Density Model for Atlantic White-Sided Dolphin (*Lagenorhynchus acutus*) for the U.S. East Coast: Supplementary Report

Model Version 4.1

Duke University Marine Geospatial Ecology Laboratory[*]

2023-05-27

Citation

When citing our methodology or results generally, please cite Roberts et al. (2016, 2023). The complete references appear at the end of this document. We are preparing a new article for a peer-reviewed journal that will eventually replace those. Until that is published, those are the best general citations.

When citing this model specifically, please use this reference:

Roberts JJ, Yack TM, Cañadas A, Fujioka E, Halpin PN, Barco SG, Boisseau O, Chavez-Rosales S, Cole TVN, Cotter MP, Cummings EW, Davis GE, DiGiovanni Jr. RA, Garrison LP, Gowan TA, Jackson KA, Kenney RD, Khan CB, Lockhart GG, Lomac-MacNair KS, McAlarney RJ, McLellan WA, Mullin KD, Nowacek DP, O'Brien O, Pabst DA, Palka DL, Quintana-Rizzo E, Redfern JV, Rickard ME, White M, Whitt AD, Zoidis AM (2022) Density Model for Atlantic White-Sided Dolphin (*Lagenorhynchus acutus*) for the U.S. East Coast, Version 4.1, 2023-05-27, and Supplementary Report. Marine Geospatial Ecology Laboratory, Duke University, Durham, North Carolina.

Copyright and License

Model Version History

Version	Date	Description
1	2014-11-15	Initial version.
2	2014-12-04	Fixed bug that applied the wrong detection function to segments NE_narwss_1999_widgeon_hapo dataset. Refitted model. Updated documentation.
2.1	2015-03-06	Updated the documentation. No changes to the model.
2.2	2015-05-14	Updated calculation of CVs. Switched density rasters to logarithmic breaks. No changes to the model.
2.3	2015-09-03	Updated the documentation. No changes to the model.

---

[*]For questions or to offer feedback please contact Jason Roberts (jason.roberts@duke.edu) and Tina Yack (tina.yack@duke.edu)

Version	Date	Description
2.4	2016-04-21	Switched calculation of monthly 5% and 95% confidence interval rasters to the method used to produce the year-round rasters. (We intended this to happen in version 2.2 but I did not implement it properly.) Updated the monthly CV rasters to have value 0 where we assumed the species was absent, consistent with the year-round CV raster. No changes to the other (non-zero) CV values, the mean abundance rasters, or the model itself. Model files released as supplementary information to Roberts et al. (2016).
3	2018-04-14	Began update to Roberts et al. (2015) model. Introduced new surveys from AMAPPS, NARWSS, UNCW, VAMSC, and the SEUS NARW teams. Updated modeling methodology. Refitted detection functions and spatial models from scratch using new and reprocessed covariates. Model released as part of a scheduled update to the U.S. Navy Marine Species Density Database (NMSDD).
4	2022-06-20	This model is a major update over the prior version, with substantial additional data, improved statistical methods, and an increased spatial resolution. It was released as part of the final delivery of the U.S. Navy Marine Species Density Database (NMSDD) for the Atlantic Fleet Testing and Training (AFTT) Phase IV Environmental Impact Statement. Several new collaborators joined and contributed survey data: New York State Department of Environmental Conservation, TetraTech, HDR, and Marine Conservation Research. We incorporated additional surveys from all continuing and new collaborators through the end of 2020. (Because some environmental covariates were only available through 2019, certain models only extend through 2019.) We increased the spatial resolution to 5 km and, at NOAA's request, we extended the model further inshore from New York through Maine. We reformulated and refitted all detection functions and spatial models. We updated all enviromental covariates to newer products, when available, and added several covariates to the set of candidates. For models that incorporated dynamic covariates, we estimated model uncertainty using a new method that accounts for both model parameter error and temporal variability.
4.1	2023-05-27	Completed the supplementary report documenting the details of this model. Corrected the 5 and 95 percent rasters so that they contain the value 0 where the taxon was asssumed absent, rather than NoData. Nothing else was changed.

1 Survey Data

We built this model from data collected between 1998-2020 (Table 1, Figure 1). We excluded surveys that did not target small cetaceans or were otherwise problematic for modeling them. In keeping with our primary strategy for the 2022 modeling cycle, we excluded data prior to 1998 in order to utilize biological covariates derived from satellite ocean color observations, which were only available for a few months before 1998. We restricted the model to aerial survey transects with sea states of Beaufort 4 or less (for a few surveys we used Beaufort 3 or less) and shipboard transects with Beaufort 5 or less (for a few we used Beaufort 4 or less). We also excluded transects with poor weather or visibility for surveys that reported those conditions.

Table 1: Survey effort and observations considered for this model. Effort is tallied as the cumulative length of on-effort transects. Observations are the number of groups and individuals encountered while on effort. Off effort observations and those lacking an estimate of group size or distance to the group were excluded.

			Effort	Observations		
Institution	Program	Period	1000s km	Groups	Individuals	Mean Group Size
Aerial Surveys						
HDR	Navy Norfolk Canyon	2018-2019	10	0	0	
NEFSC	AMAPPS	2010-2019	83	280	2,990	10.7
NEFSC	NARWSS	2003-2016	380	2,402	37,815	15.7
NEFSC	Pre-AMAPPS	1999-2008	45	124	3,200	25.8
SEFSC	AMAPPS	2010-2020	112	0	0	
SEFSC	MATS	2002-2005	27	0	0	
UNCW	MidA Bottlenose	2002-2002	15	0	0	
UNCW	Navy Cape Hatteras	2011-2017	34	0	0	
UNCW	Navy Jacksonville	2009-2017	92	0	0	
UNCW	Navy Norfolk Canyon	2015-2017	14	0	0	
UNCW	Navy Onslow Bay	2007-2011	49	0	0	
UNCW	SEUS NARW EWS	2005-2008	106	0	0	
VAMSC	MD DNR WEA	2013-2015	15	0	0	
VAMSC	Navy VACAPES	2016-2017	18	0	0	
VAMSC	VA CZM WEA	2012-2015	19	0	0	
	Total		**1,020**	**2,806**	**44,005**	**15.7**
Shipboard Surveys						
MCR	SOTW Visual	2012-2019	9	6	44	7.3
NEFSC	AMAPPS	2011-2016	15	24	279	11.6
NEFSC	Pre-AMAPPS	1998-2007	13	62	1,777	28.7
NJDEP	NJEBS	2008-2009	14	0	0	
SEFSC	AMAPPS	2011-2016	16	0	0	
SEFSC	Pre-AMAPPS	1998-2006	30	0	0	
	Total		**96**	**92**	**2,100**	**22.8**
	Grand Total		**1,115**	**2,898**	**46,105**	**15.9**

Table 2: Institutions that contributed surveys used in this model.

Institution	Full Name
HDR	HDR, Inc.
MCR	Marine Conservation Research
NEFSC	NOAA Northeast Fisheries Science Center
NJDEP	New Jersey Department of Environmental Protection
SEFSC	NOAA Southeast Fisheries Science Center
UNCW	University of North Carolina Wilmington
VAMSC	Virginia Aquarium & Marine Science Center

Table 3: Descriptions and references for survey programs used in this model.

| Program	Description	References
AMAPPS	Atlantic Marine Assessment Program for Protected Species	Palka et al. (2017), Palka et al. (2021)
MATS	Mid-Atlantic Tursiops Surveys	
MD DNR WEA	Aerial Surveys of the Maryland Wind Energy Area	Barco et al. (2015)
MidA Bottlenose	Mid-Atlantic Onshore/Offshore Bottlenose Dolphin Surveys	Torres et al. (2005)
NARWSS	North Atlantic Right Whale Sighting Surveys	Cole et al. (2007)
Navy Cape Hatteras	Aerial Surveys of the Navy's Cape Hatteras Study Area	McLellan et al. (2018)
Navy Jacksonville	Aerial Surveys of the Navy's Jacksonville Study Area	Foley et al. (2019)
Navy Norfolk Canyon	Aerial Surveys of the Navy's Norfolk Canyon Study Area	Cotter (2019), McAlarney et al. (2018)
Navy Onslow Bay	Aerial Surveys of the Navy's Onslow Bay Study Area	Read et al. (2014)
Navy VACAPES	Aerial Survey Baseline Monitoring in the Continental Shelf Region of the VACAPES OPAREA	Mallette et al. (2017)
NJEBS	New Jersey Ecological Baseline Study	Geo-Marine, Inc. (2010), Whitt et al. (2015)
Pre-AMAPPS	Pre-AMAPPS Marine Mammal Abundance Surveys	Mullin and Fulling (2003), Garrison et al. (2010), Palka (2006)
SEUS NARW EWS	Southeast U.S. Right Whale Early Warning System Surveys	
SOTW Visual	R/V Song of the Whale Visual Surveys	Ryan et al. (2013)
VA CZM WEA	Virginia CZM Wind Energy Area Surveys	Mallette et al. (2014), Mallette et al. (2015)
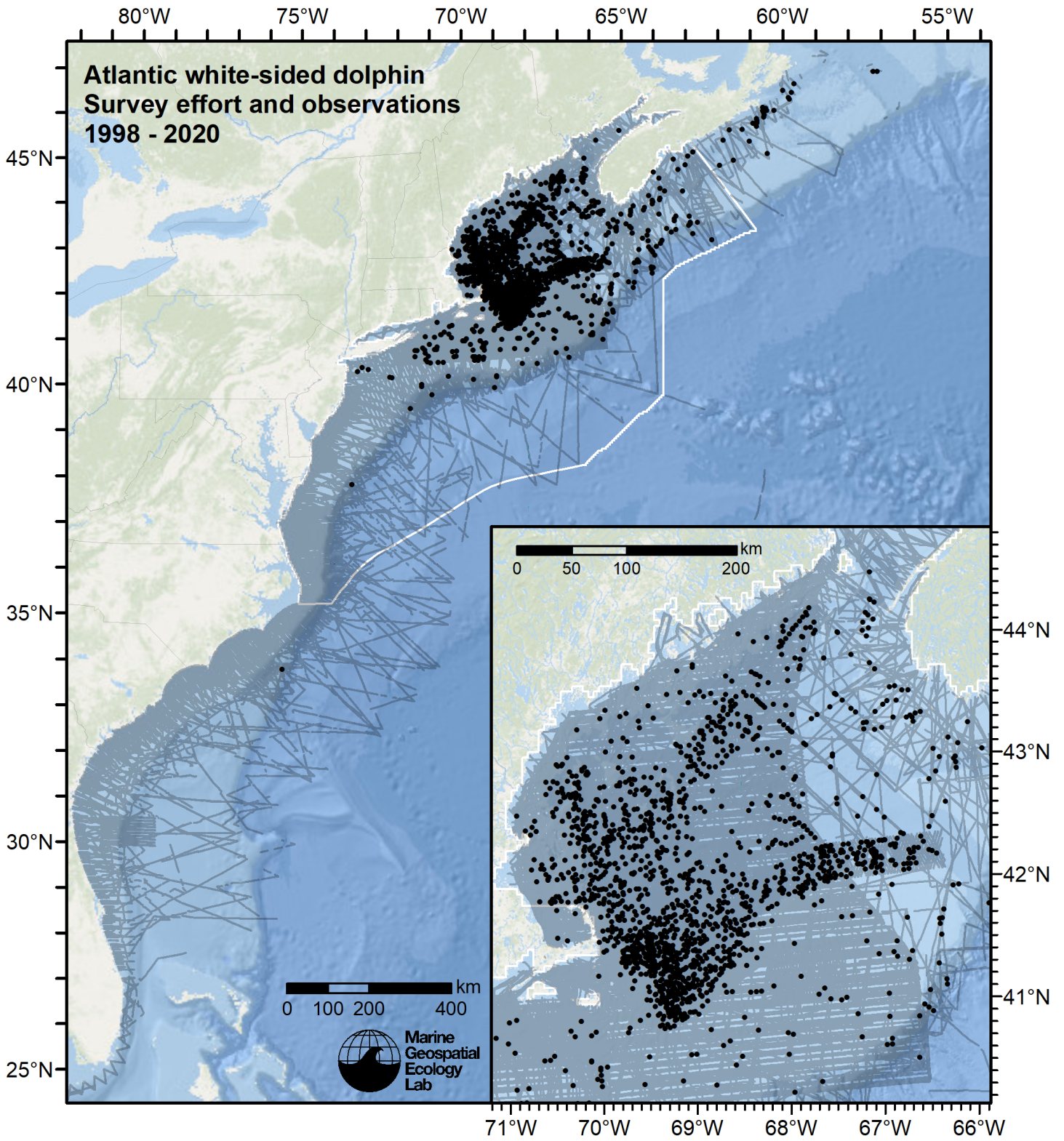
Figure 1: Survey effort and Atlantic white-sided dolphin observations available for density modeling, after detection functions were applied, and excluded segments and truncated observations were removed.

2 Classification of Ambiguous Sightings

Observers occasionally experience difficulty identifying species, due to poor sighting conditions or phenotypic similarities between the possible choices. For example, observers may not always be able to distinguish fin whales from sei whales due their similiar size and shape. When this happens, observers will report an ambiguous identification, such as "fin or sei whale". In our density models, we handled ambiguous identifications in three ways:

1. For sightings with very generic identifications such as "large whale", we discarded the sightings. These sightings represented a clear minority when compared to those with definitive species identifications, but they are uncounted animals and our density models may therefore underestimate density to some degree.

2. For sightings of certain taxa in which a large majority of identifications were ambiguous (e.g. "unidentified pilot whale") rather than specific (e.g. "short-finned pilot whale" or "long-finned pilot whale"), it was not tractable to model the individual species so we modeled the generic taxon instead.

3. For sightings that reported an ambiguous identification of two species (e.g. "fin or sei whale") that are known to exhibit different habitat preferences or typically occur in different group sizes, and for which we had sufficient number of definitive sightings of both species, we first fitted a predictive model that classified the ambiguous sightings into one species or the other and then included the resulting classified sightings in the density models for each of the two species.

This section describes how we classified the third category of ambiguous sightings reported as "common or white-sided dolphin" into one species or the other.

For the predictive model, we used the cforest classifier (Hothorn et al. 2006), an elaboration of the classic random forest classifier (Breiman 2001). First, we trained a binary classifier using the sightings that reported definitive species identifications ("short-beaked common dolphin" and "Atlantic white-sided dolphin"). To increase the range of sampling of the classification model's covariates, the training data may have included additional surveys not considered for the density model, as well as transects from outside the spatial and temporal extents of the density model. Only on-effort sightings were used. We used the species ID as the response variable and environmental variables as covariates.

We used receiver operating characteristic (ROC) curve analysis to select a threshold for classifying the probabilistic predictions of species identifications made by the model into a binary result of one species or another. For the classification threshold, we selected the value that maximized the Youden index (Perkins and Schisterman 2006). Then, for all sightings reporting the ambiguous identification, we classified each as either one species or the other by processing the covariate values observed for it through the fitted model. We then included the classified sightings in the detection functions and density models. The sightings reported elsewhere in this document incorporate both the definitive sightings and the classified sightings, unless otherwise noted.

2.1 Classification Model

```
MODEL SUMMARY:
==============

Random Forest using Conditional Inference Trees

Number of trees: 750

Response: factor(OriginalScientificName)
Inputs: ClimChl, ClimDistToFront207, ClimMnkEpi, ClimPP_CAFE, ClimSST_CMC, ClimWindSpeed,
ClimZoo_SEAPODYM, Depth, DistTo125m, DistTo300m, Slope
Number of observations: 4877

Number of variables tried at each split: 5

Estimated predictor variable importance (conditional = FALSE):

Importance
DistTo300m 0.0818
ClimZoo_SEAPODYM 0.0688
ClimMnkEpi 0.0659
```

```
ClimWindSpeed 0.0343
ClimSST_CMC 0.0266
ClimPP_CAFE 0.0250
ClimDistToFront207 0.0244
DistTo125m 0.0204
ClimChl 0.0180
Depth 0.0111
Slope 0.0063
```

```
MODEL PERFORMANCE SUMMARY:
==========================
```

Statistics calculated from the training data.

```
Area under the ROC curve (auc)          = 0.981
Mean cross-entropy (mxe)                = 0.210
Precision-recall break-even point (prbe) = 0.907
Root-mean square error (rmse)           = 0.244
```

User-specified cutoff = 0.524

Confusion matrix for that cutoff:

	Actual Lagenorhynchus acutus	Actual Delphinus delphis	Total
Predicted Lagenorhynchus acutus	1880	193	2073
Predicted Delphinus delphis	192	2612	2804
Total	2072	2805	4877

Model performance statistics for that cutoff:

```
Accuracy (acc)                          = 0.921
Error rate (err)                        = 0.079
Rate of positive predictions (rpp)      = 0.425
Rate of negative predictions (rnp)      = 0.575

True positive rate (tpr, or sensitivity) = 0.907
False positive rate (fpr, or fallout)   = 0.069
True negative rate (tnr, or specificity) = 0.931
False negative rate (fnr, or miss)      = 0.093

Positive prediction value (ppv, or precision) = 0.907
Negative prediction value (npv)         = 0.932
Prediction-conditioned fallout (pcfall) = 0.093
Prediction-conditioned miss (pcmiss)    = 0.068

Matthews correlation coefficient (mcc)  = 0.838
Odds ratio (odds)                       = 132.517
SAR                                     = 0.715

Cohen's kappa (K)                       = 0.838
```
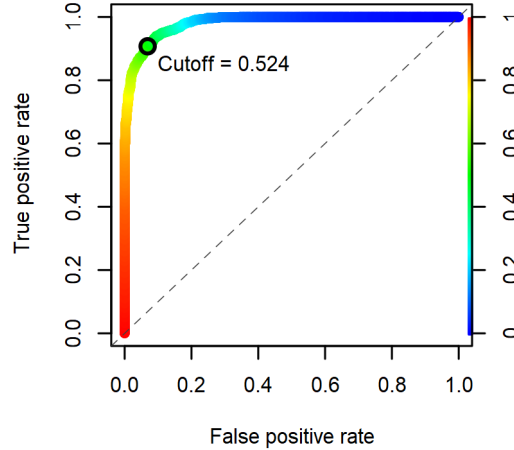
Figure 2: Receiver operating characteristic (ROC) curve summarizing the predictive performance of the ambiguous sighting classification model.

Table 4: Covariates used in the ambiguous sighting classification model.

| Covariate	Description
ClimChl	Climatological monthly mean chlorophyll a concentration (mg m^{-3}) from Copernicus GlobColour (Garnesson et al. (2019)), provided by E.U. Copernicus Marine Service (product OCEANCOLOUR_GLO_CHL_L4_REP_OBSERVATIONS_009_082)
ClimDistToFront207	Climatological monthly mean distance (km) to the closest sea surface temperature front detected in daily GHRSST Level 4 CMC0.2deg and CMC0.1deg images (Brasnett (2008); Canada Meteorological Center (2012); Meissner et al. (2016); Canada Meteorological Center (2016)) with MGET's implementation of the Canny edge detector (Roberts et al. (2010); Canny (1986))
ClimMnkEpi	Climatological monthly mean micronekton biomass available in the epipelagic zone, expressed as wet weight (g m^{-2}), from SEAPODYM (Lehodey et al. (2008); Lehodey et al. (2015)), provided by E.U. Copernicus Marine Service. doi: 10.48670/moi-00020. Computed as the sum of the SEAPODYM mnkc_epi, mnkc_mumeso, and mnkc_hmlmeso variables.
ClimPP_CAFE	Climatological monthly mean net primary productivity (mg C m^{-2} day^{-1}) from the Carbon, Absorption, and Fluorescence Euphotic-resolving (CAFE) model (Silsbe et al. (2016))
ClimSST_CMC	Climatological monthly mean sea surface temperature (°C) from GHRSST Level 4 CMC0.2deg and CMC0.1deg (Brasnett (2008); Canada Meteorological Center (2012); Meissner et al. (2016); Canada Meteorological Center (2016))
ClimWindSpeed	Climatological monthly mean wind speed (m s^{-1}) 10 m above sea level from CCMP V2 Level 3 surface wind vectors (Atlas et al. (2011); Wentz et al. (2015))
ClimZoo_SEAPODYM	Climatological monthly mean zooplankton biomass expressed in carbon (g C m^{-2}) from SEAPODYM (Lehodey et al. (2008); Lehodey et al. (2015)), provided by E.U. Copernicus Marine Service. doi: 10.48670/moi-00020
Depth	Depth (m) of the seafloor, from SRTM30_PLUS (Becker et al. (2009))
DistTo125m	Distance (km) to the 125m isobath, derived from SRTM30_PLUS (Becker et al. (2009))
DistTo300m	Distance (km) to the 300m isobath, derived from SRTM30_PLUS (Becker et al. (2009))
Slope	Slope (percent rise) of the seafloor, derived from SRTM30_PLUS (Becker et al. (2009))
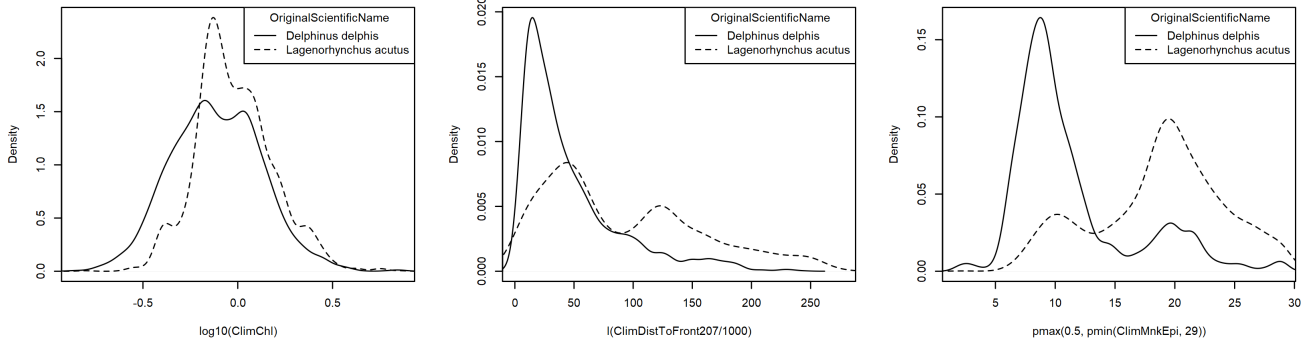
(a) Chlorophyll a concentration (mg m^{-3}) (b) Climatological distance to SST front (km)(c) Climatological epipelagic micronekton biomass (g m^{-2})
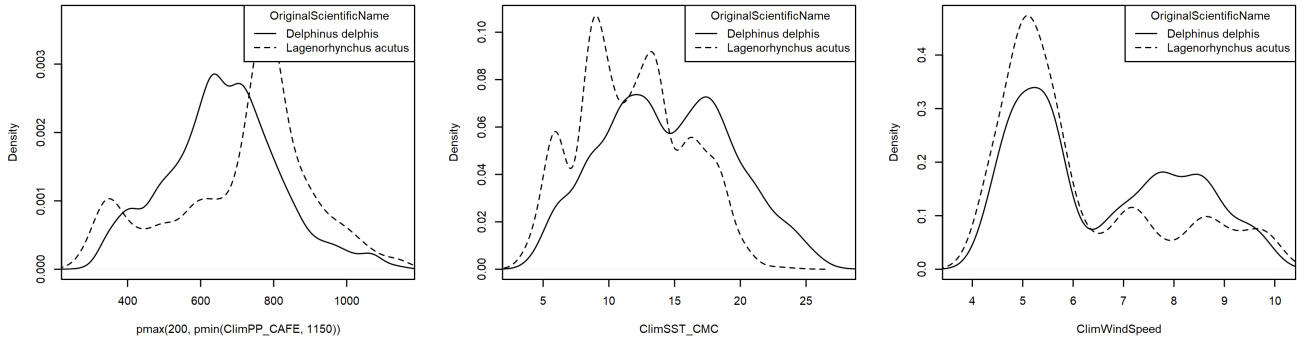
(d) Climatological net primary productivity (mg C m^{-2} day^{-1}) (CAFE model) (e) Climatological sea surface temperature (°C) (f) Climatological wind speed (m s^{-1})
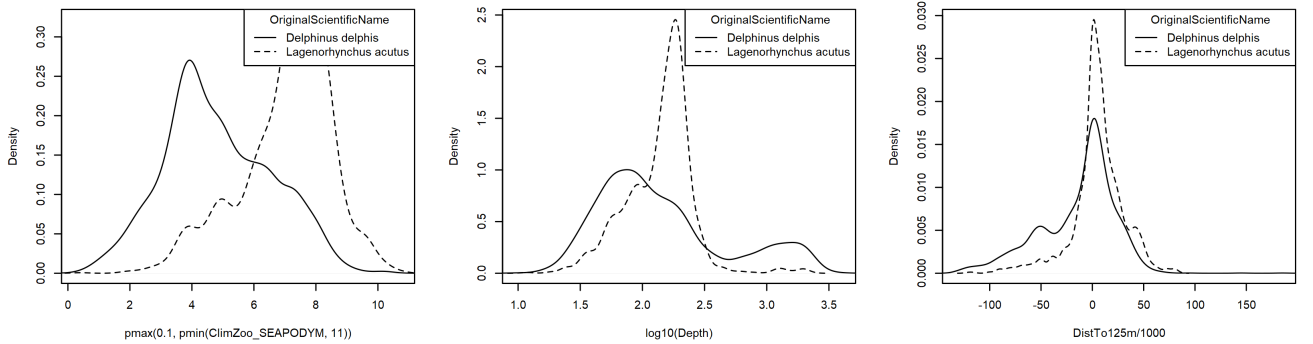
(g) Climatological zooplankton biomass (g C m^{-2}) (h) Seafloor depth (m) (i) Distance to 125m isobath (km)
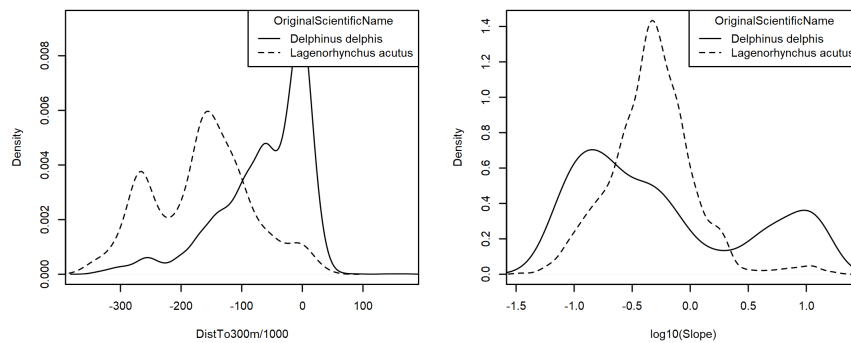
(j) Distance to 300m isobath (km) (k) Seafloor slope (percent rise)

Figure 3: Density histograms showing the per-species distribution of each covariate in the ambiguous sighting classification model. When a covariate exhibits a substantially different distribution for each species, it is a good candidate for differentiating the species. Transforms and other treatments are indicated in axis labels. *log10* indicates the covariate was $\log_{10}$ transformed. *pmax* and *pmin* indicate the covariate's minimum and maximum values, respectively, were Winsorized to the values shown. */1000* indicates meters were transformed to kilometers for interpretation convenience.

9

2.2 Classifications Performed

Table 5: Summary of the definitive sightings used to train the classification model, the ambiguous sightings to which the model was applied, and their resulting classifications. To increase the range of sampling of the classification model's covariates, the training data may have included additional surveys not considered for the density model, as well as transects from outside the spatial and temporal extents of the density model. Only on-effort sightings were used.

Institution	Program	Definitive		Ambiguous	Classified	
		D. delphis	L. acutus		D. delphis	L. acutus
Aerial Surveys						
HDR	Navy Norfolk Canyon	84	0	0	0	0
NEAq	CNM	21	0	0	0	0
NEAq	MMS-WEA	61	8	3	3	0
NEAq	NLPSC	44	6	5	4	1
NEFSC	AMAPPS	742	225	165	103	62
NEFSC	NARWSS	372	1,536	1,472	325	1,147
NEFSC	Pre-AMAPPS	302	207	9	7	2
NJDEP	NJEBS	5	0	0	0	0
NYS-DEC/TT	NYBWM	67	0	0	0	0
SEFSC	AMAPPS	300	0	0	0	0
SEFSC	MATS	3	0	0	0	0
UNCW	MidA Bottlenose	5	0	0	0	0
UNCW	Navy Cape Hatteras	30	0	0	0	0
UNCW	Navy Norfolk Canyon	51	0	0	0	0
UNCW	Navy Onslow Bay	1	0	0	0	0
UNCW	SEUS NARW EWS	26	0	0	0	0
VAMSC	MD DNR WEA	44	0	0	0	0
VAMSC	Navy VACAPES	9	0	0	0	0
VAMSC	VA CZM WEA	25	0	0	0	0
	Total	**2,192**	**1,982**	**1,654**	**442**	**1,212**
Shipboard Surveys						
MCR	SOTW Visual	9	1	0	0	0
NEFSC	AMAPPS	368	24	2	2	0
NEFSC	Pre-AMAPPS	173	65	0	0	0
NJDEP	NJEBS	19	0	0	0	0
SEFSC	AMAPPS	2	0	0	0	0
SEFSC	Pre-AMAPPS	42	0	0	0	0
	Total	**613**	**90**	**2**	**2**	**0**
	Grand Total	**2,805**	**2,072**	**1,656**	**444**	**1,212**
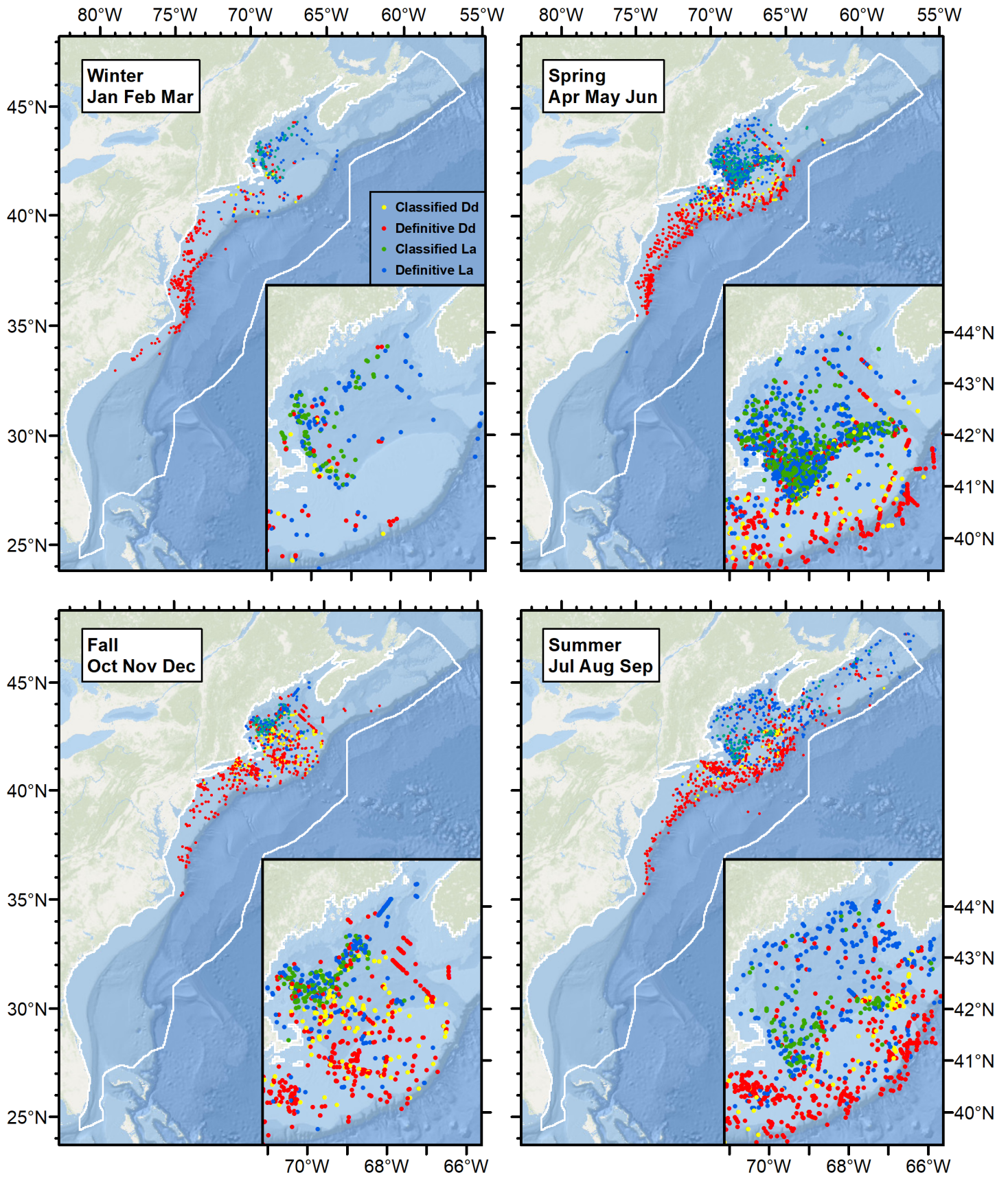
Figure 4: Definitive sightings used to train the model and ambiguous sightings classified by the model.

3 Detection Functions

3.1 With a Taxonomic Covariate

We fitted the detection functions in this section to pools of species with similar detectability characteristics and used the taxonomic identification as a covariate (ScientificName) to account for differences between them. We consulted the literature and observer teams to determine appropriate poolings. We usually employed this approach to boost the counts of observations in the detection functions, which increased the chance that other covariates such as Beaufort sea state could be used to account for differences in observing conditions. When defining the taxonomic covariate, we sometimes had too few observations of species to allocate each of them their own level of the covariate and had to group them together, again consulting the literature and observers for advice on species similarity. Also, when species were observed frequently enough to be allocated their own levels but statistical tests indicated no significant difference between the levels, we usually grouped them together into a single level.

3.1.1 Aerial Surveys
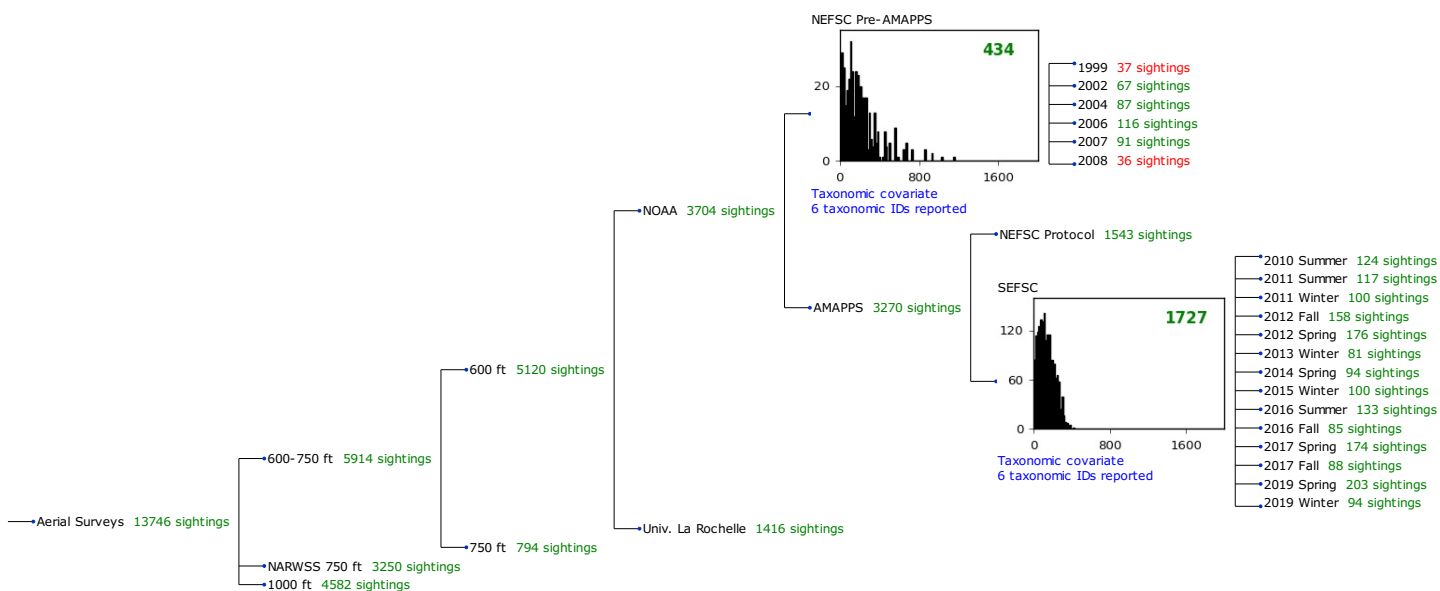
Figure 5: Detection hierarchy for aerial surveys, showing how they were pooled during detectability modeling, for detection functions that pooled multiple taxa and used used a taxonomic covariate to account for differences between them. Each histogram represents a detection function and summarizes the perpendicular distances of observations that were pooled to fit it, prior to truncation. Observation counts, also prior to truncation, are shown in green when they met the recommendation of Buckland et al. (2001) that detection functions utilize at least 60 sightings, and red otherwise. For rare taxa, it was not always possible to meet this recommendation, yielding higher statistical uncertainty. During the spatial modeling stage of the analysis, effective strip widths were computed for each survey using the closest detection function above it in the hierarchy (i.e. moving from right to left in the figure). Surveys that do not have a detection function above them in this figure were either addressed by a detection function presented in a different section of this report, or were omitted from the analysis.

3.1.1.1 NEFSC Pre-AMAPPS

After right-truncating observations greater than 600 m, we fitted the detection function to the 413 observations that remained (Table 6). The selected detection function (Figure 6) used a hazard rate key function with Beaufort (Figure 7) and ScientificName (Figure 8) as covariates.

Table 6: Observations used to fit the NEFSC Pre-AMAPPS detection function.

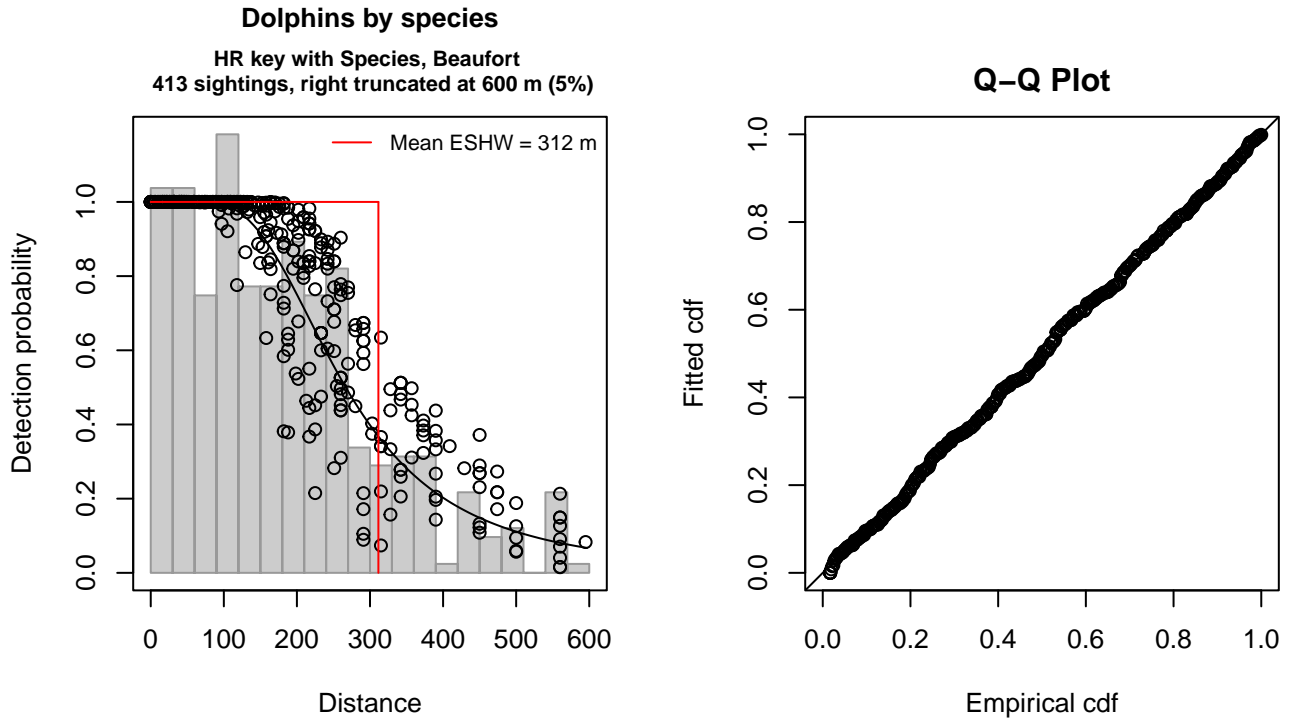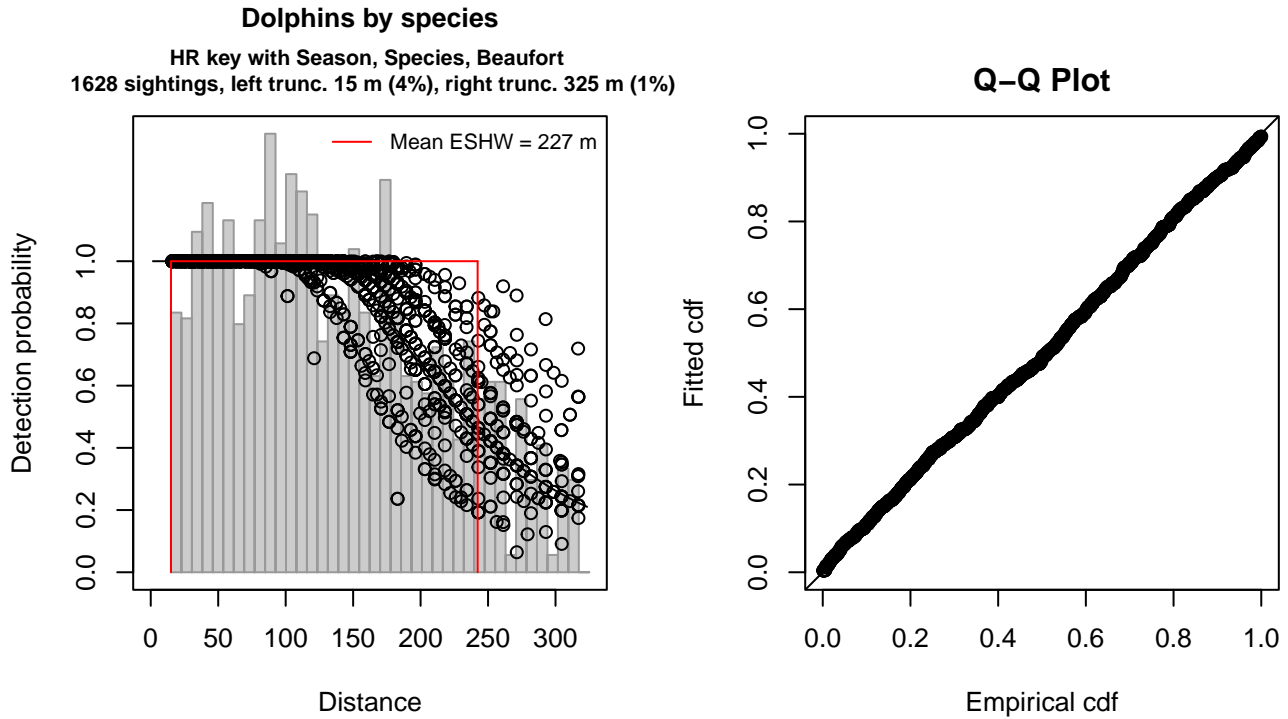| ScientificName	n
Delphinus, Lagenodelphis, Stenella	239
Lagenorhynchus	128
Tursiops, Steno	46
Total	**413**

Figure 6: NEFSC Pre-AMAPPS detection function and Q-Q plot showing its goodness of fit.

Statistical output for this detection function:

```
Summary for ds object
Number of observations :   413
Distance range         :   0  -   600
AIC                    :   5043.994

Detection function:
 Hazard-rate key function

Detection function parameters
Scale coefficient(s):
                              estimate          se
(Intercept)                  5.3188665 0.15126469
ScientificNameLagenorhynchus -0.1872175 0.11165678
ScientificNameTursiops, Steno -0.5457529 0.14785313
Beaufort                      0.1451869 0.05844944

Shape coefficient(s):
            estimate        se
(Intercept) 1.107015 0.1176733

                Estimate         SE          CV
```

```
Average p               0.4982478  0.02373666 0.04764026
N in covered region 828.9047438 49.28440455 0.05945726


Distance sampling Cramer-von Mises test (unweighted)
Test statistic = 0.023324  p = 0.992716
```
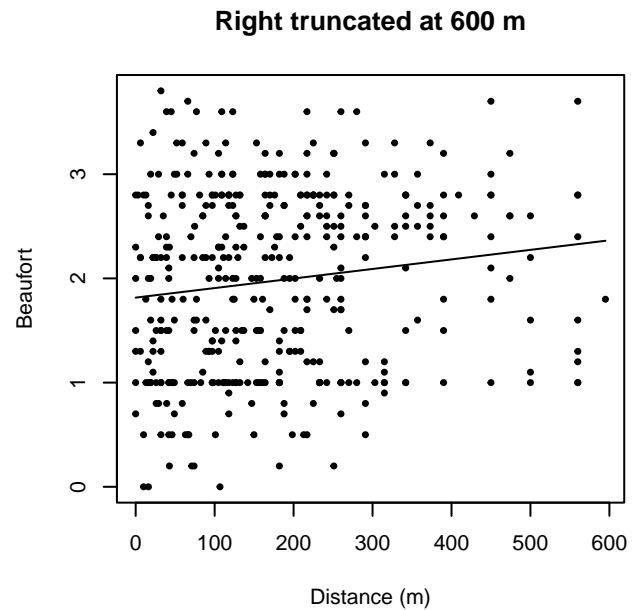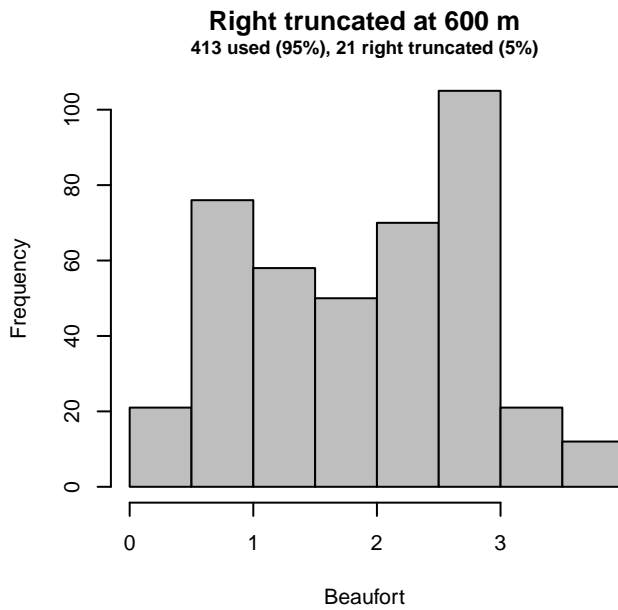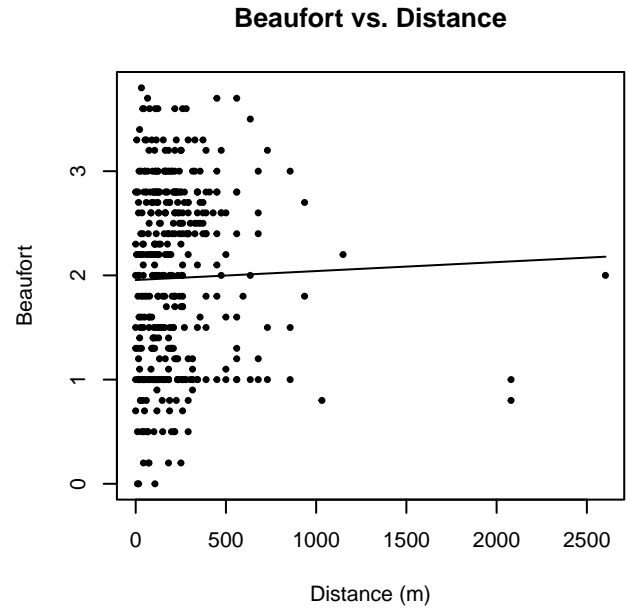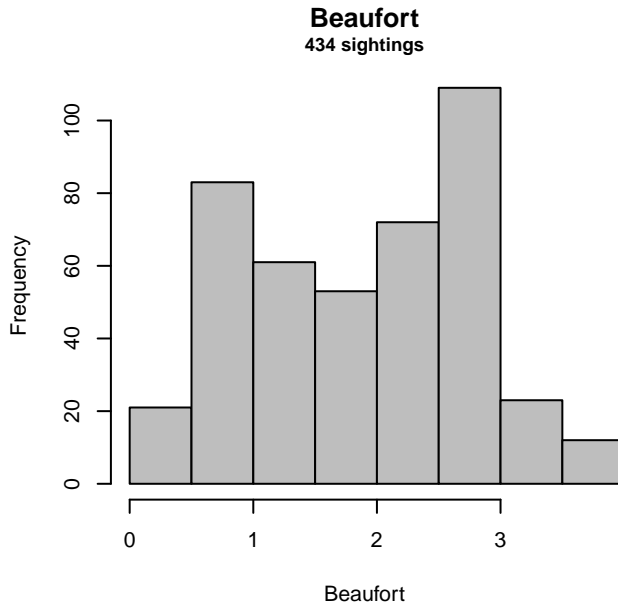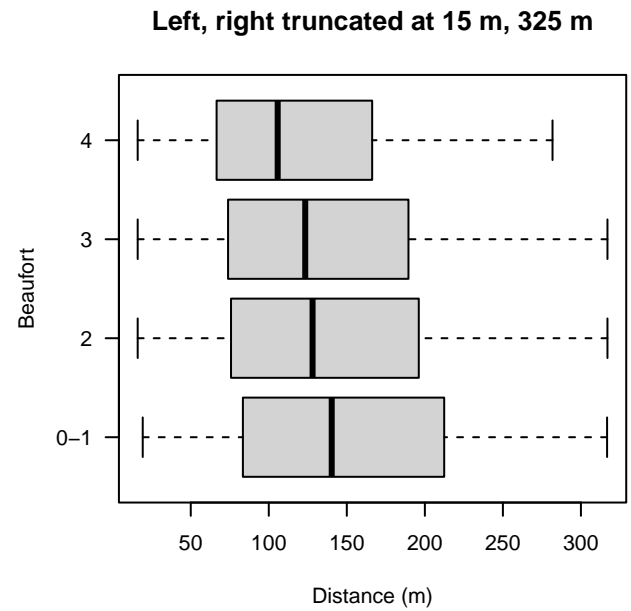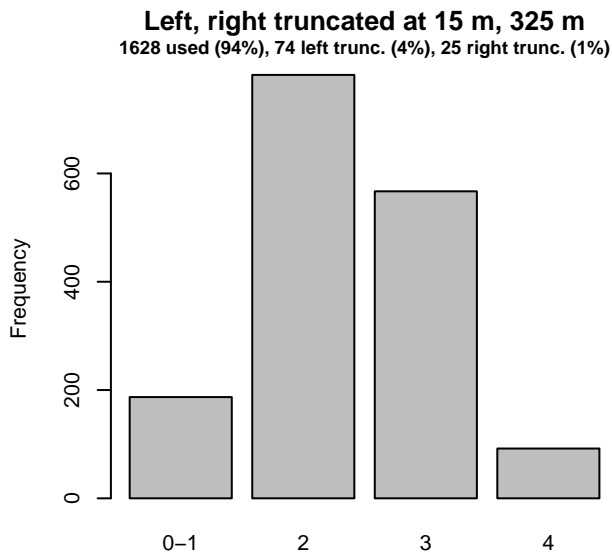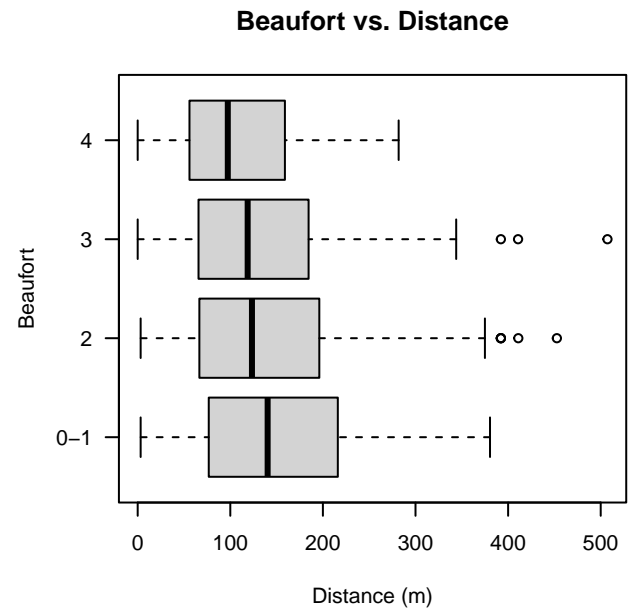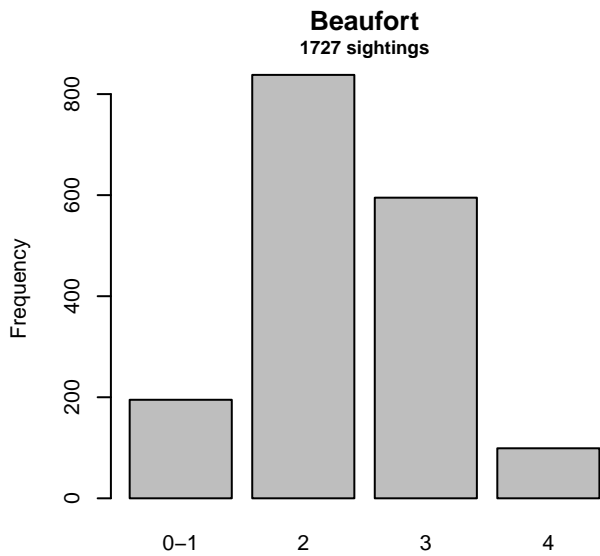

Figure 7: Distribution of the Beaufort covariate before (top row) and after (bottom row) observations were truncated to fit the NEFSC Pre-AMAPPS detection function.
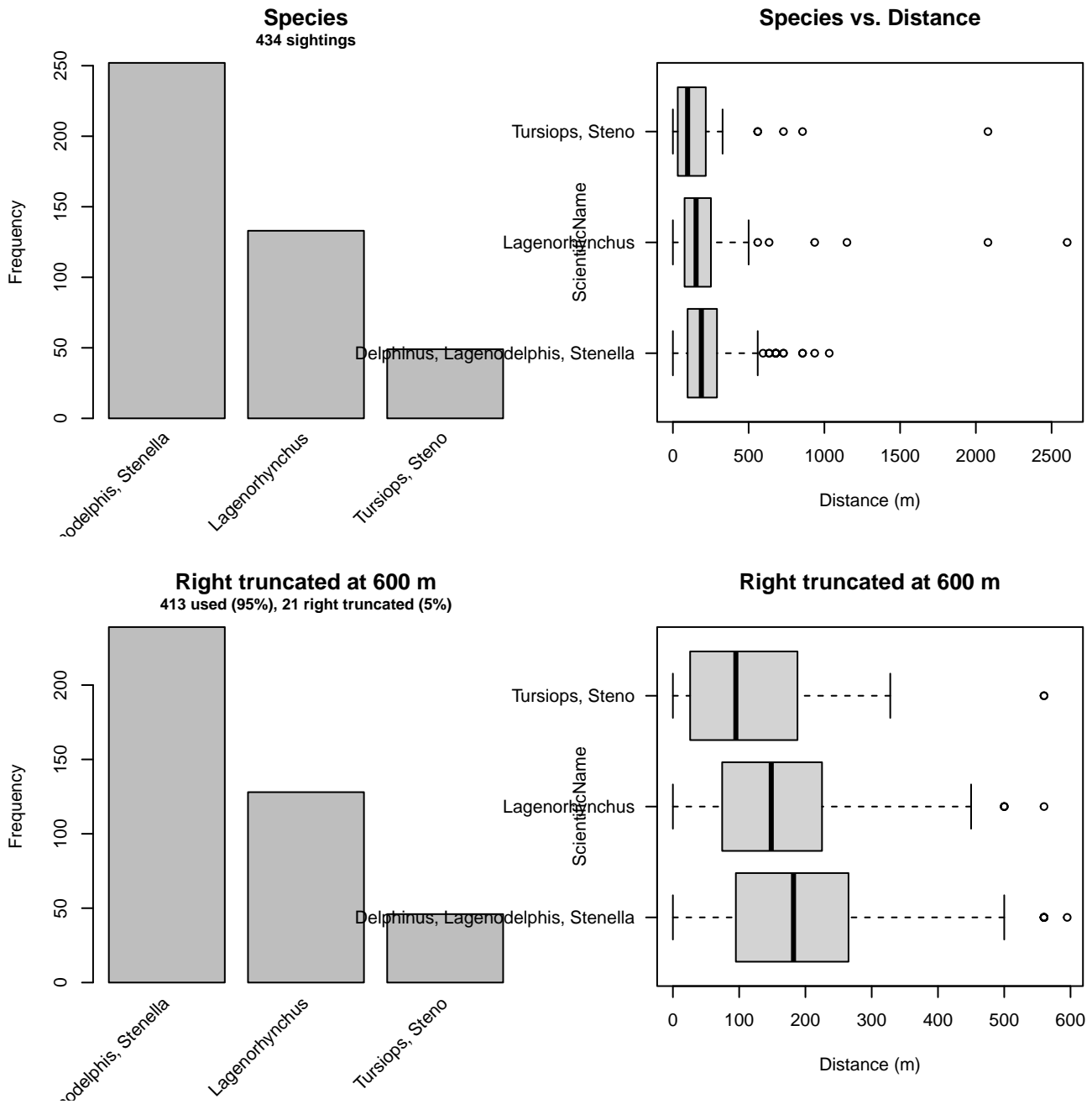
Figure 8: Distribution of the ScientificName covariate before (top row) and after (bottom row) observations were truncated to fit the NEFSC Pre-AMAPPS detection function.

3.1.1.2 SEFSC AMAPPS

After right-truncating observations greater than 325 m and left-truncating observations less than 15 m (Figure 10), we fitted the detection function to the 1628 observations that remained (Table 7). The selected detection function (Figure 9) used a hazard rate key function with Beaufort (Figure 11), ScientificName (Figure 12) and Season (Figure 13) as covariates.

Table 7: Observations used to fit the SEFSC AMAPPS detection function.

ScientificName	n
Delphinus, Tursiops, Lagenorhynchus, Steno	1422
Stenella, Lagenodelphis	206
Total	**1628**

Dolphins by species

HR key with Season, Species, Beaufort
1628 sightings, left trunc. 15 m (4%), right trunc. 325 m (1%)

Q–Q Plot

Figure 9: SEFSC AMAPPS detection function and Q-Q plot showing its goodness of fit.

Statistical output for this detection function:

```
Summary for ds object
Number of observations :  1628
Distance range         :  15  -  325
AIC                    :  18351.39

Detection function:
 Hazard-rate key function

Detection function parameters
Scale coefficient(s):
                                          estimate          se
(Intercept)                              5.4780735  0.08251975
SeasonSummer                             0.1269645  0.06172358
SeasonWinter                            -0.2356803  0.06102237
ScientificNameStenella, Lagenodelphis   0.2204074  0.08699872
Beaufort2                               -0.1192230  0.08713320
Beaufort3                               -0.1846083  0.08971655
Beaufort4                               -0.4027356  0.12330363

Shape coefficient(s):
            estimate         se
(Intercept) 1.266688 0.1150367


                    Estimate          SE          CV
Average p           0.720161  0.01522909  0.02114679
N in covered region 2260.605761 56.60731047 0.02504077

Distance sampling Cramer-von Mises test (unweighted)
Test statistic = 0.138923  p = 0.425167
```

Left trucated sightings (in red)

1628 used (94%), 74 left trunc. (4%), 25 right trunc. (1%)
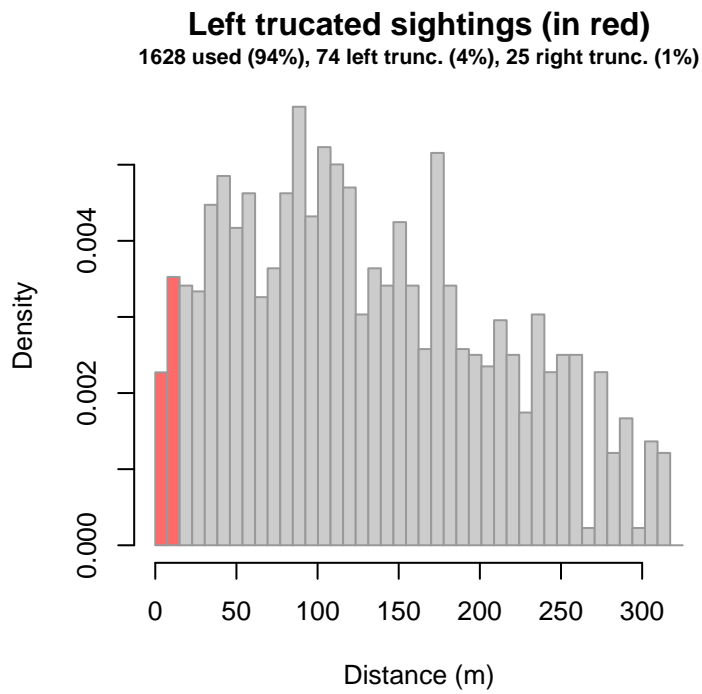
Figure 10: Density histogram of observations used to fit the SEFSC AMAPPS detection function, with the left-most bar showing observations at distances less than 15 m, which were left-truncated and excluded from the analysis [Buckland et al. (2001)]. (This bar may be very short if there were very few left-truncated sightings, or very narrow if the left truncation distance was very small; in either case it may not appear red.)

Figure 11: Distribution of the Beaufort covariate before (top row) and after (bottom row) observations were truncated to fit the SEFSC AMAPPS detection function.
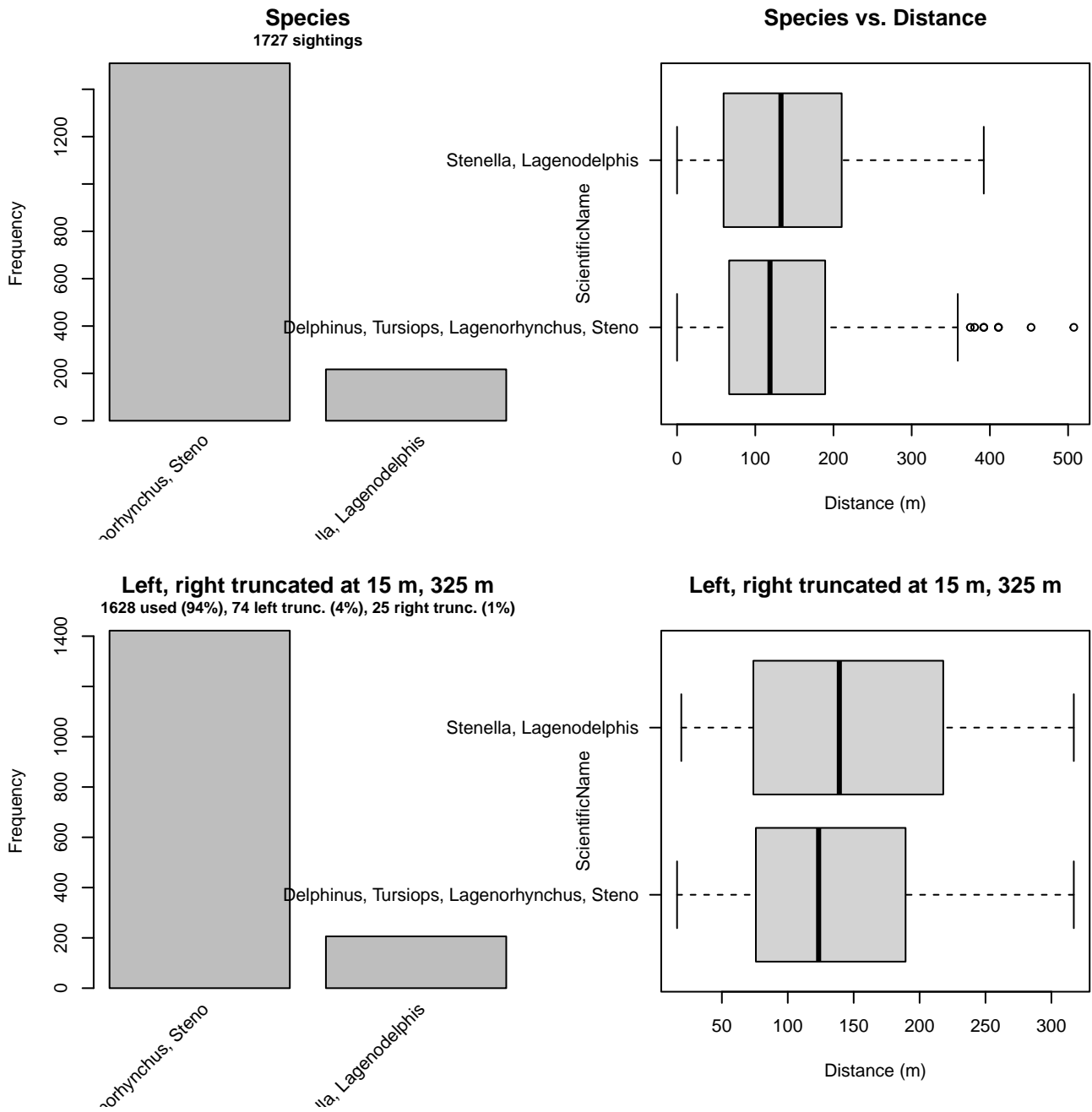
Figure 12: Distribution of the ScientificName covariate before (top row) and after (bottom row) observations were truncated to fit the SEFSC AMAPPS detection function.
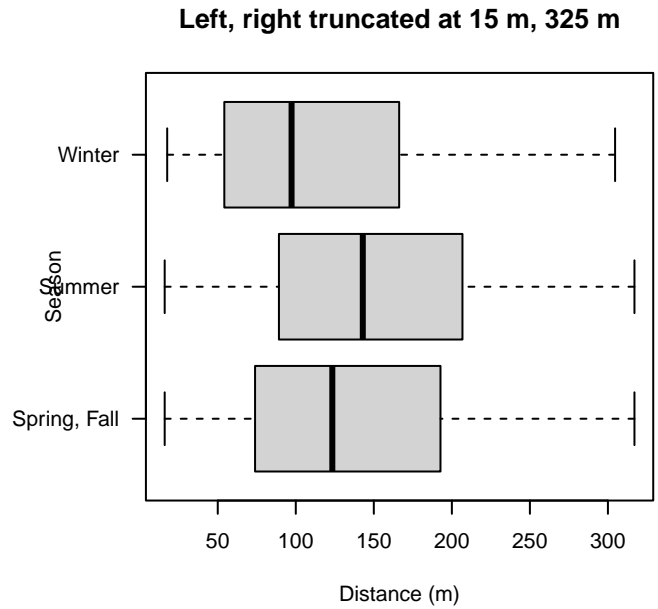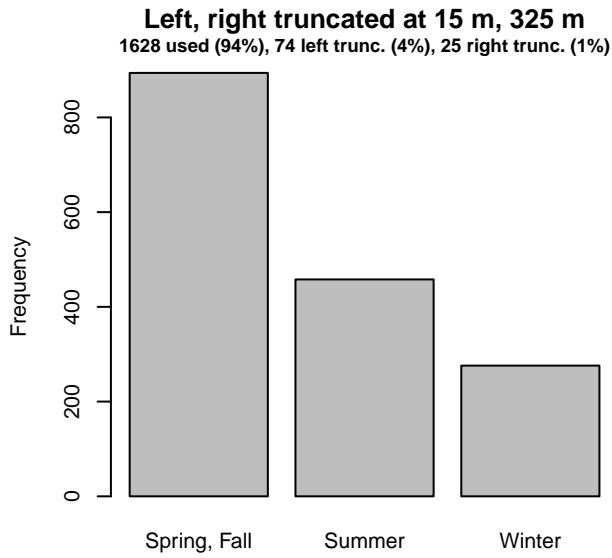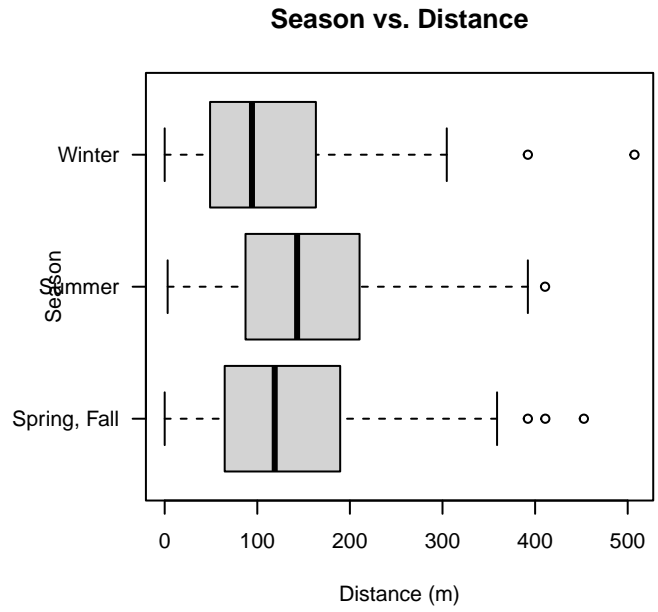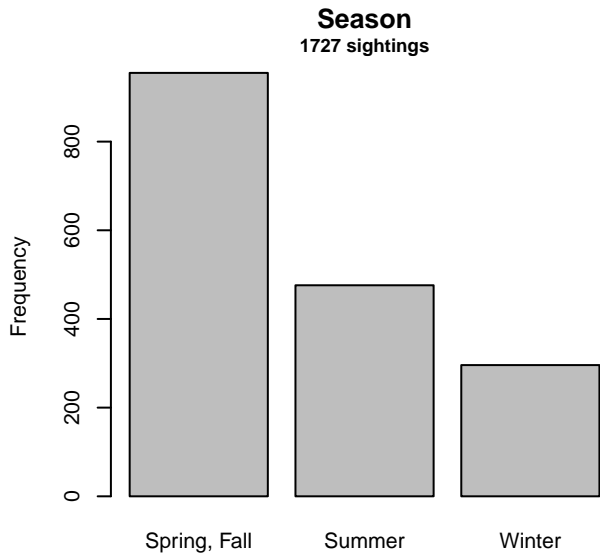
Figure 13: Distribution of the Season covariate before (top row) and after (bottom row) observations were truncated to fit the SEFSC AMAPPS detection function.

3.1.2 Shipboard Surveys
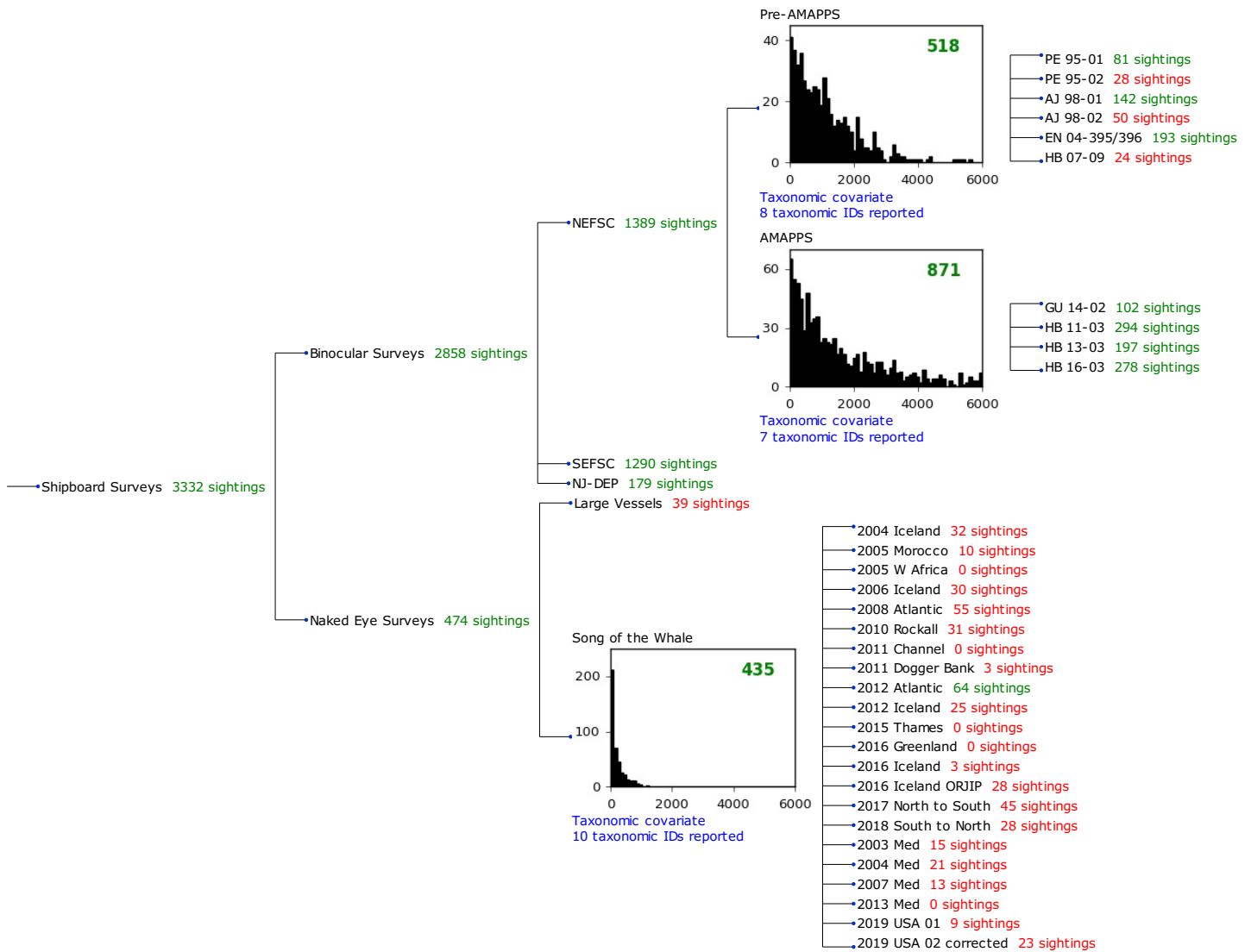
Figure 14: Detection hierarchy for shipboard surveys, showing how they were pooled during detectability modeling, for detection functions that pooled multiple taxa and used used a taxonomic covariate to account for differences between them. Each histogram represents a detection function and summarizes the perpendicular distances of observations that were pooled to fit it, prior to truncation. Observation counts, also prior to truncation, are shown in green when they met the recommendation of Buckland et al. (2001) that detection functions utilize at least 60 sightings, and red otherwise. For rare taxa, it was not always possible to meet this recommendation, yielding higher statistical uncertainty. During the spatial modeling stage of the analysis, effective strip widths were computed for each survey using the closest detection function above it in the hierarchy (i.e. moving from right to left in the figure). Surveys that do not have a detection function above them in this figure were either addressed by a detection function presented in a different section of this report, or were omitted from the analysis.

3.1.2.1 NEFSC Pre-AMAPPS

After right-truncating observations greater than 4000 m, we fitted the detection function to the 508 observations that remained (Table 8). The selected detection function (Figure 15) used a hazard rate key function with Beaufort (Figure 16), ScientificName (Figure 17) and VesselName (Figure 18) as covariates.

Table 8: Observations used to fit the NEFSC Pre-AMAPPS detection function.

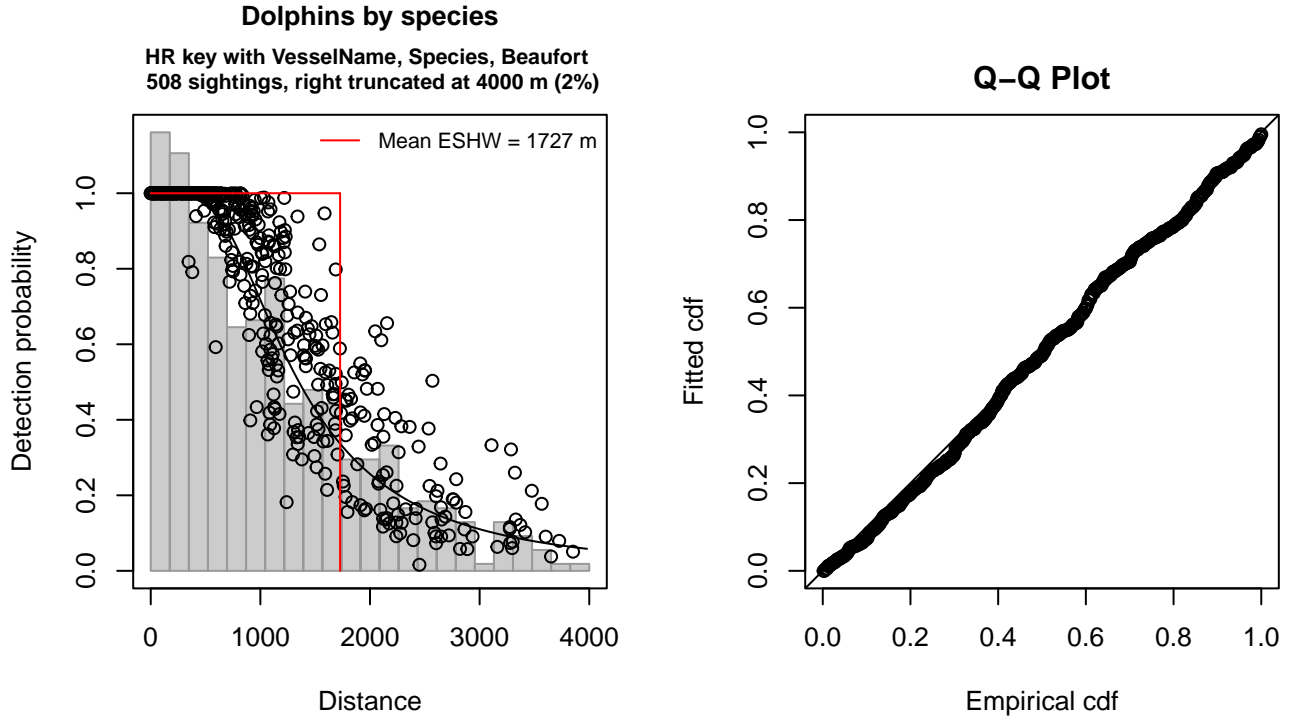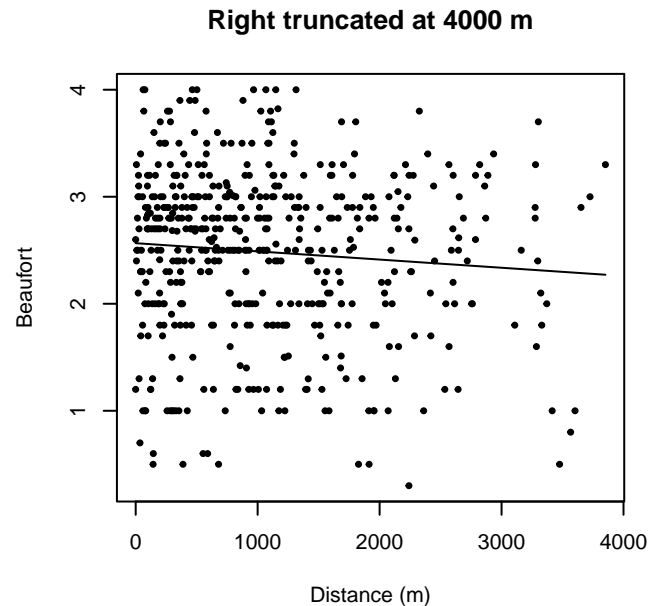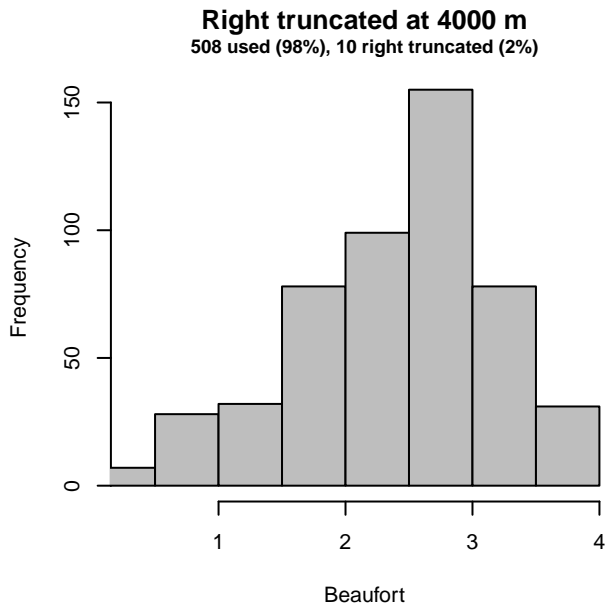| ScientificName	n
Delphinus, Lagenorhynchus, Tursiops, Steno	365
Other Stenella, Lagenodelphis	130
Stenella frontalis	13
Total	**508**

Figure 15: NEFSC Pre-AMAPPS detection function and Q-Q plot showing its goodness of fit.

Statistical output for this detection function:

```
Summary for ds object
Number of observations :   508
Distance range         :   0  -  4000
AIC                    :   8058.614

Detection function:
 Hazard-rate key function

Detection function parameters
Scale coefficient(s):
                                              estimate          se
(Intercept)                                  7.3979634 0.1986065
VesselNameEndeavor, Bigelow                  0.2529041 0.1095209
ScientificNameOther Stenella, Lagenodelphis  0.3555978 0.1258179
ScientificNameStenella frontalis            -0.8556981 0.3078540
Beaufort                                    -0.1897812 0.0694737

Shape coefficient(s):
            estimate        se
(Intercept) 0.8752144 0.1006522
```

```
                        Estimate          SE          CV
Average p               0.4071518  0.02118698 0.05203705
N in covered region  1247.6919609 78.15195776 0.06263722


Distance sampling Cramer-von Mises test (unweighted)
Test statistic = 0.120847   p = 0.492001
```
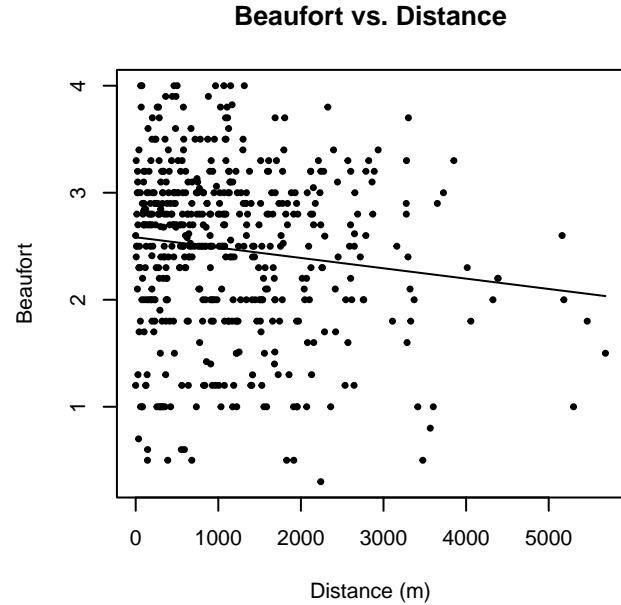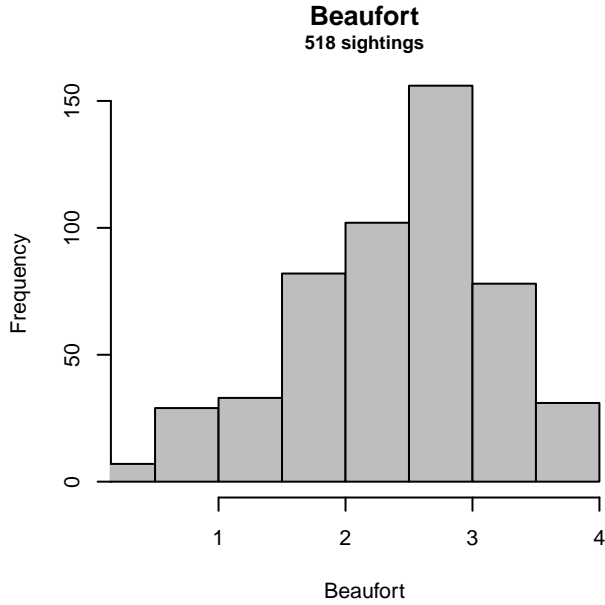

Figure 16: Distribution of the Beaufort covariate before (top row) and after (bottom row) observations were truncated to fit the NEFSC Pre-AMAPPS detection function.
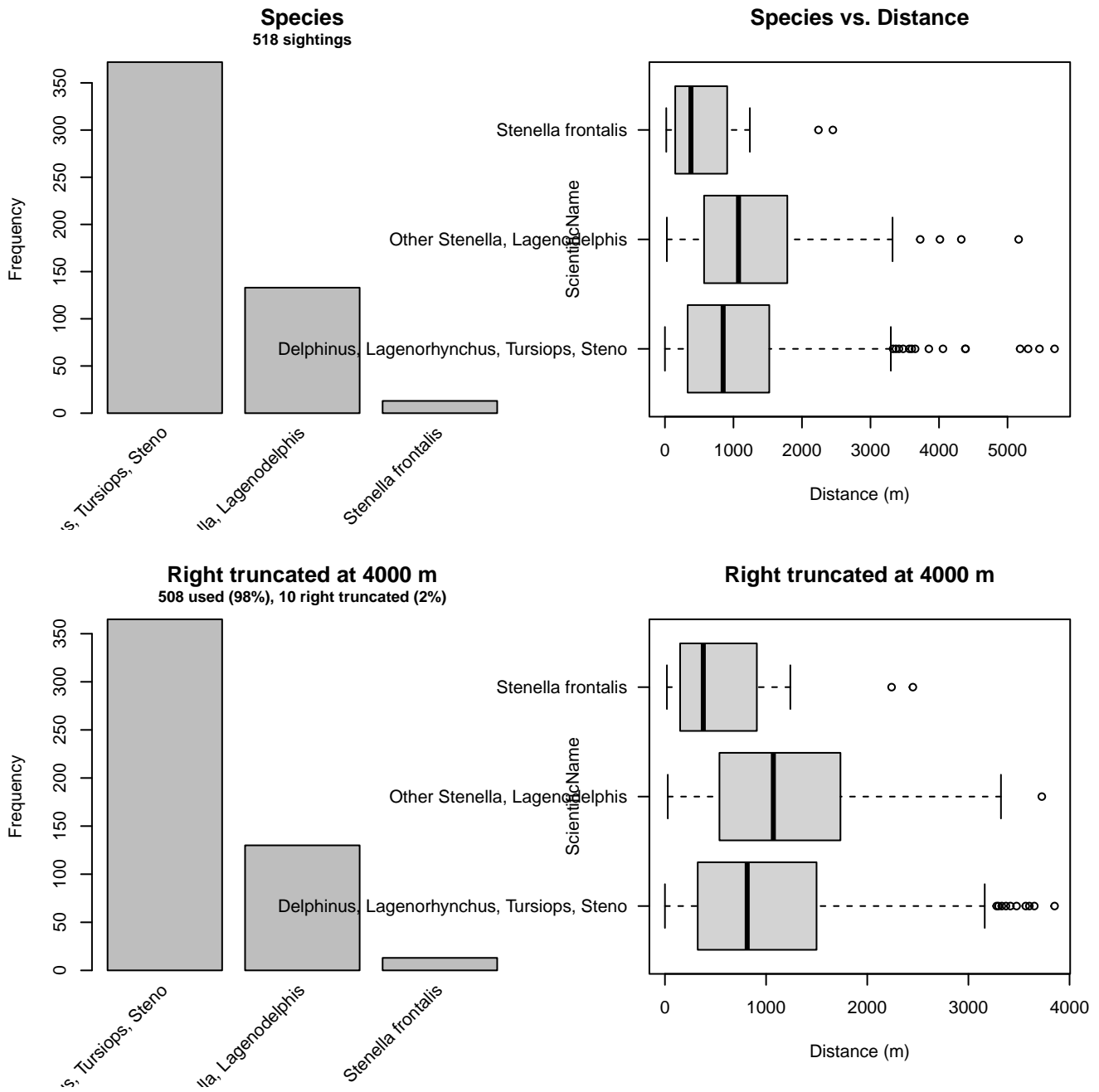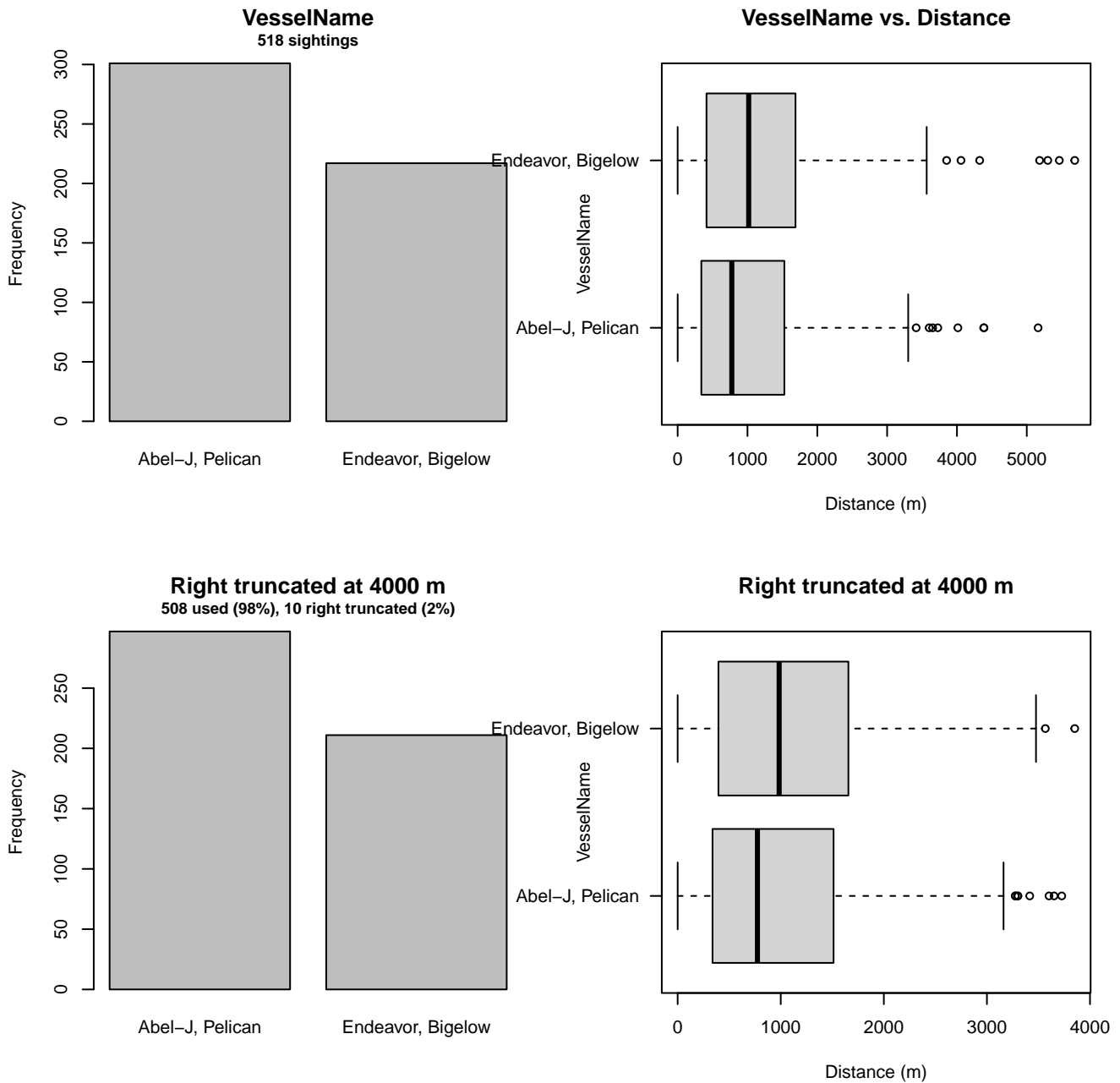
Figure 17: Distribution of the ScientificName covariate before (top row) and after (bottom row) observations were truncated to fit the NEFSC Pre-AMAPPS detection function.

Figure 18: Distribution of the VesselName covariate before (top row) and after (bottom row) observations were truncated to fit the NEFSC Pre-AMAPPS detection function.

3.1.2.2 NEFSC AMAPPS

After right-truncating observations greater than 6000 m, we fitted the detection function to the 857 observations that remained (Table 9). The selected detection function (Figure 19) used a hazard rate key function with Beaufort (Figure 20) and ScientificName (Figure 21) as covariates.

Table 9: Observations used to fit the NEFSC AMAPPS detection function.

ScientificName	n
Delphinus, Lagenorhynchus	358
Other Stenella, Lagenodelphis	175
Stenella frontalis	53
Tursiops, Steno	271
Total	**857**
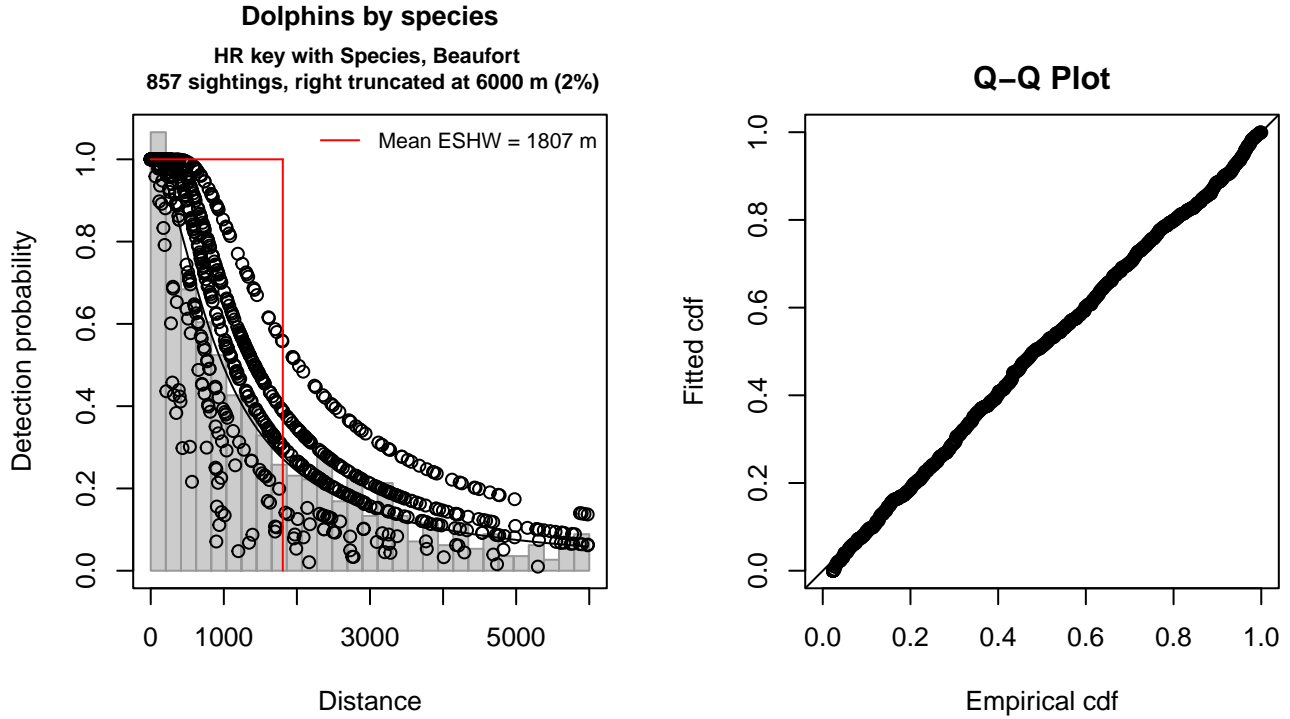
Figure 19: NEFSC AMAPPS detection function and Q-Q plot showing its goodness of fit.

Statistical output for this detection function:

```
Summary for ds object
Number of observations :   857
Distance range         :   0  -  6000
AIC                    :   14222.66

Detection function:
 Hazard-rate key function

Detection function parameters
Scale coefficient(s):
                                             estimate          se
(Intercept)                                 7.0022801  0.1342692
ScientificNameOther Stenella, Lagenodelphis  0.3515378  0.1854896
ScientificNameStenella frontalis           -0.5910499  0.3033455
ScientificNameTursiops, Steno              -0.2176361  0.1602756
Beaufort3-4                                -0.5842019  0.1839783
Beaufort4-5                                -1.4374209  0.2667762

Shape coefficient(s):
          estimate          se
```

```
(Intercept) 0.356339 0.0663051


                         Estimate           SE          CV
Average p               0.2624967   0.01868208  0.07117073
N in covered region 3264.8026106 252.27662296  0.07727163


Distance sampling Cramer-von Mises test (unweighted)
Test statistic = 0.089267  p = 0.640081
```
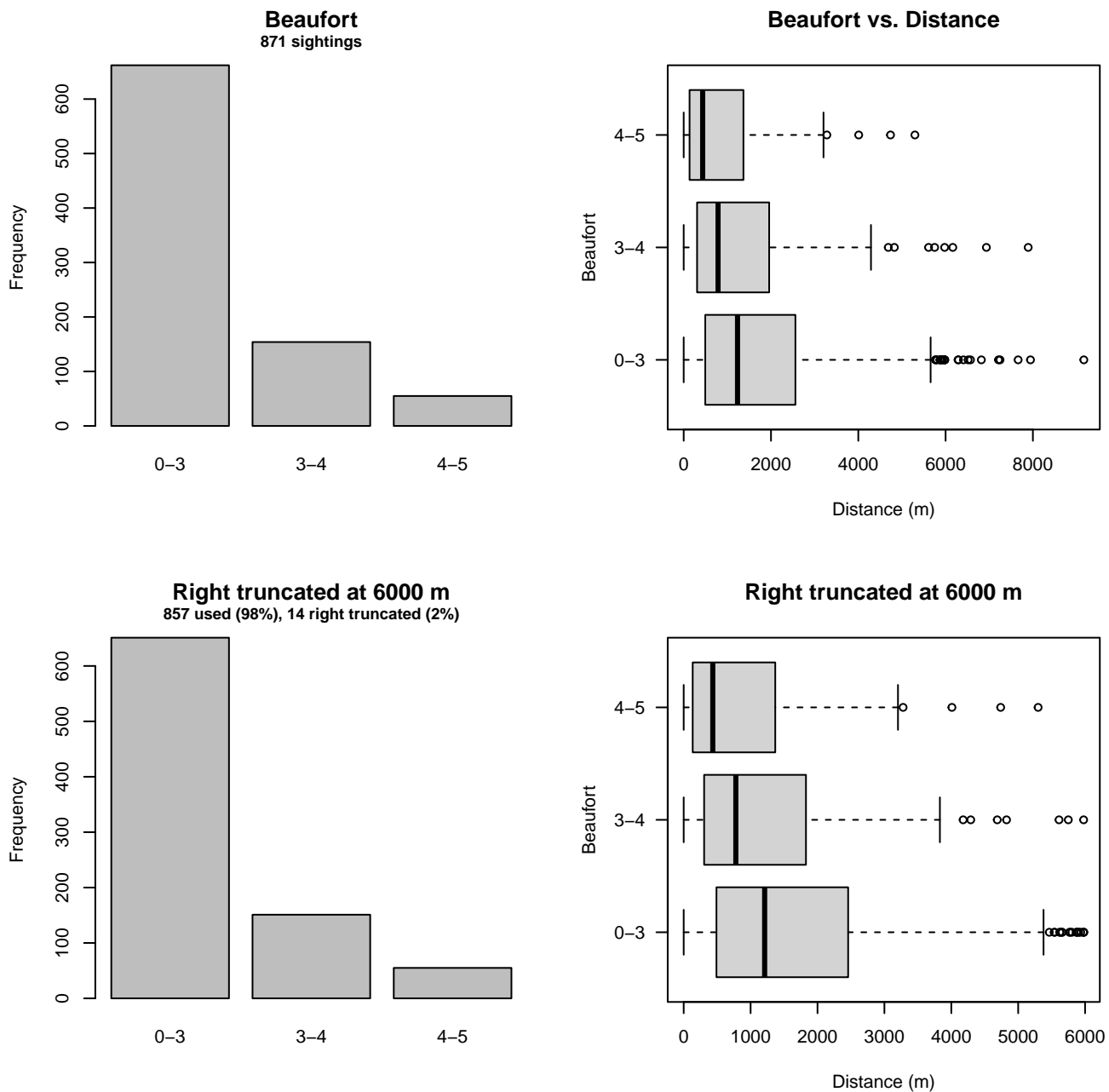

Figure 20: Distribution of the Beaufort covariate before (top row) and after (bottom row) observations were truncated to fit the NEFSC AMAPPS detection function.
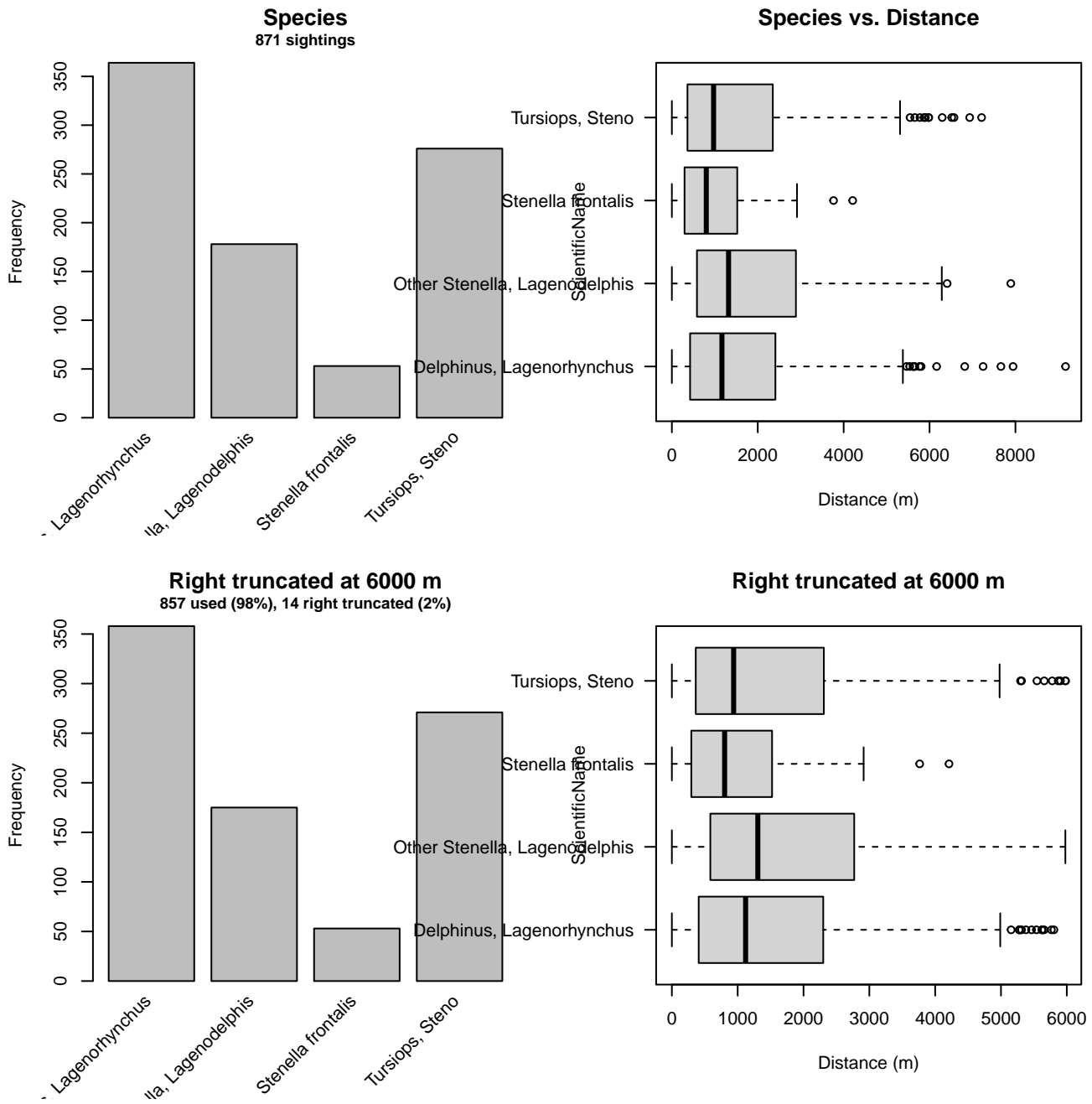
Figure 21: Distribution of the ScientificName covariate before (top row) and after (bottom row) observations were truncated to fit the NEFSC AMAPPS detection function.

3.1.2.3 Song of the Whale

After right-truncating observations greater than 700 m and left-truncating observations less than 1 m (Figure 23), we fitted the detection function to the 360 observations that remained (Table 10). The selected detection function (Figure 22) used a hazard rate key function with Beaufort (Figure 24), ScientificName (Figure 25) and Visibility (Figure 26) as covariates.

Table 10: Observations used to fit the Song of the Whale detection function.

ScientificName	n
All others	211
Delphinus	149
Total	**360**

28

Dolphins by species

HR key with Species, Beaufort, Visibility
360 sightings, left trunc. 1 m (10%), right trunc. 700 m (8%)
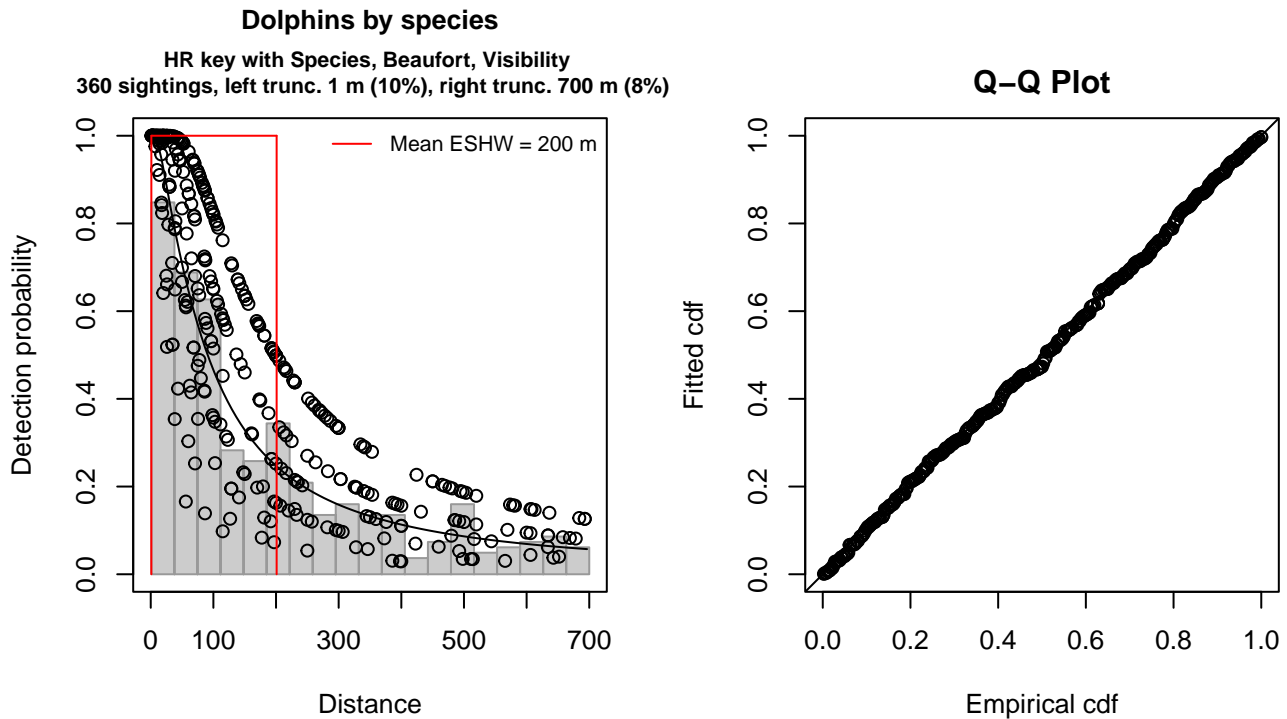
Q–Q Plot

Figure 22: Song of the Whale detection function and Q-Q plot showing its goodness of fit.

Statistical output for this detection function:

```
Summary for ds object
Number of observations :  360
Distance range         :  1  -  700
AIC                    :  4434.06

Detection function:
 Hazard-rate key function

Detection function parameters
Scale coefficient(s):
                              estimate         se
(Intercept)                  5.0168382 0.2118228
ScientificNameDelphinus     -0.3746003 0.2526245
Beaufort3                   -0.6586604 0.2922112
Beaufort3.5-4               -1.3223280 0.3841776
VisibilityModerate (2-5nmi) -0.9687696 0.4363084

Shape coefficient(s):
            estimate         se
(Intercept) 0.2728327 0.09542948


                   Estimate          SE         CV
Average p          0.232512   0.02944422 0.1266352
N in covered region 1548.306965 209.54903632 0.1353408

Distance sampling Cramer-von Mises test (unweighted)
Test statistic = 0.019198  p = 0.997687
```

Left trucated sightings (in red)
360 used (83%), 42 left trunc. (10%), 33 right trunc. (8%)
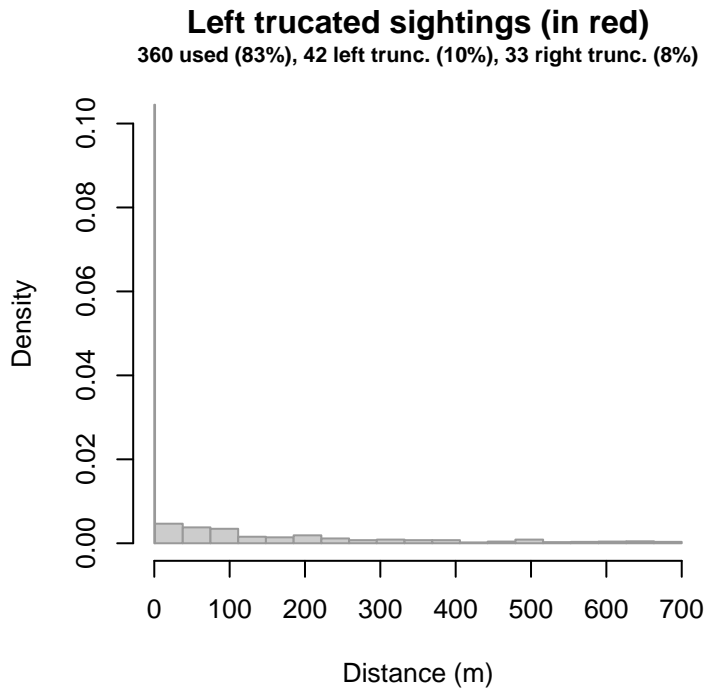
Figure 23: Density histogram of observations used to fit the Song of the Whale detection function, with the left-most bar showing observations at distances less than 1 m, which were left-truncated and not used to fit the detection function. (This bar may be very short if there were very few left-truncated sightings, or very narrow if the left truncation distance was very small; in either case it may not appear red.) These were excluded because they formed a problematic "spike" in detections close to the trackline, suggesting that animals approached the vessel (e.g. to bow-ride) prior to being detected. To address this, we fitted the detection function to the observations beyond the spike and assumed that within it, detection probability was 1, effectively treating it like a strip transect. We then added the left-truncated observations back into the analysis as if they occurred in this strip. This treatment may have resulted in an underestimation of detection probability.
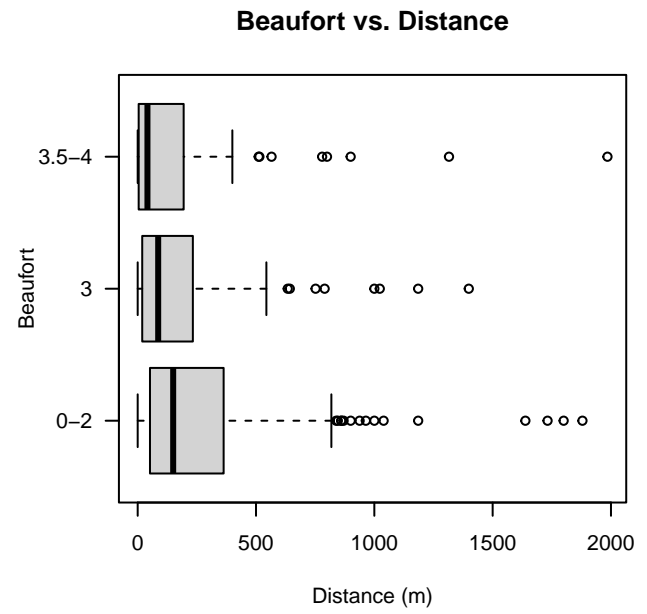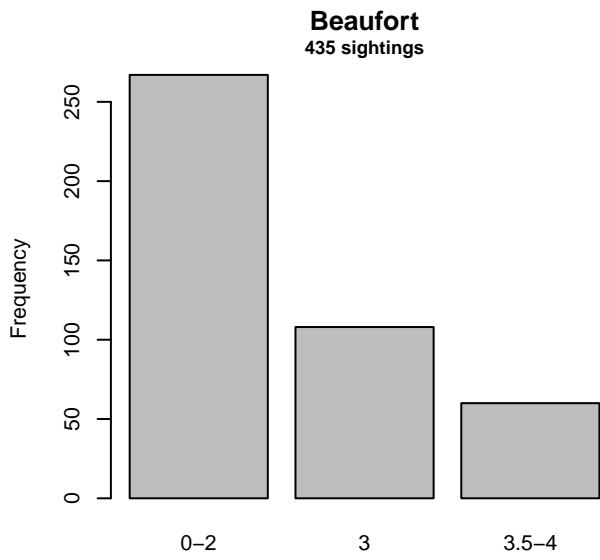
Figure 24: Distribution of the Beaufort covariate before (top row) and after (bottom row) observations were truncated to fit the Song of the Whale detection function.
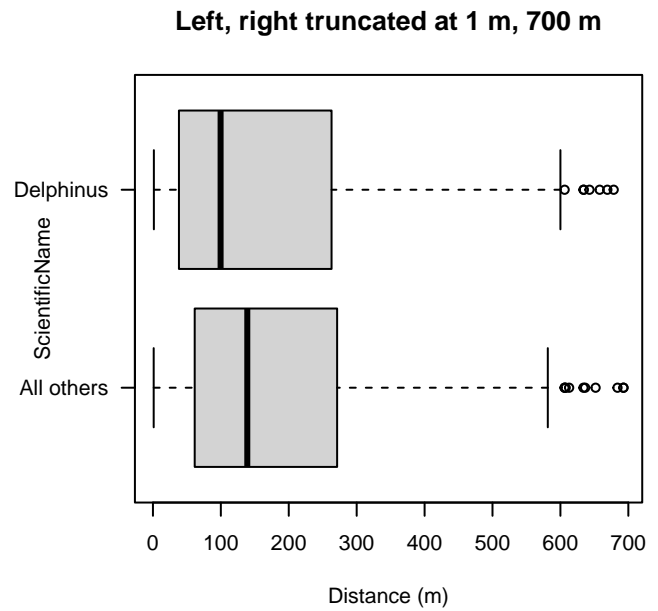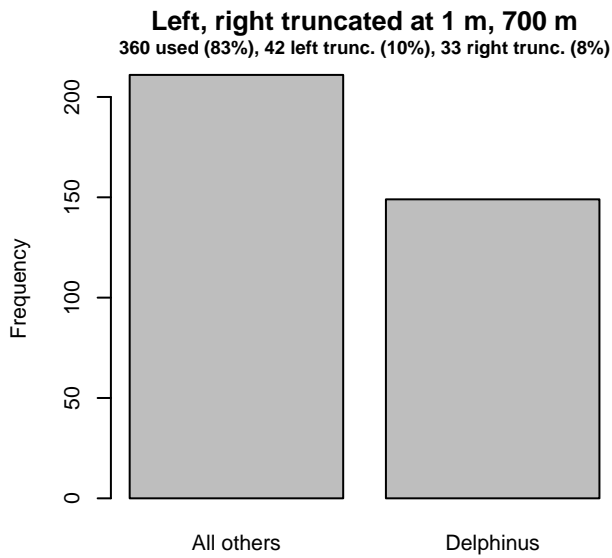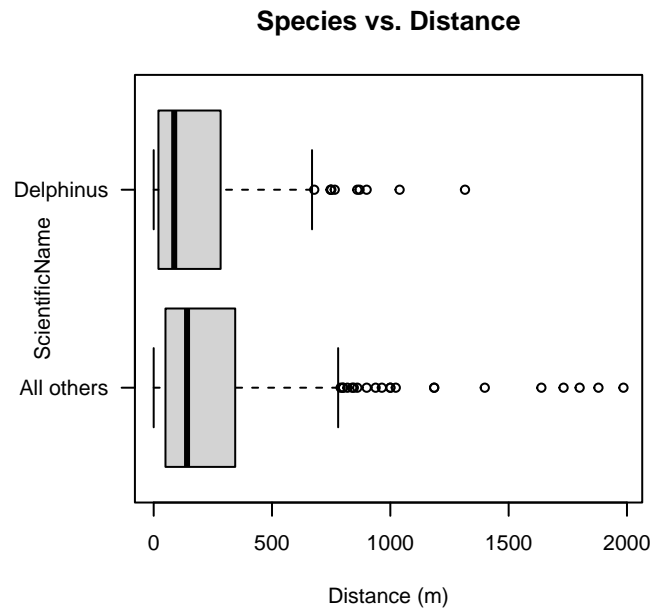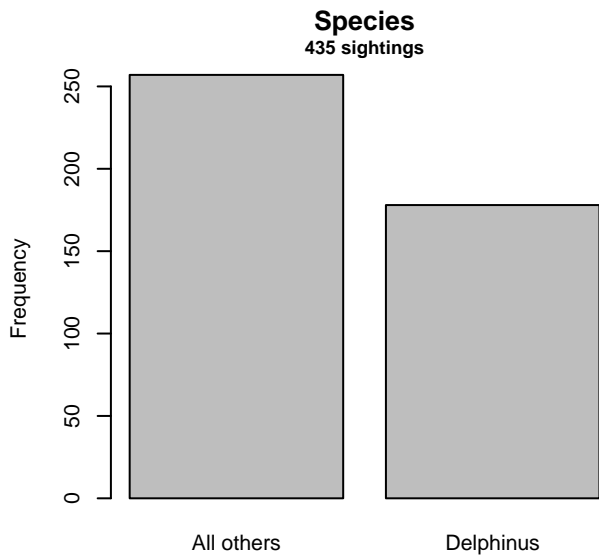
Figure 25: Distribution of the ScientificName covariate before (top row) and after (bottom row) observations were truncated to fit the Song of the Whale detection function.
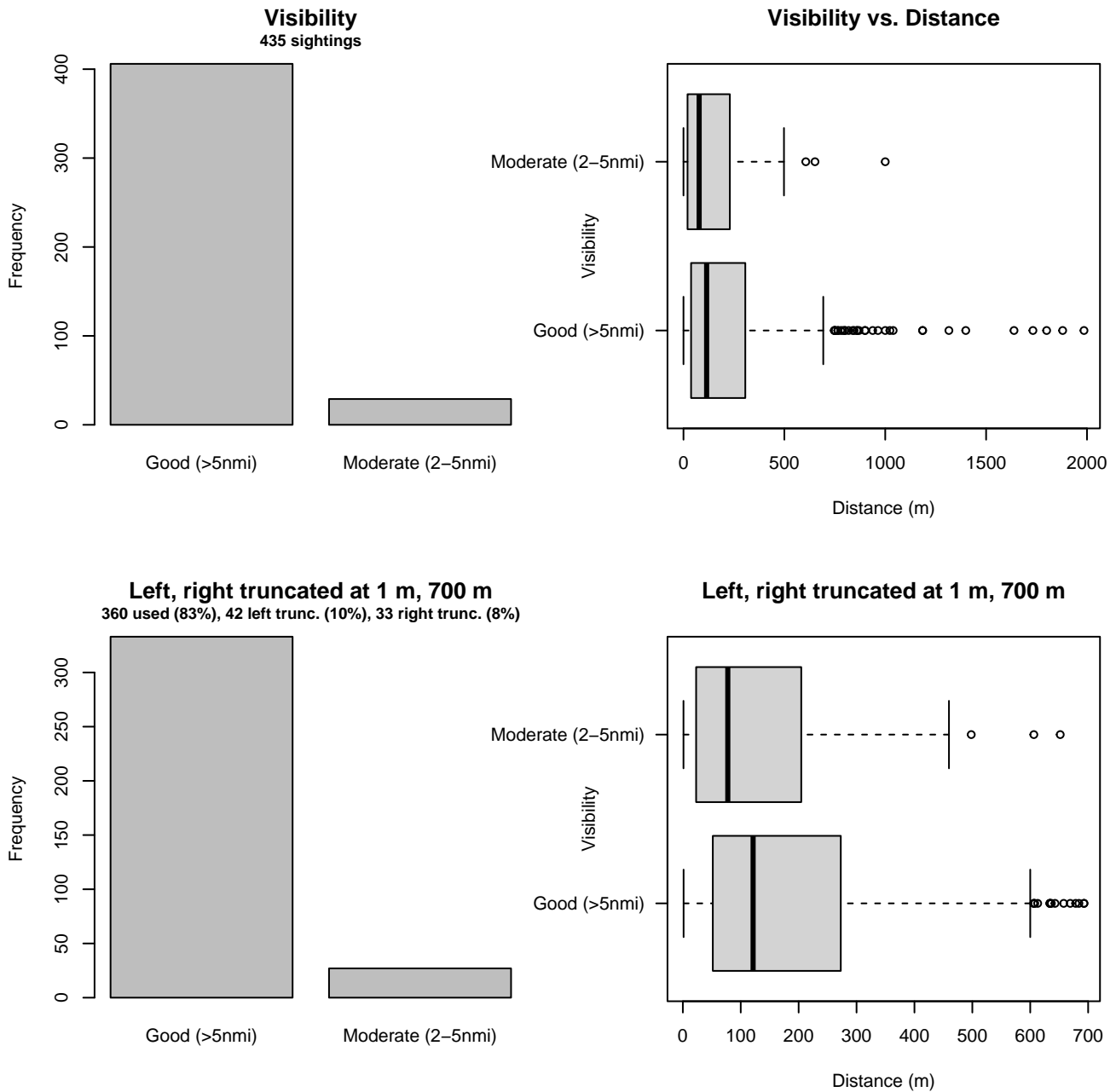
Figure 26: Distribution of the Visibility covariate before (top row) and after (bottom row) observations were truncated to fit the Song of the Whale detection function.

3.2 Without a Taxonomic Covariate

We fitted the detection functions in this section to pools of species with similar detectability characteristics but could not use a taxonomic identification as a covariate to account for differences between them. We usually took this approach after trying the taxonomic covariate and finding it had insufficient statistical power to be retained. We also resorted to it when the focal taxon being modeled had too few observations to be allocated its own taxonomic covariate level and was too poorly known for us to confidently determine which other taxa we could group it with.
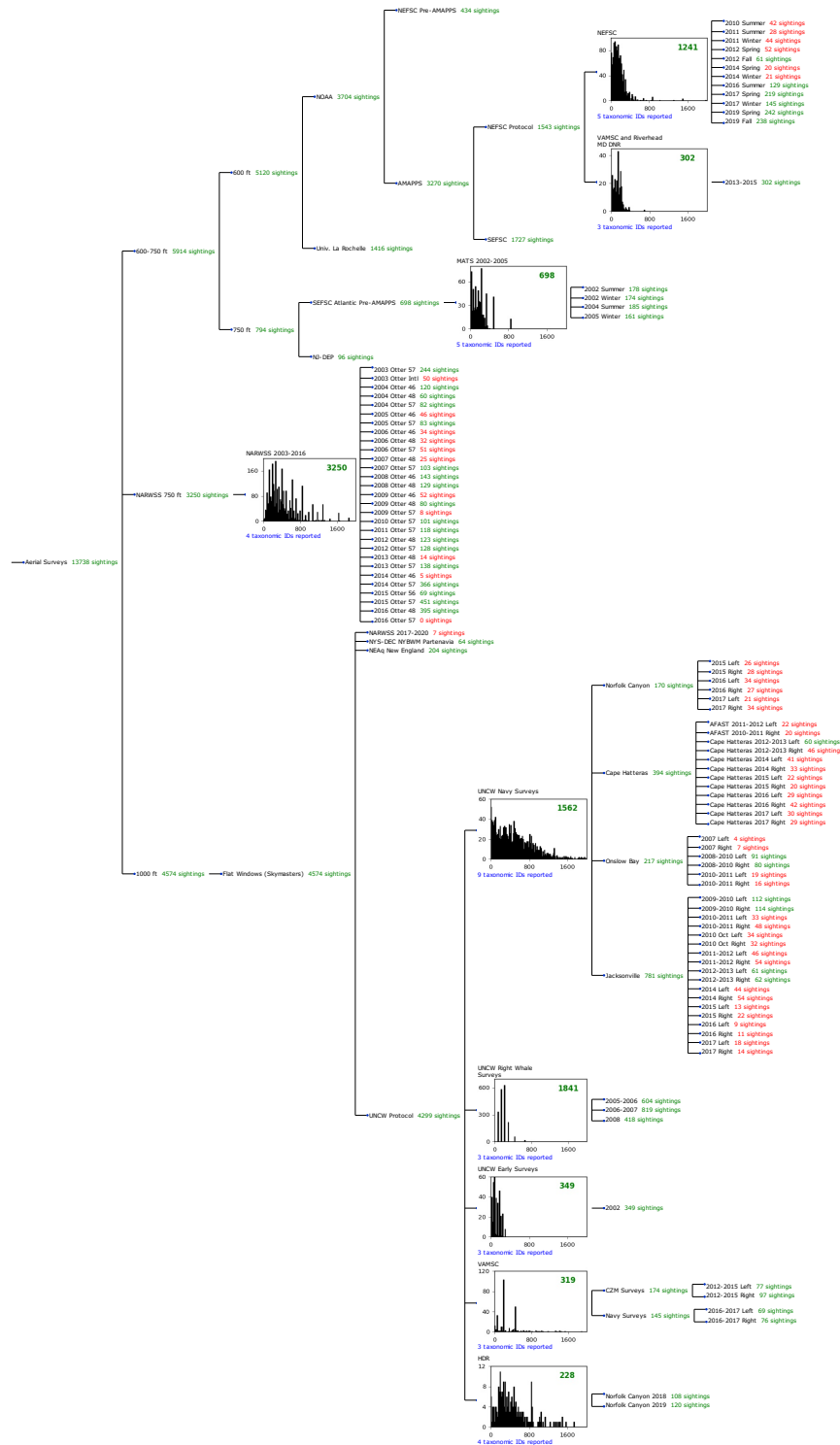
3.2.1 Aerial Surveys

Figure 27: Detection hierarchy for aerial surveys, showing how they were pooled during detectability modeling, for detection functions that pooled multiple taxa but could not use a taxonomic covariate to account for differences between them. Each histogram represents a detection function and summarizes the perpendicular distances of observations that were pooled to fit it, prior to truncation. Observation counts, also prior to truncation, are shown in green when they met the recommendation of Buckland et al. (2001) that detection functions utilize at least 60 sightings, and red otherwise. For rare taxa, it was not always possible to meet this recommendation, yielding higher statistical uncertainty. During the spatial modeling stage of the analysis, effective strip widths were computed for each survey using the closest detection function above it in the hierarchy (i.e. moving from right to left in the figure). Surveys that do not have a detection function above them in this figure were either addressed by a detection function presented in a different section of this report, or were omitted from the analysis.

34

3.2.1.1 NEFSC AMAPPS

After right-truncating observations greater than 600 m, we fitted the detection function to the 1218 observations that remained (Table 11). The selected detection function (Figure 28) used a hazard rate key function with Season (Figure 29) as a covariate.

Table 11: Observations used to fit the NEFSC AMAPPS detection function.

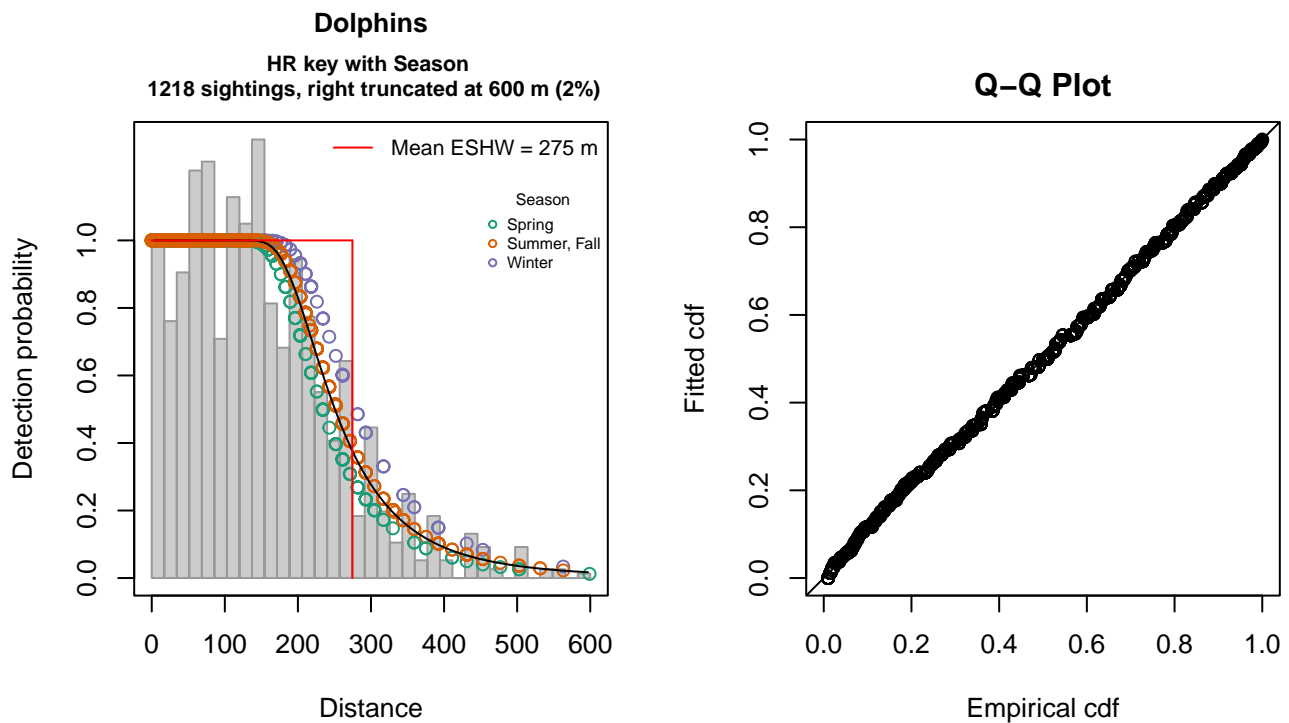| ScientificName	n
Delphinus delphis	817
Lagenorhynchus acutus	280
Lagenorhynchus albirostris	3
Stenella coeruleoalba	13
Tursiops truncatus	105
Total	**1218**

Figure 28: NEFSC AMAPPS detection function and Q-Q plot showing its goodness of fit.

Statistical output for this detection function:

```
Summary for ds object
Number of observations :  1218
Distance range         :  0  -  600
AIC                    :  14460.69

Detection function:
 Hazard-rate key function

Detection function parameters
Scale coefficient(s):
                   estimate          se
(Intercept)        5.36944749 0.04422696
SeasonSummer, Fall 0.08083579 0.04638562
SeasonWinter       0.17600218 0.07702020
```

```
Shape coefficient(s):
            estimate        se
(Intercept) 1.452854 0.065484


                      Estimate         SE         CV
Average p             0.456561   0.00970389 0.02125431
N in covered region 2667.770370 79.97999993 0.02998009


Distance sampling Cramer-von Mises test (unweighted)
Test statistic = 0.126854   p = 0.468488
```
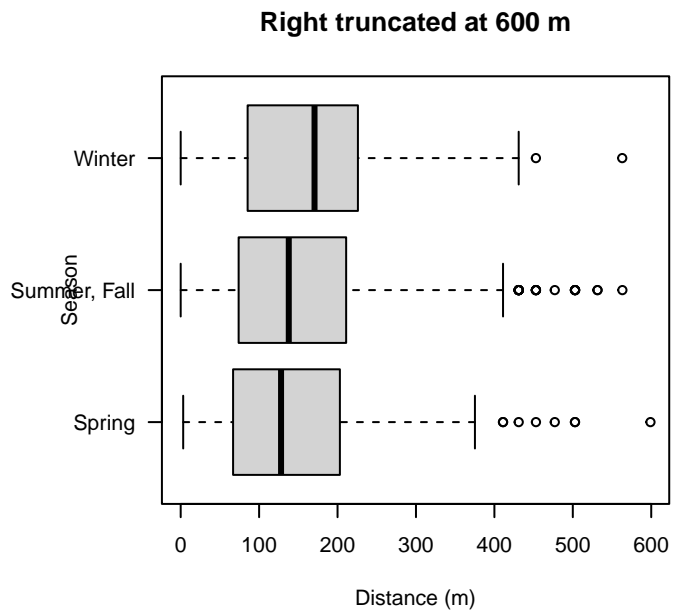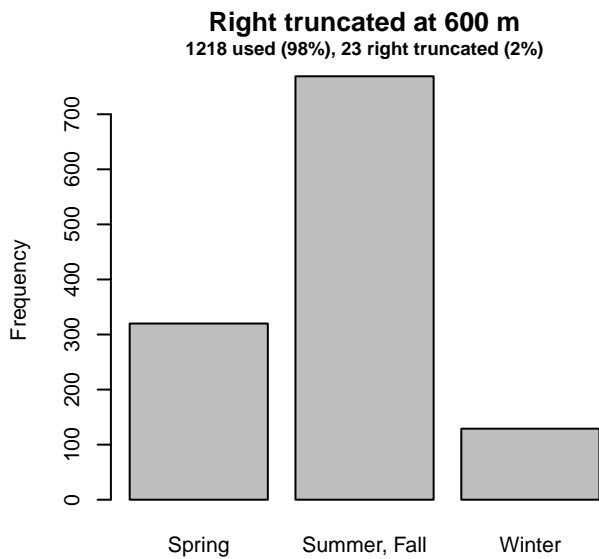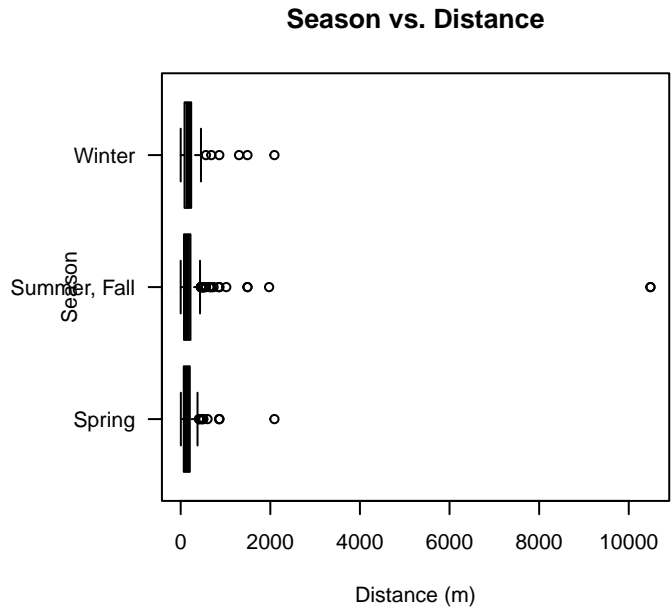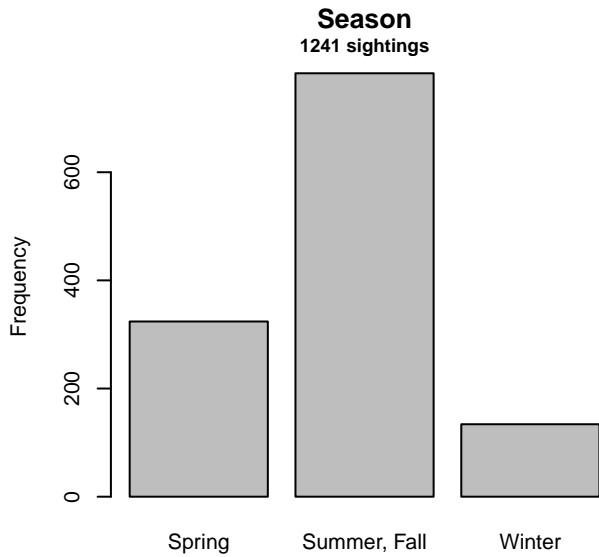

Figure 29: Distribution of the Season covariate before (top row) and after (bottom row) observations were truncated to fit the NEFSC AMAPPS detection function.

3.2.1.2 VAMSC and Riverhead MD DNR

After right-truncating observations greater than 400 m, we fitted the detection function to the 301 observations that remained (Table 12). The selected detection function (Figure 30) used a hazard rate key function with no covariates.

Table 12: Observations used to fit the VAMSC and Riverhead MD DNR detection function.

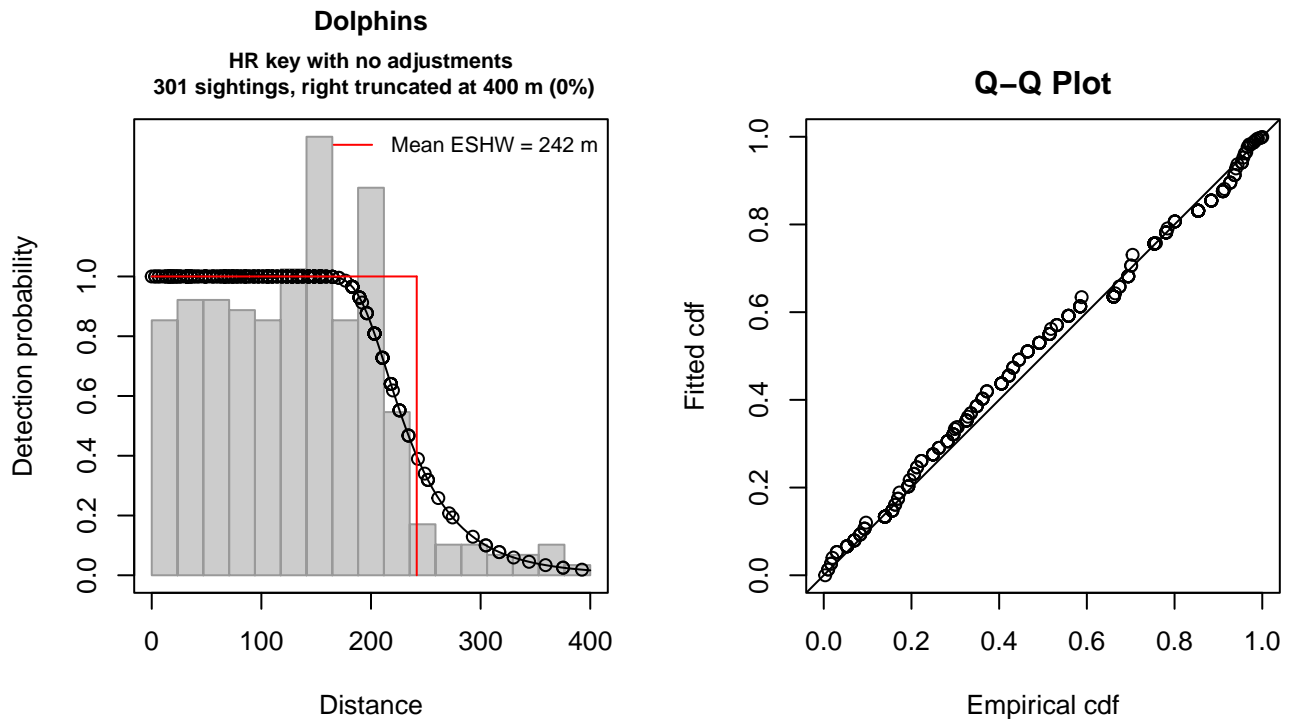| ScientificName	n
Delphinus delphis	22
Stenella frontalis	1
Tursiops truncatus	278
Total	**301**

Figure 30: VAMSC and Riverhead MD DNR detection function and Q-Q plot showing its goodness of fit.

Statistical output for this detection function:

```
Summary for ds object
Number of observations :  301
Distance range         :  0  -  400
AIC                    :  3426.124

Detection function:
 Hazard-rate key function

Detection function parameters
Scale coefficient(s):
           estimate         se
(Intercept) 5.388208 0.04209556

Shape coefficient(s):
           estimate         se
(Intercept)  1.91525 0.1331166
```

```
                       Estimate         SE          CV
Average p               0.6042969  0.0203517 0.03367831
N in covered region 498.0995265 24.6489147 0.04948592


Distance sampling Cramer-von Mises test (unweighted)
Test statistic = 0.302011  p = 0.133421
```

3.2.1.3 MATS 2002-2005

After right-truncating observations greater than 629 m, we fitted the detection function to the 684 observations that remained (Table 13). The selected detection function (Figure 31) used a hazard rate key function with Beaufort (Figure 32) as a covariate.

Table 13: Observations used to fit the MATS 2002-2005 detection function.

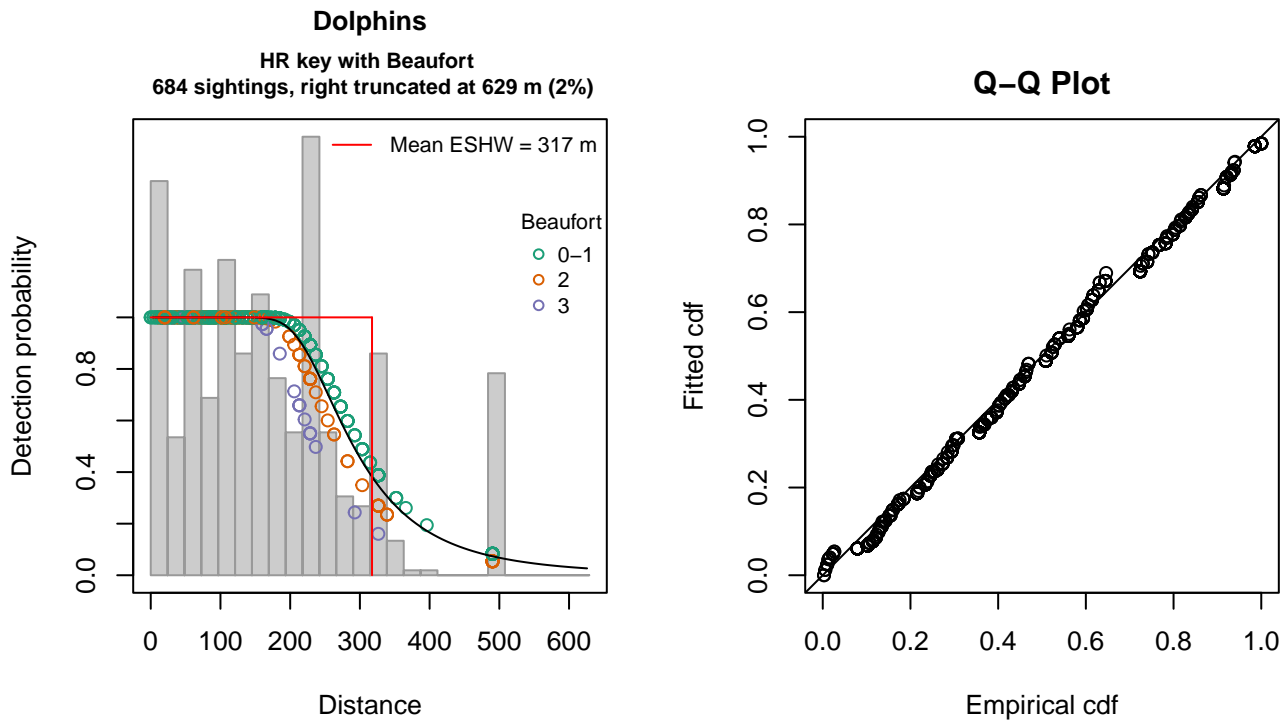| ScientificName	n
Delphinus delphis	2
Stenella attenuata	2
Stenella frontalis	104
Tursiops truncatus	576
Total	**684**

Figure 31: MATS 2002-2005 detection function and Q-Q plot showing its goodness of fit.

Statistical output for this detection function:

```
Summary for ds object
Number of observations :  684
Distance range         :  0  -  629
AIC                    :  8306.088

Detection function:
```

```
 Hazard-rate key function

Detection function parameters
Scale coefficient(s):
            estimate          se
(Intercept)  5.6213531 0.04325709
Beaufort2   -0.1046854 0.06814971
Beaufort3   -0.2421057 0.13060115


Shape coefficient(s):
           estimate         se
(Intercept) 1.449025 0.08965229


                      Estimate        SE        CV
Average p            0.5026836  0.0147185 0.02927984
N in covered region 1360.6968013 54.2106880 0.03984039


Distance sampling Cramer-von Mises test (unweighted)
Test statistic = 0.194502  p = 0.278380
```
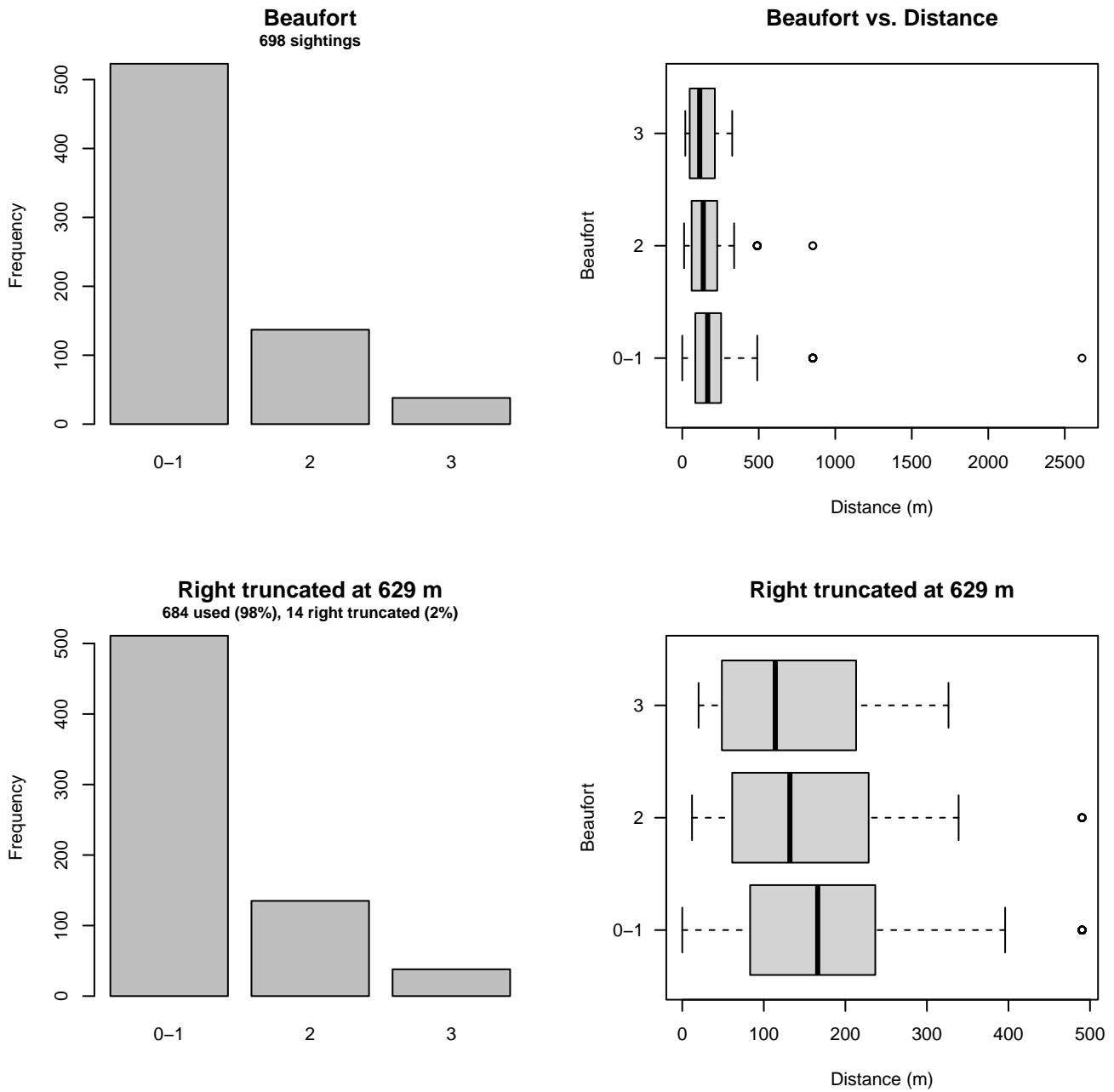
Figure 32: Distribution of the Beaufort covariate before (top row) and after (bottom row) observations were truncated to fit the MATS 2002-2005 detection function.

3.2.1.4 NARWSS 2003-2016

After right-truncating observations greater than 1367 m and left-truncating observations less than 61 m (Figure 34), we fitted the detection function to the 3073 observations that remained (Table 14). The selected detection function (Figure 33) used a hazard rate key function with Beaufort (Figure 35) and Season (Figure 36) as covariates.

Table 14: Observations used to fit the NARWSS 2003-2016 detection function.

ScientificName	n
Delphinus delphis	607
Lagenorhynchus acutus	2404
Lagenorhynchus albirostris	6
Tursiops truncatus	56
Total	**3073**

Dolphins

HR key with Season, Beaufort
3073 sightings, left trunc. 61 m (2%), right trunc. 1367 m (4%
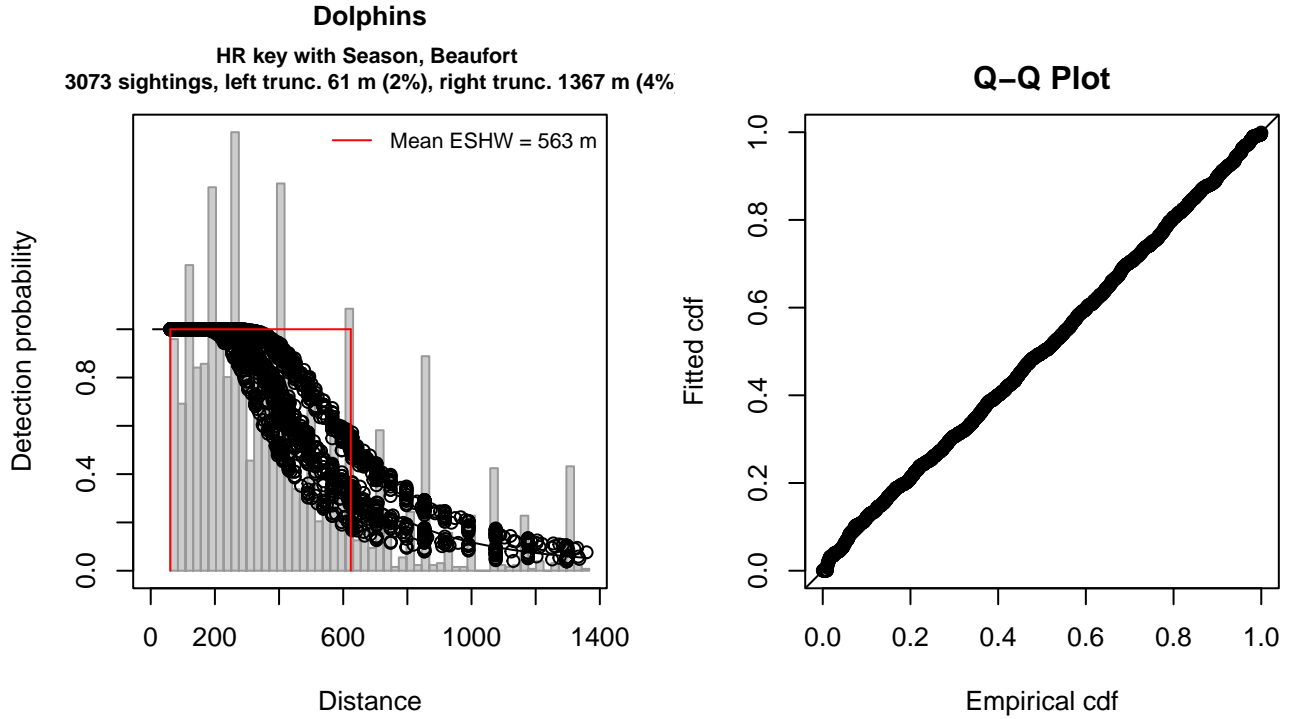
Q–Q Plot

Figure 33: NARWSS 2003-2016 detection function and Q-Q plot showing its goodness of fit.

Statistical output for this detection function:

```
Summary for ds object
Number of observations :  3073
Distance range         :  61  -  1367
AIC                    :  41850.8

Detection function:
 Hazard-rate key function

Detection function parameters
Scale coefficient(s):
               estimate          se
(Intercept)   6.10469263 0.07579397
SeasonSpring  0.06689438 0.05622050
SeasonSummer  0.29278056 0.05383279
SeasonWinter -0.15259970 0.06804643
Beaufort     -0.03572691 0.02383833

Shape coefficient(s):
           estimate         se
(Intercept) 1.009361 0.0398862
```

```
                      Estimate          SE          CV
Average p             0.4196247 8.827249e-03 0.02103606
N in covered region 7323.2113220 1.845410e+02 0.02519946


Distance sampling Cramer-von Mises test (unweighted)
Test statistic = 0.246036  p = 0.193531
```

Left trucated sightings (in red)

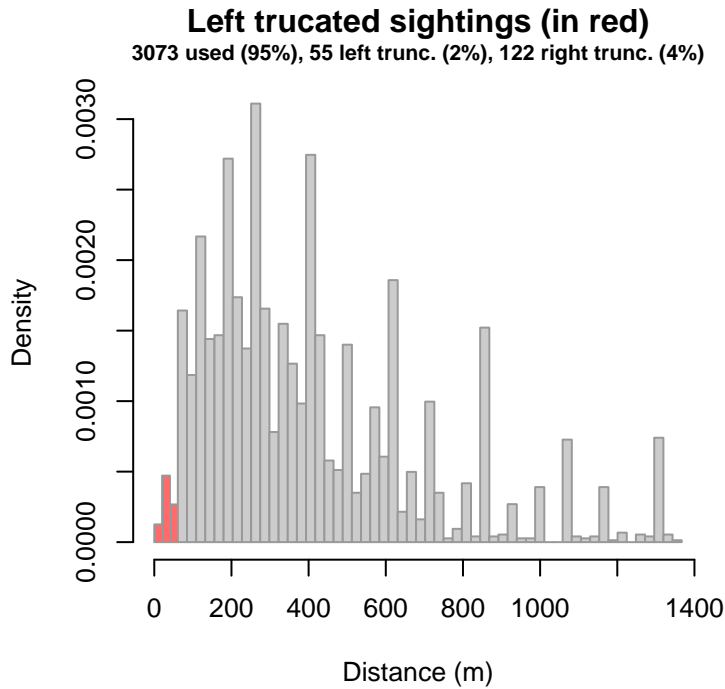**3073 used (95%), 55 left trunc. (2%), 122 right trunc. (4%)**

Figure 34: Density histogram of observations used to fit the NARWSS 2003-2016 detection function, with the left-most bar showing observations at distances less than 61 m, which were left-truncated and excluded from the analysis [Buckland et al. (2001)]. (This bar may be very short if there were very few left-truncated sightings, or very narrow if the left truncation distance was very small; in either case it may not appear red.)
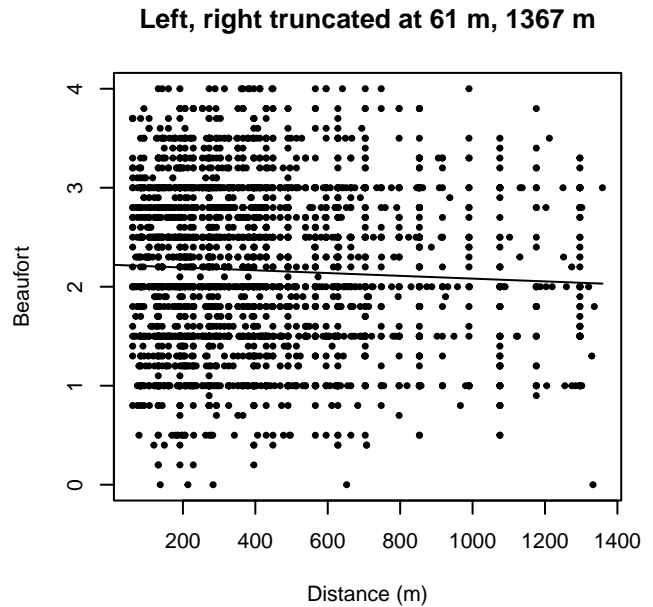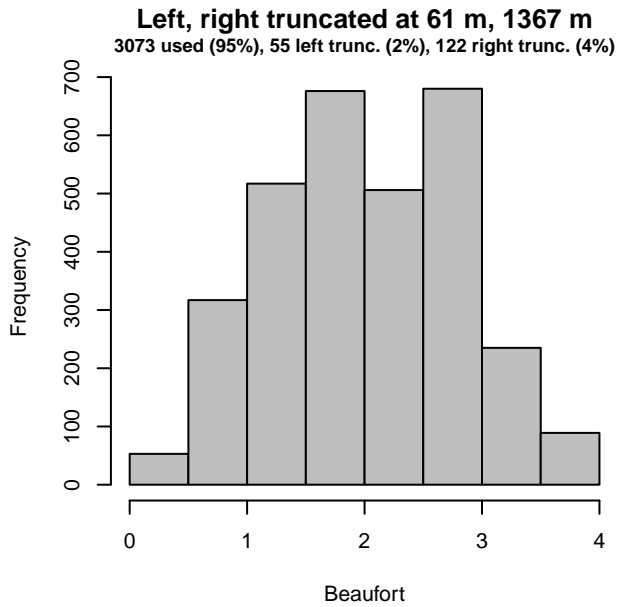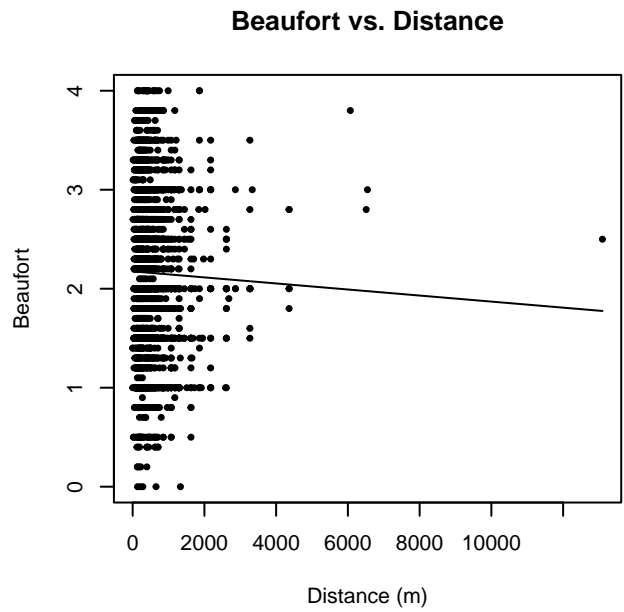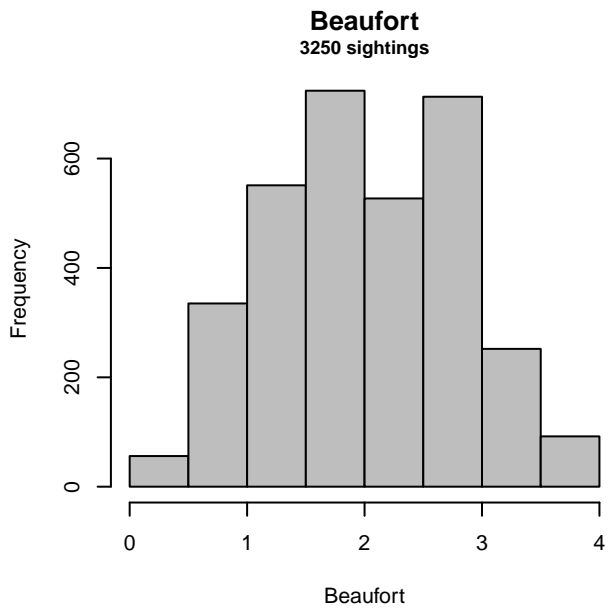
Figure 35: Distribution of the Beaufort covariate before (top row) and after (bottom row) observations were truncated to fit the NARWSS 2003-2016 detection function.

Figure 36: Distribution of the Season covariate before (top row) and after (bottom row) observations were truncated to fit the NARWSS 2003-2016 detection function.

3.2.1.5 UNCW Navy Surveys

After right-truncating observations greater than 1600 m, we fitted the detection function to the 1523 observations that remained (Table 15). The selected detection function (Figure 37) used a half normal key function with Glare (Figure 38) and Visibility (Figure 39) as covariates.

Table 15: Observations used to fit the UNCW Navy Surveys detection function.

ScientificName	n
Delphinus delphis	77
Lagenodelphis hosei	1
Stenella attenuata	2
Stenella clymene	11
Stenella coeruleoalba	19
Stenella frontalis	480
Stenella longirostris	1
Steno bredanensis	14
Tursiops truncatus	918
Total	**1523**
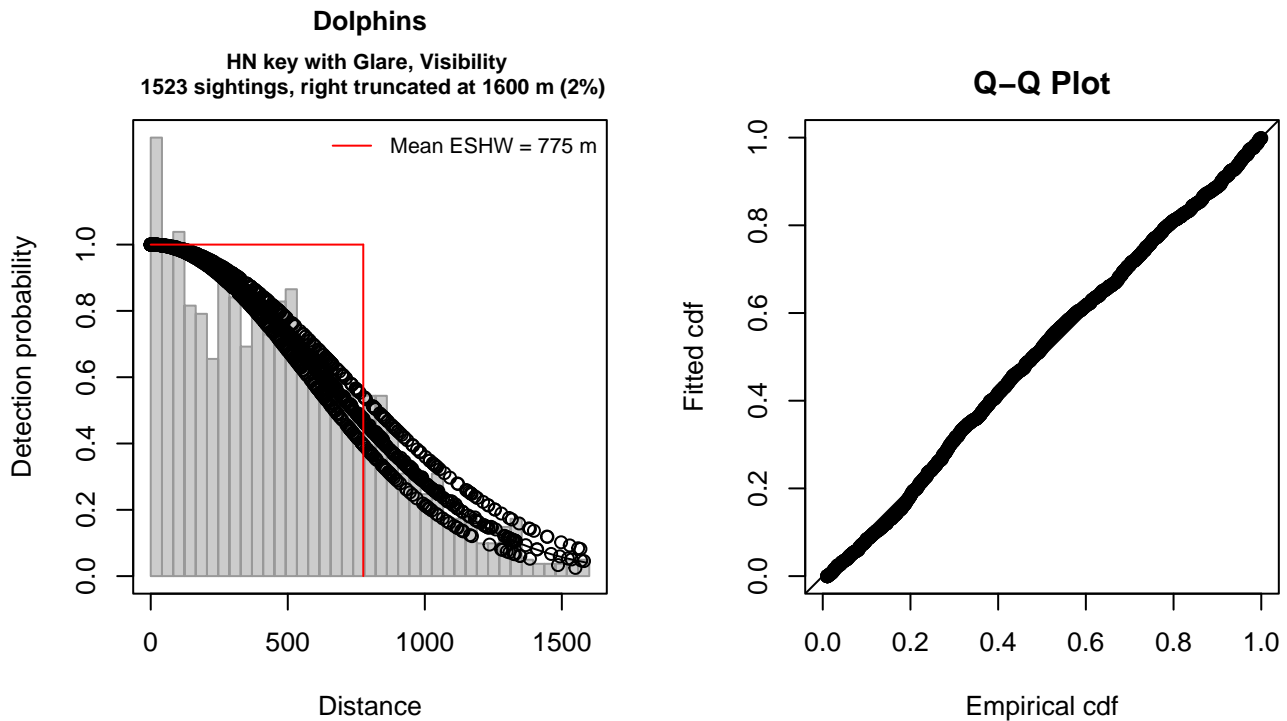
Figure 37: UNCW Navy Surveys detection function and Q-Q plot showing its goodness of fit.

Statistical output for this detection function:

```
Summary for ds object
Number of observations :  1523
Distance range         :  0  -  1600
AIC                    :  21665.78

Detection function:
 Half-normal key function

Detection function parameters
Scale coefficient(s):
                          estimate          se
(Intercept)             6.55223233 0.04798577
GlareNone, 0-25%, Unk. -0.10934970 0.05247015
VisibilityHalf         -0.09759271 0.04601702
```

```
                       Estimate         SE         CV
Average p             0.4827398   0.01003395 0.02078542
N in covered region 3154.9084328 87.71221948 0.02780183


Distance sampling Cramer-von Mises test (unweighted)
Test statistic = 0.331909  p = 0.110182
```
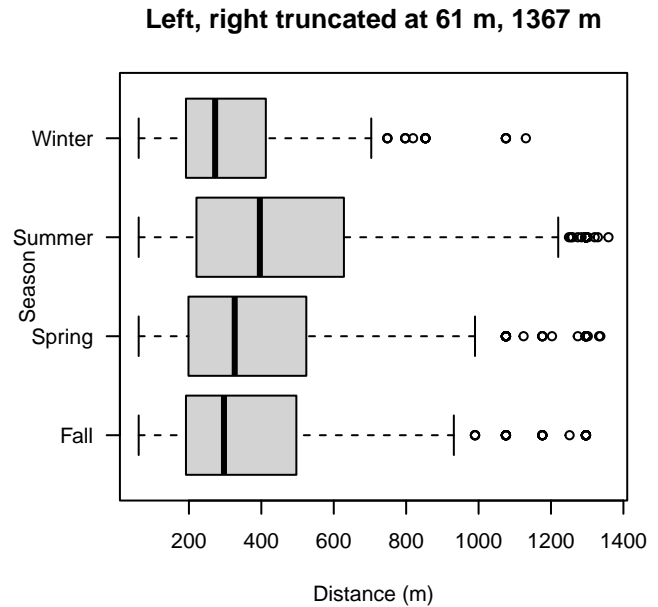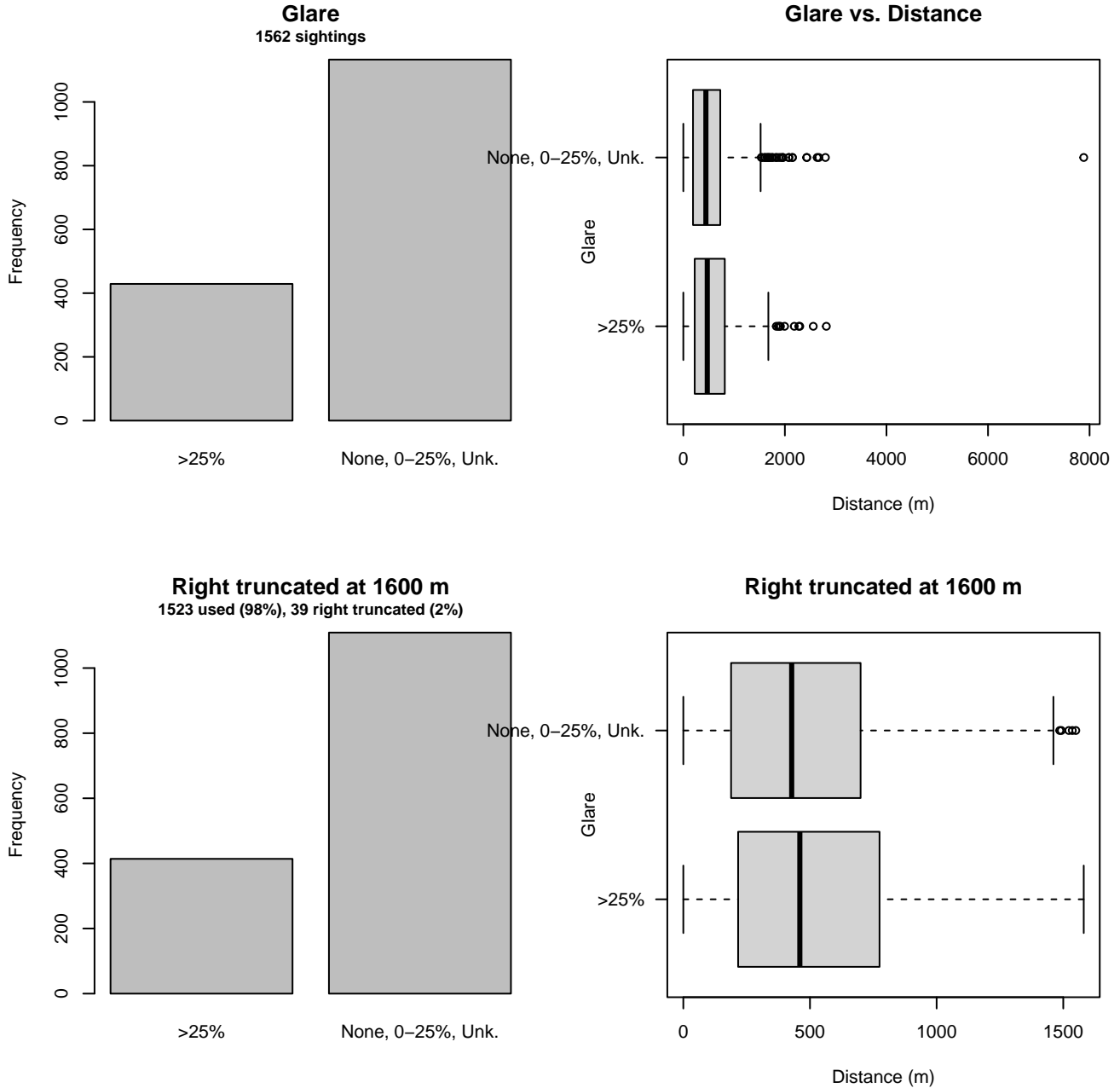

Figure 38: Distribution of the Glare covariate before (top row) and after (bottom row) observations were truncated to fit the UNCW Navy Surveys detection function.
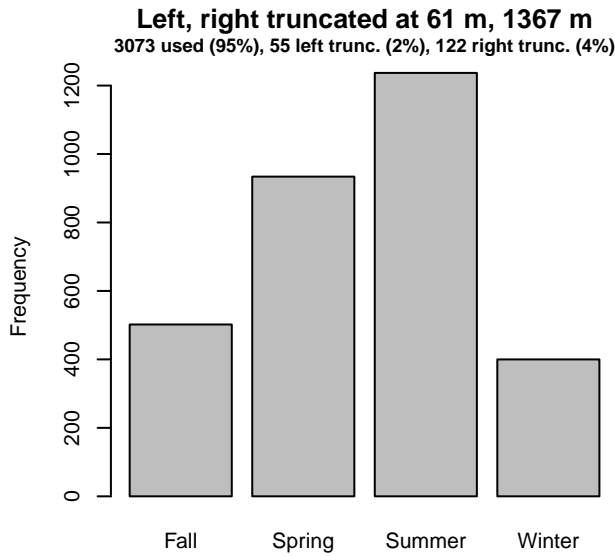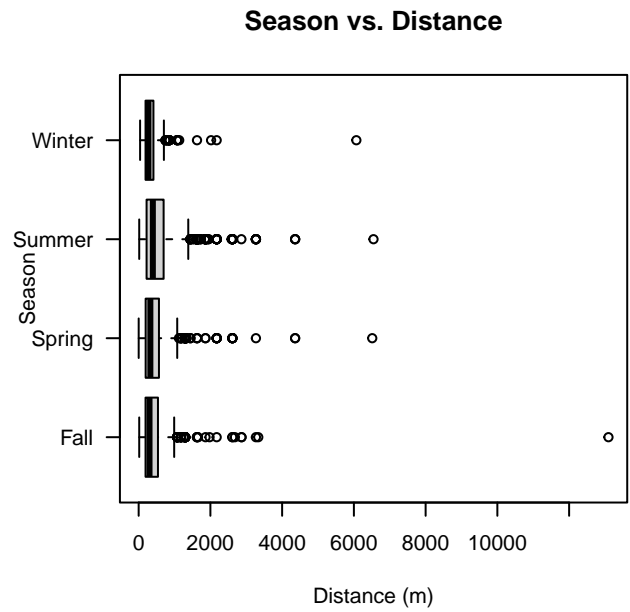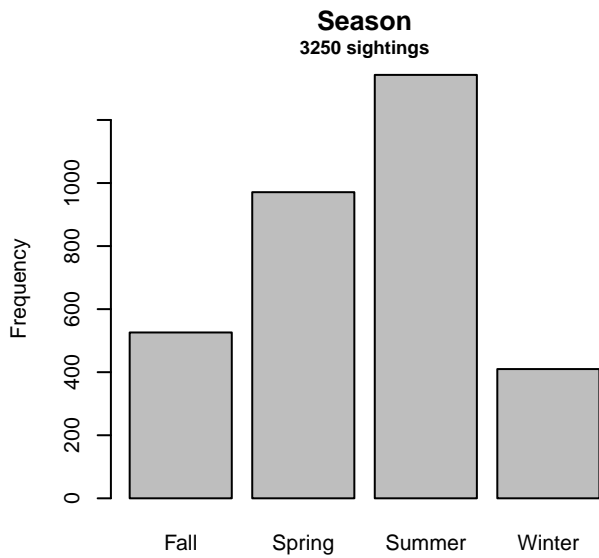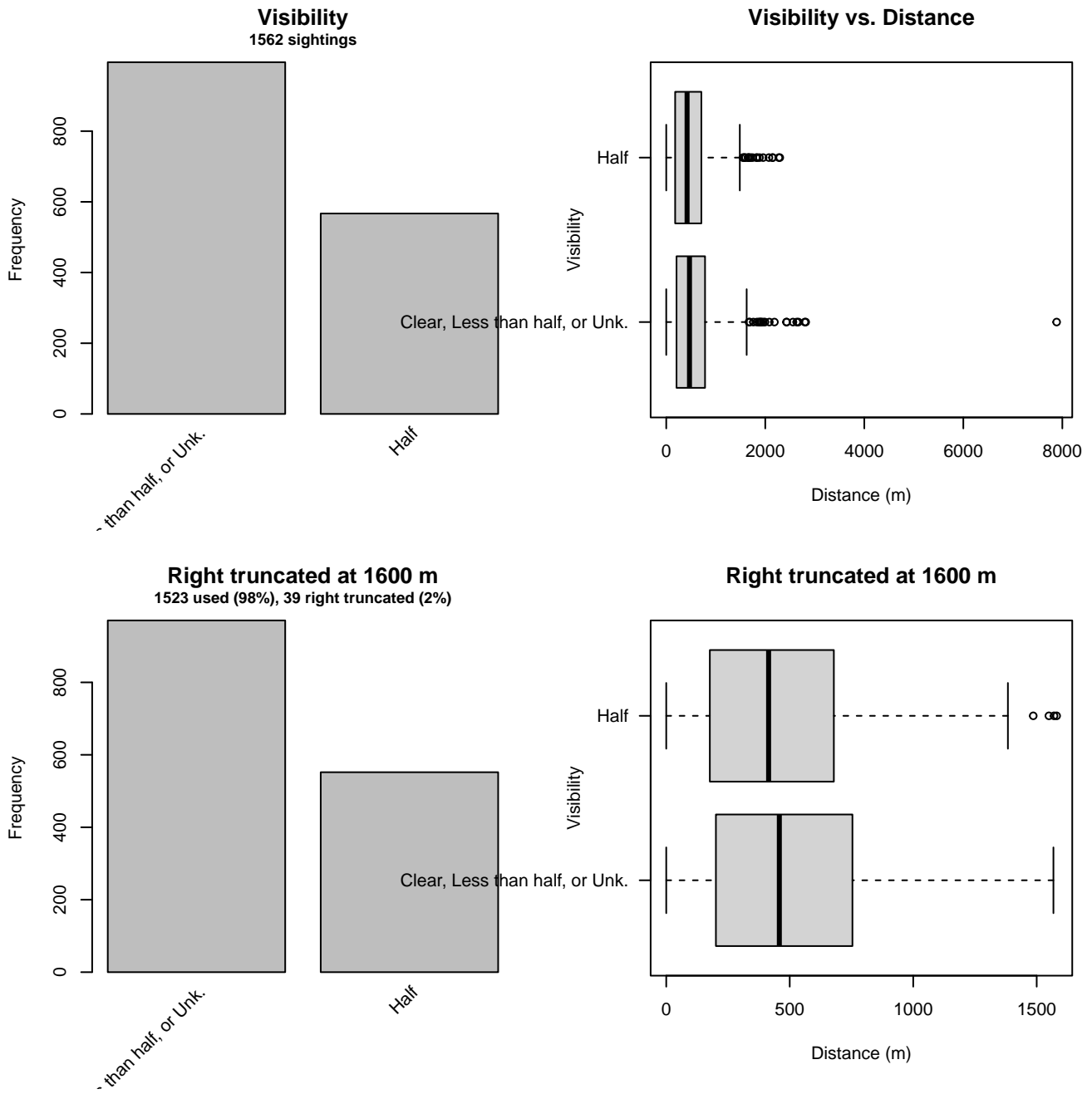
Figure 39: Distribution of the Visibility covariate before (top row) and after (bottom row) observations were truncated to fit the UNCW Navy Surveys detection function.

3.2.1.6 UNCW Right Whale Surveys

After right-truncating observations greater than 528 m and left-truncating observations less than 54 m (Figure 41), we fitted the detection function to the 1821 observations that remained (Table 16). The selected detection function (Figure 40) used a hazard rate key function with no covariates.

Table 16: Observations used to fit the UNCW Right Whale Surveys detection function.

| ScientificName	n
Delphinus delphis	26
Stenella frontalis	4
Tursiops truncatus	1791
Total	**1821**
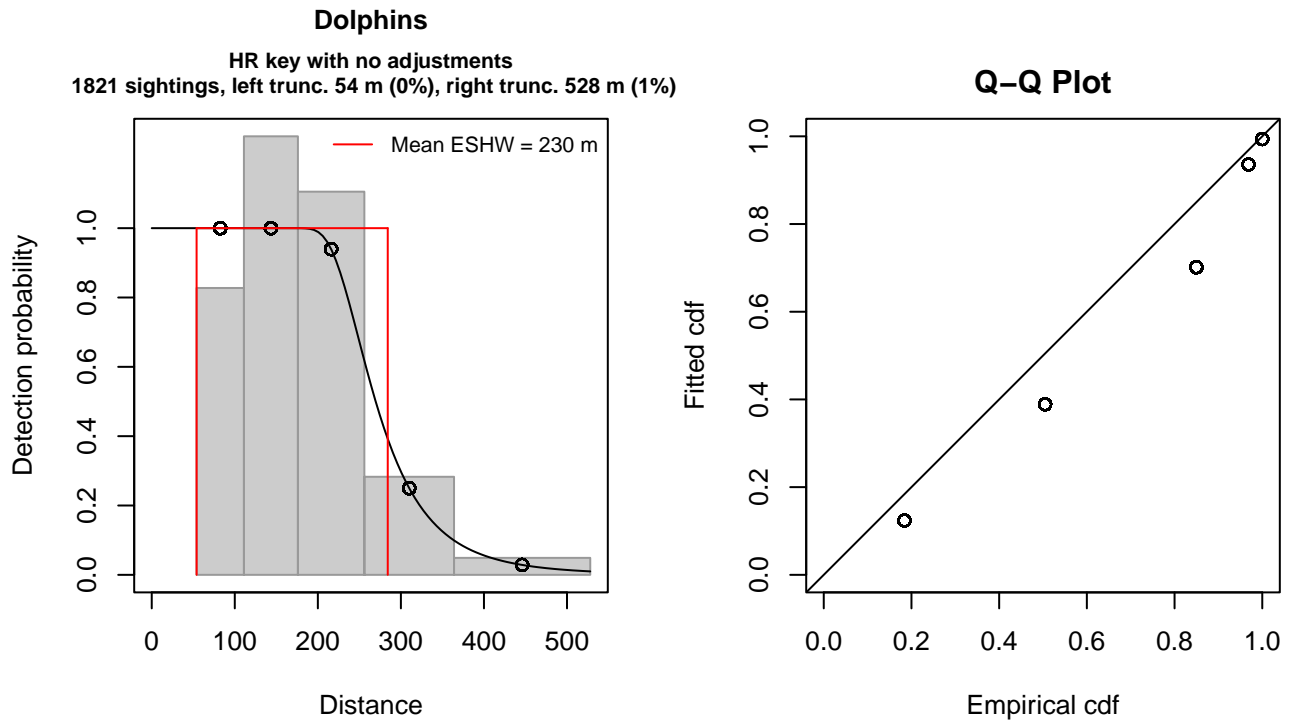
Figure 40: UNCW Right Whale Surveys detection function and Q-Q plot showing its goodness of fit.

Statistical output for this detection function:

```
Summary for ds object
Number of observations :  1821
Distance range         :  54  -  528
AIC                    :  5176.116

Detection function:
 Hazard-rate key function

Detection function parameters
Scale coefficient(s):
            estimate          se
(Intercept) 5.538954 0.02098751

Shape coefficient(s):
            estimate          se
(Intercept) 1.841299 0.06464608


                      Estimate          SE         CV
Average p            0.4855453  0.009233858 0.01901750
N in covered region 3750.4226341 95.188173832 0.02538065
```

```
Distance sampling Cramer-von Mises test (unweighted)
Test statistic = 14.468539  p = 0.010416
```


Left trucated sightings (in red)
1821 used (99%), 2 left trunc. (0%), 18 right trunc. (1%)
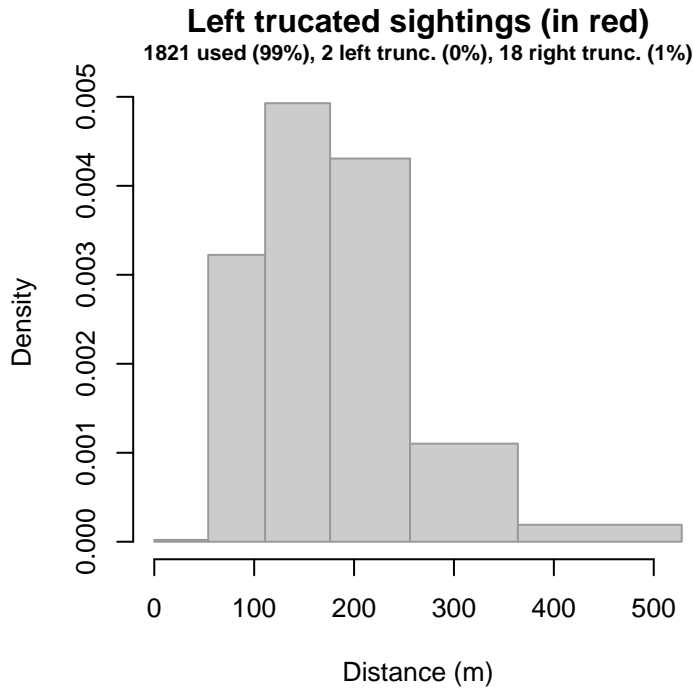
Figure 41: Density histogram of observations used to fit the UNCW Right Whale Surveys detection function, with the left-most bar showing observations at distances less than 54 m, which were left-truncated and excluded from the analysis [Buckland et al. (2001)]. (This bar may be very short if there were very few left-truncated sightings, or very narrow if the left truncation distance was very small; in either case it may not appear red.)

3.2.1.7 UNCW Early Surveys

After right-truncating observations greater than 333 m and left-truncating observations less than 14 m (Figure 43), we fitted the detection function to the 349 observations that remained (Table 17). The selected detection function (Figure 42) used a half normal key function with Beaufort (Figure 44) as a covariate.

Table 17: Observations used to fit the UNCW Early Surveys detection function.

| ScientificName	n
Delphinus delphis	5
Stenella frontalis	1
Tursiops truncatus	343
Total	**349**
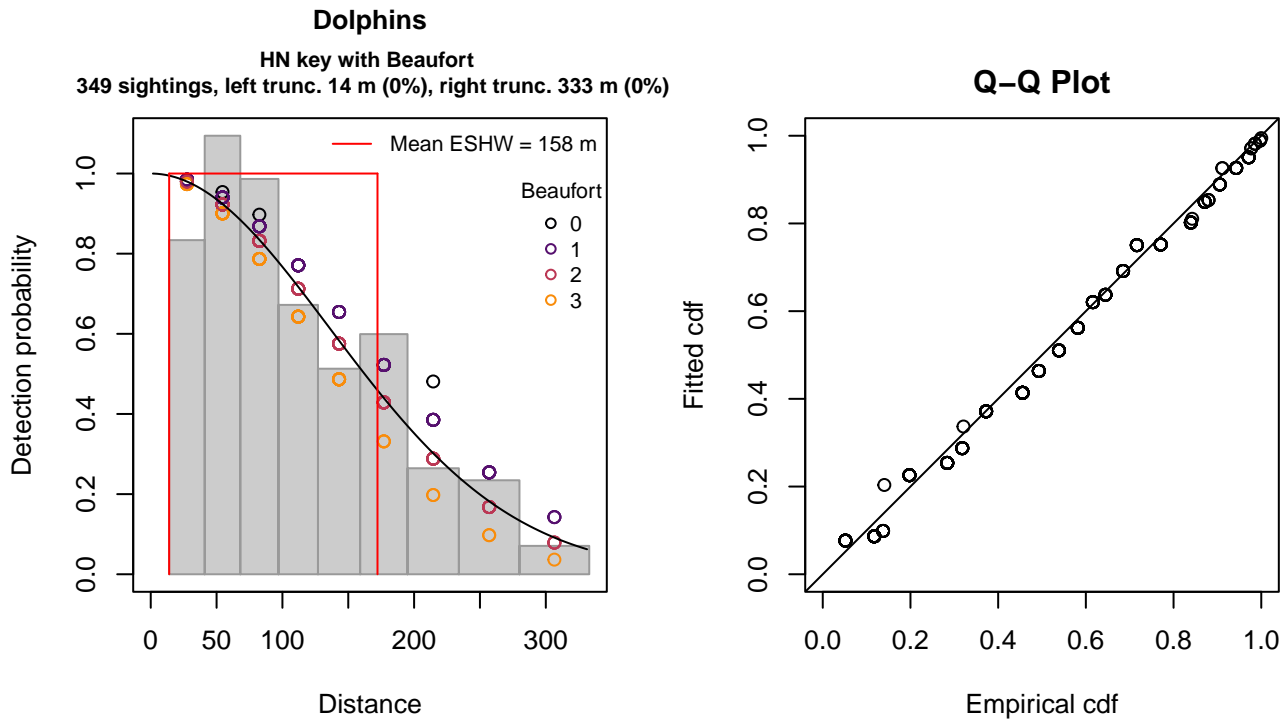
Figure 42: UNCW Early Surveys detection function and Q-Q plot showing its goodness of fit.

Statistical output for this detection function:

```
Summary for ds object
Number of observations :   349
Distance range         :   14  -  333
AIC                    :   1464.597

Detection function:
 Half-normal key function

Detection function parameters
Scale coefficient(s):
              estimate          se
(Intercept)  5.1778911 0.14575211
Beaufort    -0.1325498 0.07066838


                  Estimate          SE          CV
Average p         0.4915207   0.02352103 0.04785360
N in covered region 710.0413079 43.53534195 0.06131382

Distance sampling Cramer-von Mises test (unweighted)
Test statistic = 0.278162  p = 0.155953
```

Left trucated sightings (in red)

349 used (100%), 0 left trunc. (0%), 0 right trunc. (0%)

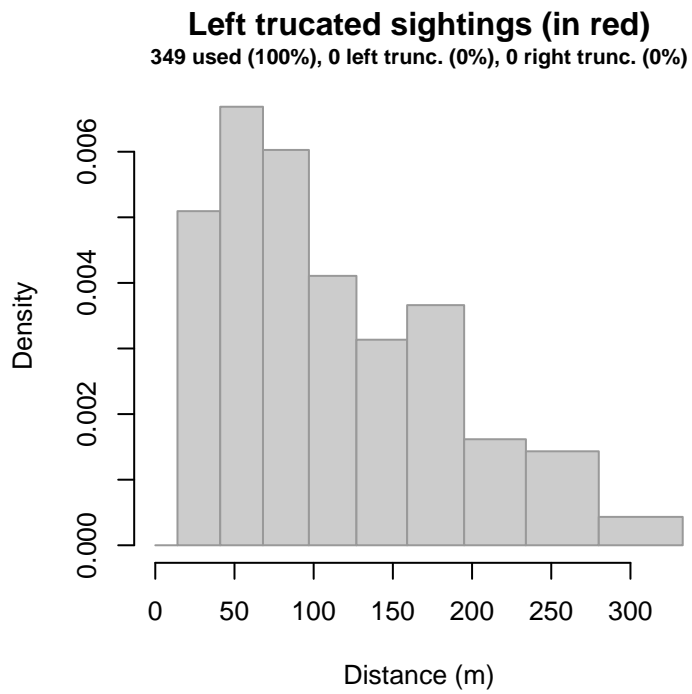Figure 43: Density histogram of observations used to fit the UNCW Early Surveys detection function, with the left-most bar showing observations at distances less than 14 m, which were left-truncated and excluded from the analysis [Buckland et al. (2001)]. (This bar may be very short if there were very few left-truncated sightings, or very narrow if the left truncation distance was very small; in either case it may not appear red.)
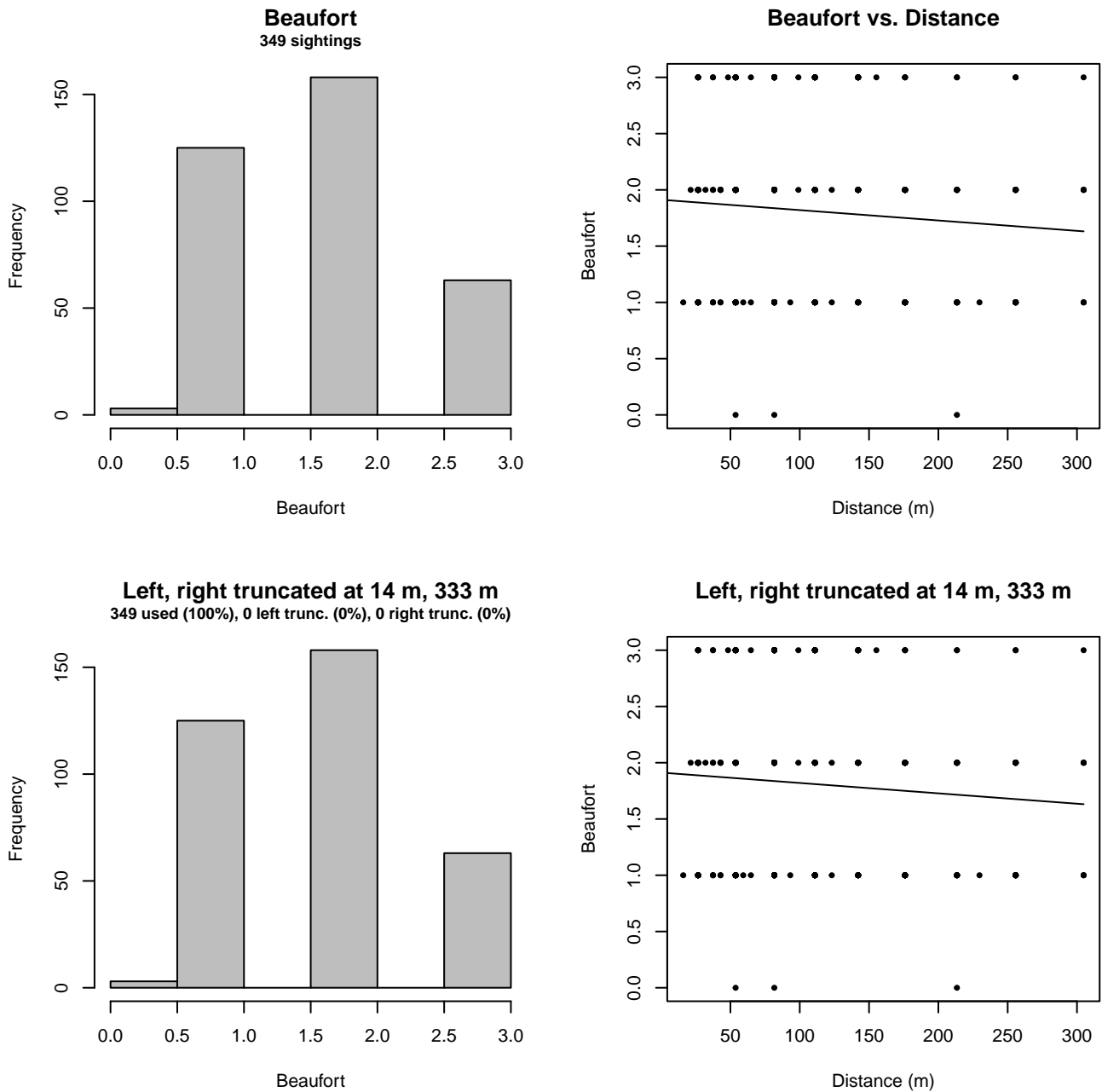
Figure 44: Distribution of the Beaufort covariate before (top row) and after (bottom row) observations were truncated to fit the UNCW Early Surveys detection function.

3.2.1.8   VAMSC

After right-truncating observations greater than 1000 m, we fitted the detection function to the 303 observations that remained (Table 18). The selected detection function (Figure 45) used a hazard rate key function with no covariates.

Table 18: Observations used to fit the VAMSC detection function.

ScientificName	n
Delphinus delphis	30
Stenella frontalis	4
Tursiops truncatus	269
Total	**303**

52
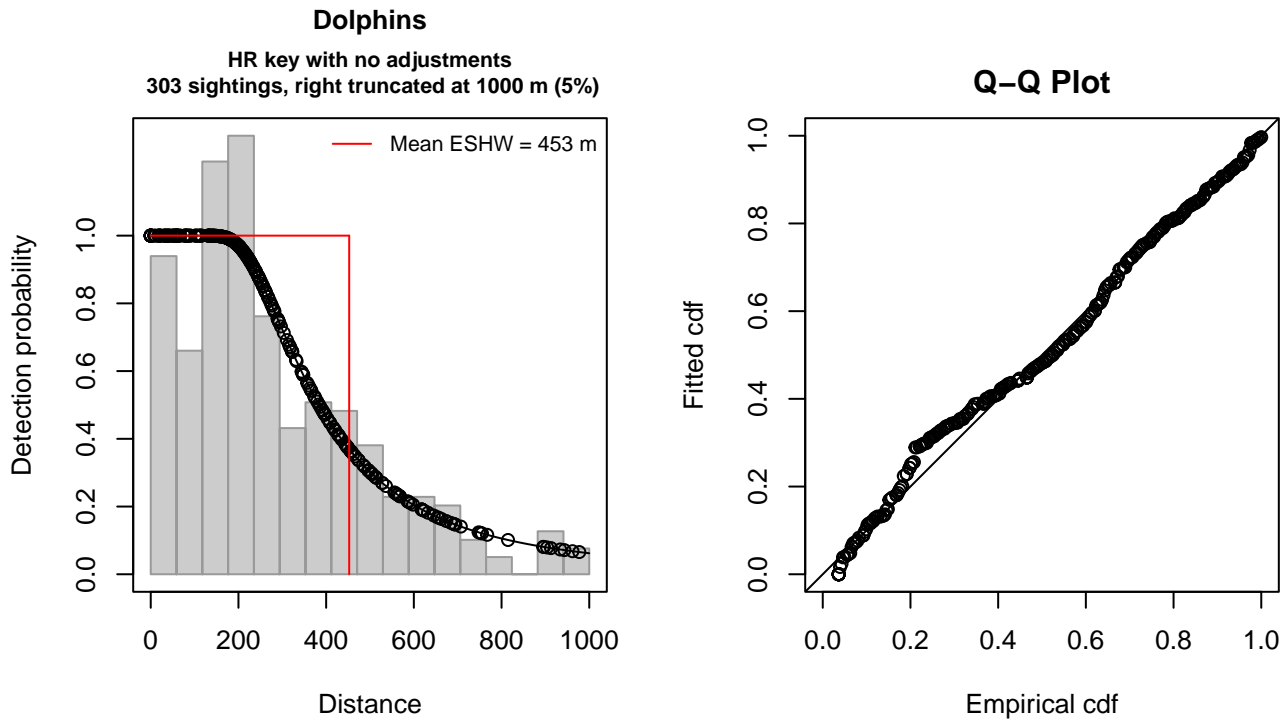
Figure 45: VAMSC detection function and Q-Q plot showing its goodness of fit.

Statistical output for this detection function:

```
Summary for ds object
Number of observations :   303
Distance range         :   0  -  1000
AIC                    :   3992.632

Detection function:
 Hazard-rate key function

Detection function parameters
Scale coefficient(s):
            estimate         se
(Intercept) 5.803823 0.1019737

Shape coefficient(s):
            estimate         se
(Intercept) 0.9119562 0.1438459


                      Estimate         SE         CV
Average p            0.4525805  0.02853931 0.06305908
N in covered region 669.4942067 50.91287837 0.07604678


Distance sampling Cramer-von Mises test (unweighted)
Test statistic = 0.212402  p = 0.244680
```

3.2.1.9   HDR

After right-truncating observations greater than 1500 m and left-truncating observations less than 111 m (Figure 47), we fitted the detection function to the 203 observations that remained (Table 19). The selected detection function (Figure 46) used a hazard rate key function with Season (Figure 48) and Swell (Figure 49) as covariates.

53

Table 19: Observations used to fit the HDR detection function.

| ScientificName	n
Delphinus delphis	47
Stenella coeruleoalba	14
Stenella frontalis	19
Tursiops truncatus	123
Total	**203**
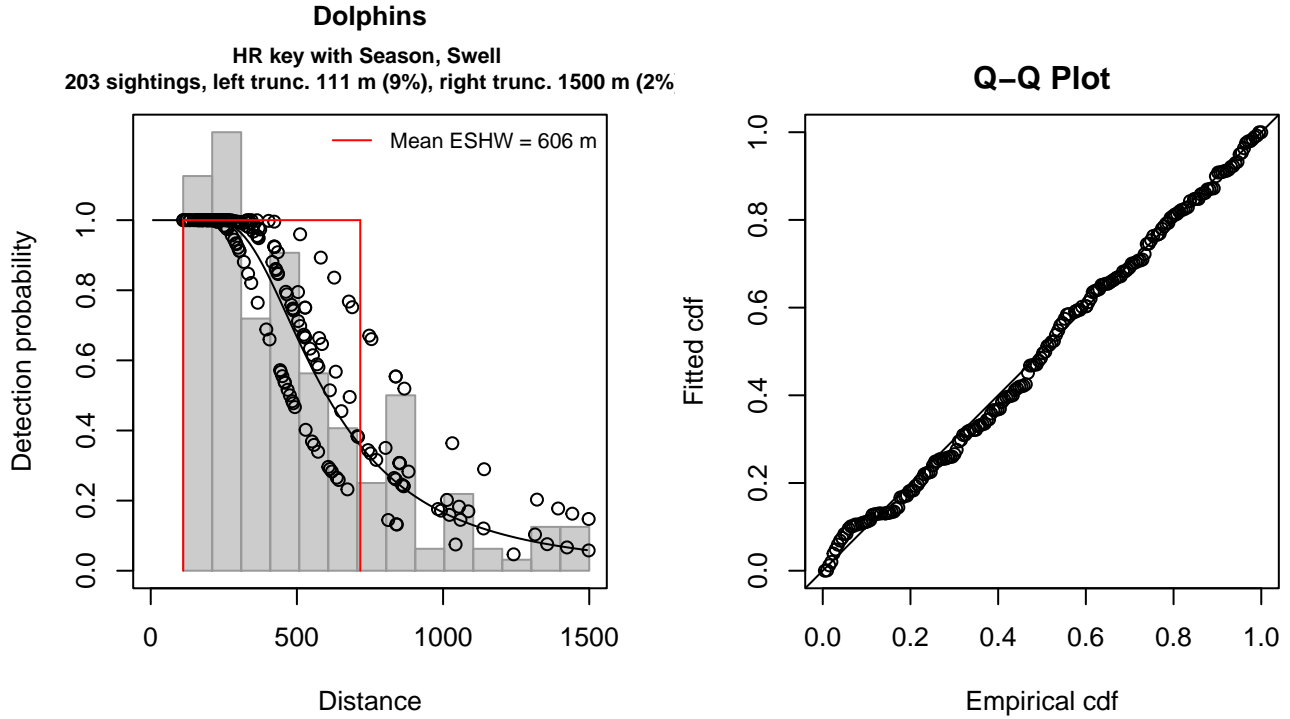
Figure 46: HDR detection function and Q-Q plot showing its goodness of fit.

Statistical output for this detection function:

```
Summary for ds object
Number of observations :  203
Distance range         :  111  -  1500
AIC                    :  2802.845

Detection function:
 Hazard-rate key function

Detection function parameters
Scale coefficient(s):
                        estimate          se
(Intercept)            6.3015171 0.1328018
SeasonWinter, Spring  -0.2671651 0.1458664
Swell3-4               0.3527933 0.1530784

Shape coefficient(s):
            estimate          se
(Intercept) 1.026101 0.1620057

                    Estimate          SE          CV
```

```
Average p               0.419883  0.03654238 0.08702991
N in covered region 483.467993 49.56848062 0.10252691


Distance sampling Cramer-von Mises test (unweighted)
Test statistic = 0.059652  p = 0.816171
```

Left trucated sightings (in red)

203 used (89%), 21 left trunc. (9%), 4 right trunc. (2%)
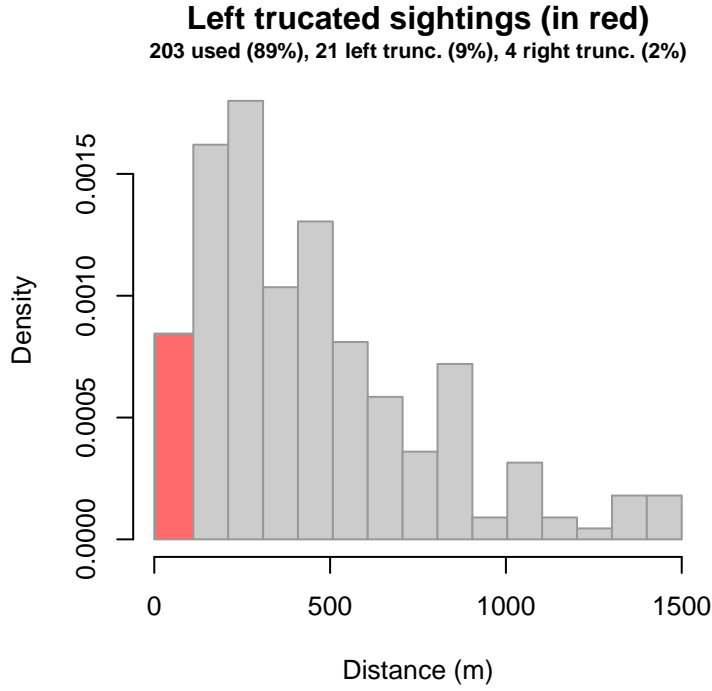
Figure 47: Density histogram of observations used to fit the HDR detection function, with the left-most bar showing observations at distances less than 111 m, which were left-truncated and excluded from the analysis [Buckland et al. (2001)]. (This bar may be very short if there were very few left-truncated sightings, or very narrow if the left truncation distance was very small; in either case it may not appear red.)

Figure 48: Distribution of the Season covariate before (top row) and after (bottom row) observations were truncated to fit the HDR detection function.

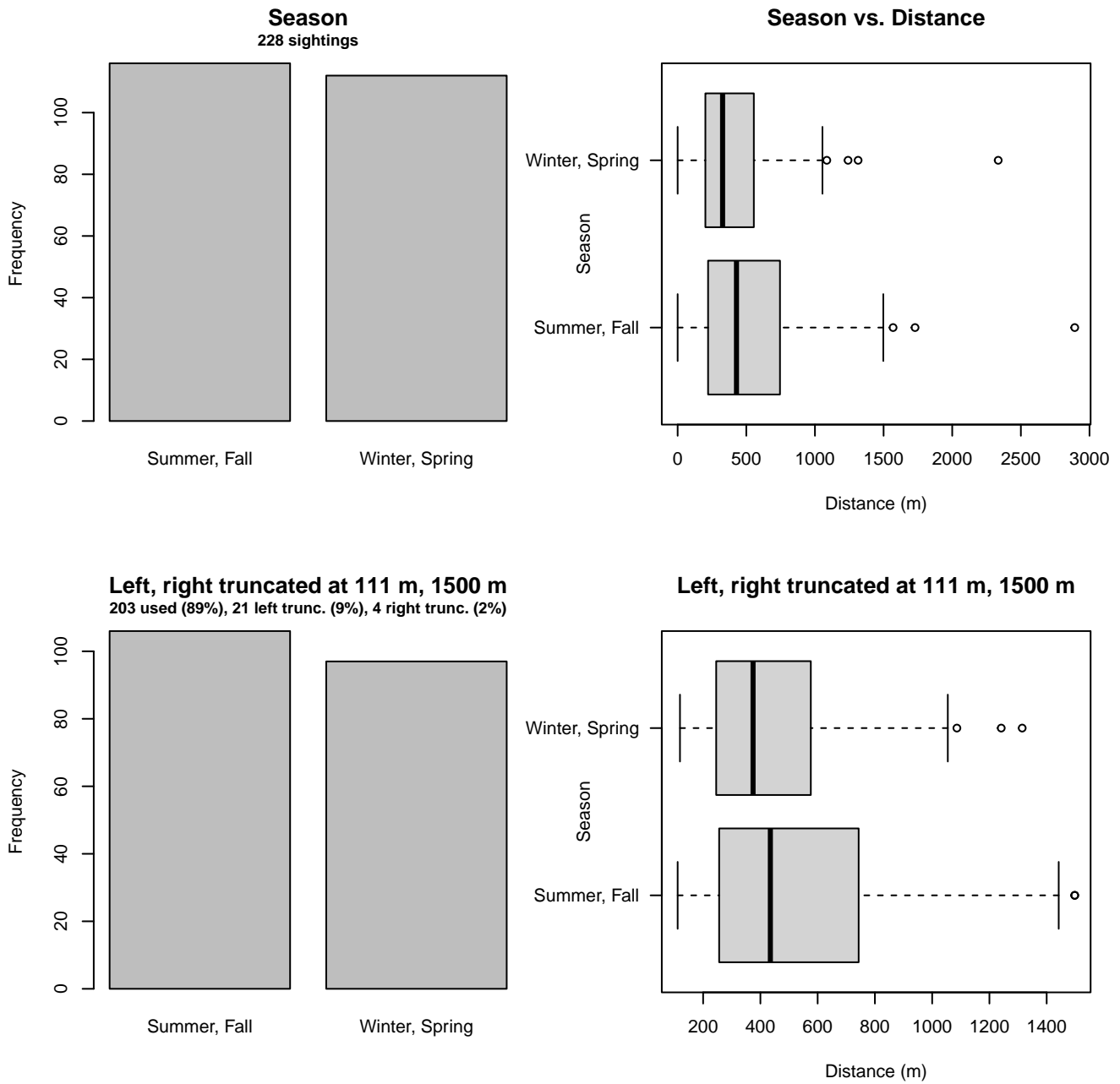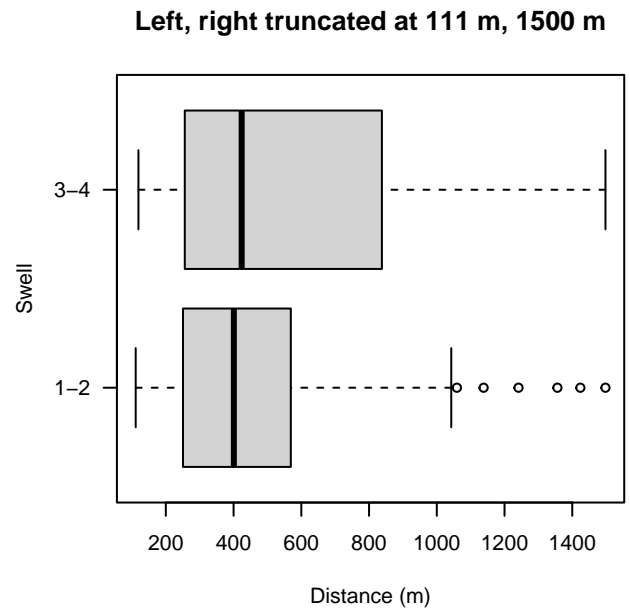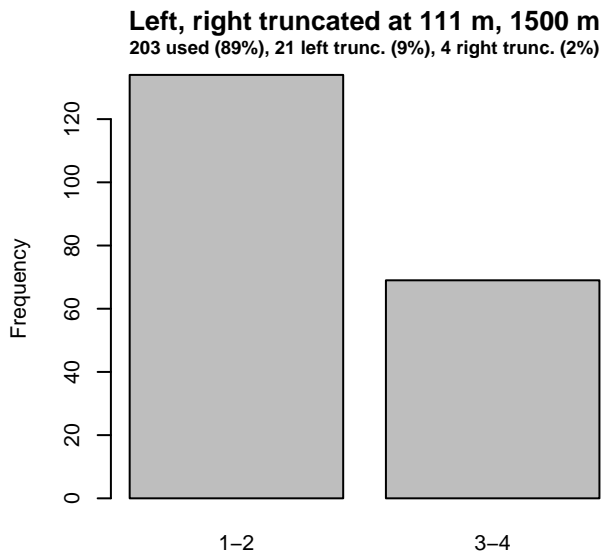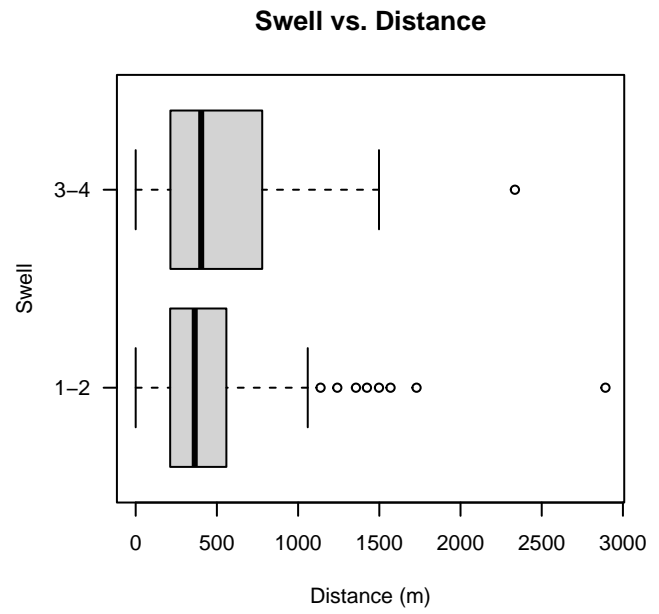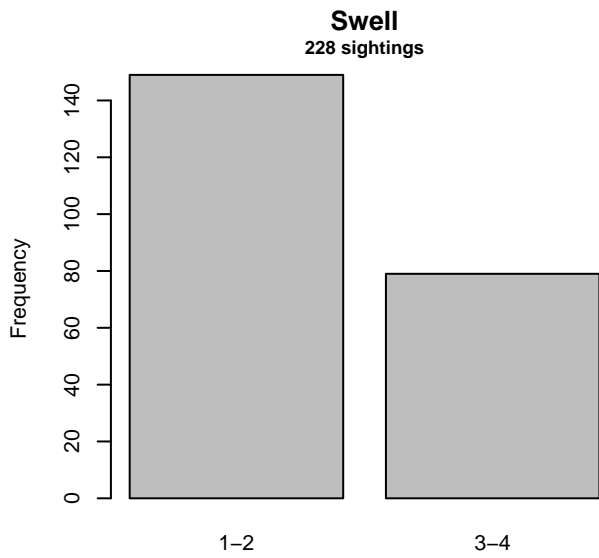Figure 49: Distribution of the Swell covariate before (top row) and after (bottom row) observations were truncated to fit the HDR detection function.
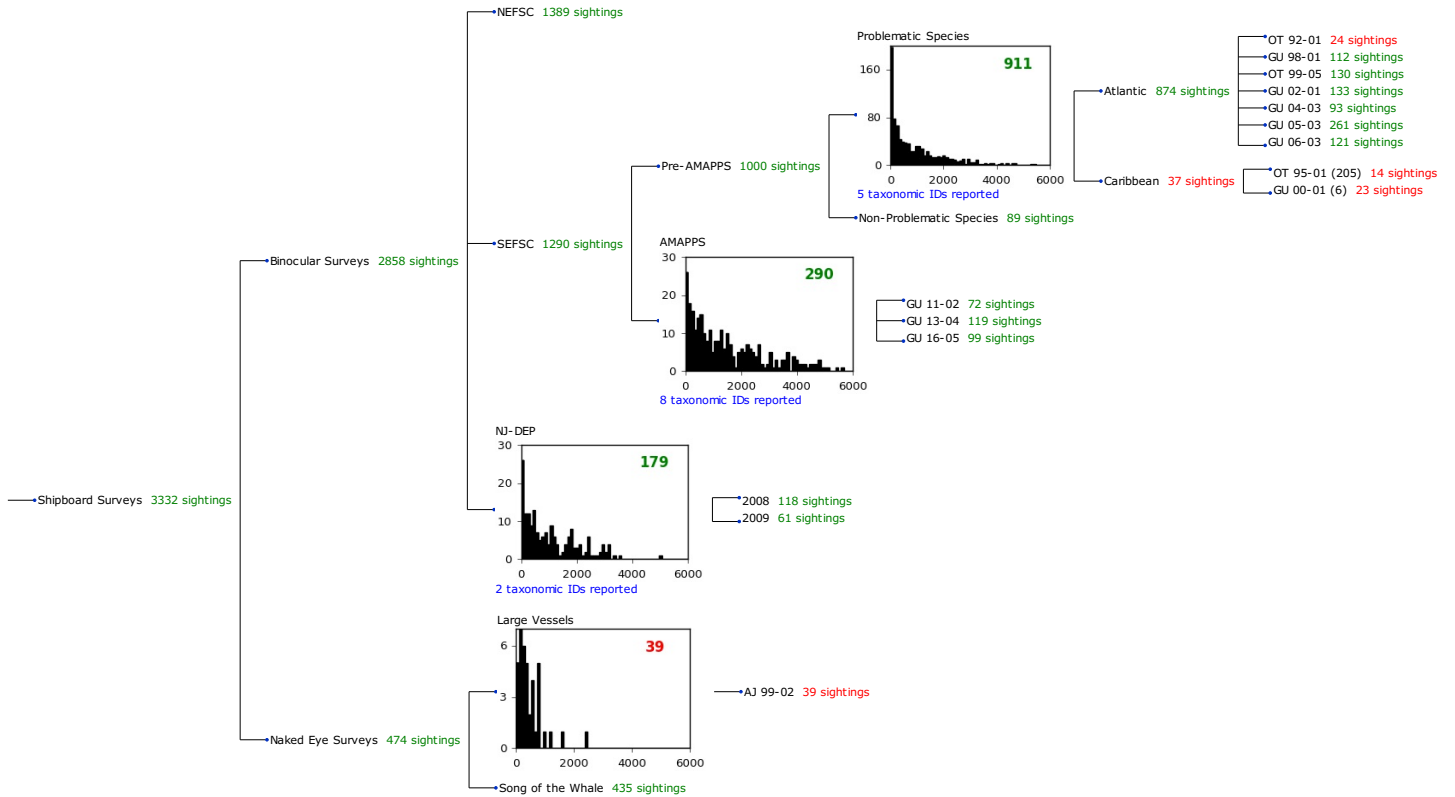
3.2.2 Shipboard Surveys

Figure 50: Detection hierarchy for shipboard surveys, showing how they were pooled during detectability modeling, for detection functions that pooled multiple taxa but could not use a taxonomic covariate to account for differences between them. Each histogram represents a detection function and summarizes the perpendicular distances of observations that were pooled to fit it, prior to truncation. Observation counts, also prior to truncation, are shown in green when they met the recommendation of Buckland et al. (2001) that detection functions utilize at least 60 sightings, and red otherwise. For rare taxa, it was not always possible to meet this recommendation, yielding higher statistical uncertainty. During the spatial modeling stage of the analysis, effective strip widths were computed for each survey using the closest detection function above it in the hierarchy (i.e. moving from right to left in the figure). Surveys that do not have a detection function above them in this figure were either addressed by a detection function presented in a different section of this report, or were omitted from the analysis.

3.2.2.1 SEFSC Pre-AMAPPS Problematic Species

After right-truncating observations greater than 4000 m and left-truncating observations less than 200 m (Figure 52), we fitted the detection function to the 616 observations that remained (Table 20). The selected detection function (Figure 51) used a hazard rate key function with Beaufort (Figure 53) and VesselName (Figure 54) as covariates.

Table 20: Observations used to fit the SEFSC Pre-AMAPPS Problematic Species detection function.

ScientificName	n
Delphinus delphis	34
Stenella attenuata	14
Stenella frontalis	262
Steno bredanensis	4
Tursiops truncatus	302
Total	**616**
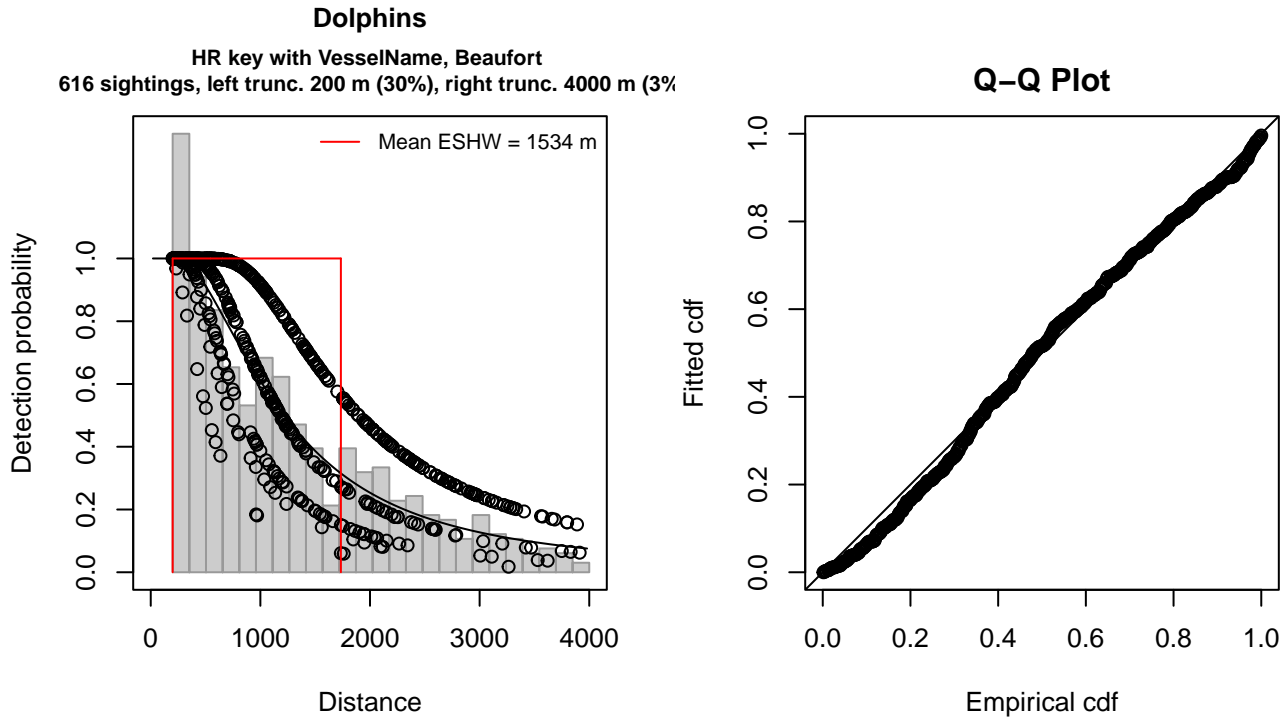
Figure 51: SEFSC Pre-AMAPPS Problematic Species detection function and Q-Q plot showing its goodness of fit.

Statistical output for this detection function:

```
Summary for ds object
Number of observations :  616
Distance range         :  200  -  4000
AIC                    :  9753.004

Detection function:
 Hazard-rate key function

Detection function parameters
Scale coefficient(s):
                      estimate          se
(Intercept)          7.3628462 0.09422017
VesselNameOregon II -0.4793018 0.17480366
Beaufort3           -0.4668391 0.14302976
Beaufort4-5         -0.8137669 0.16103824

Shape coefficient(s):
          estimate          se
(Intercept) 0.689867 0.09372714

                      Estimate         SE          CV
Average p            0.3555714   0.02671315 0.07512737
N in covered region 1732.4228173 142.52885613 0.08227140

Distance sampling Cramer-von Mises test (unweighted)
Test statistic = 0.313292  p = 0.124062
```
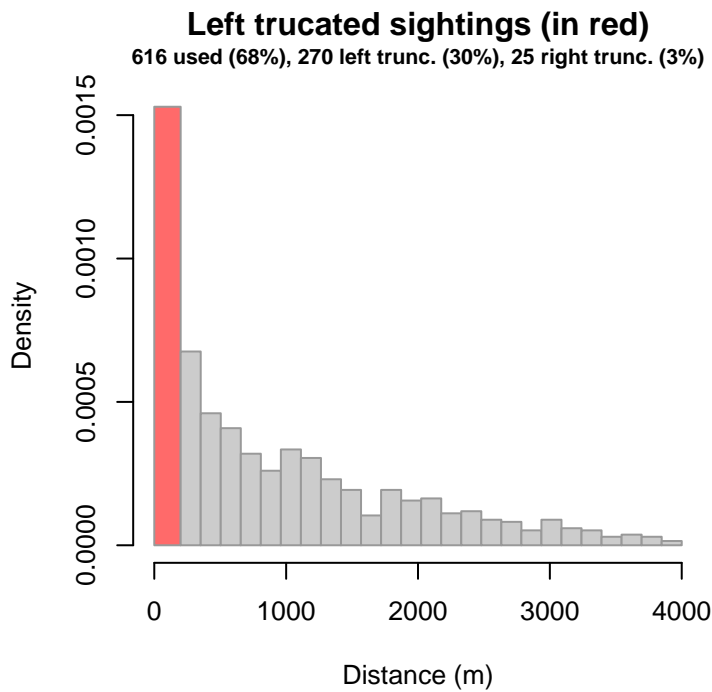
Figure 52: Density histogram of observations used to fit the SEFSC Pre-AMAPPS Problematic Species detection function, with the left-most bar showing observations at distances less than 200 m, which were left-truncated and not used to fit the detection function. (This bar may be very short if there were very few left-truncated sightings, or very narrow if the left truncation distance was very small; in either case it may not appear red.) These were excluded because they formed a problematic "spike" in detections close to the trackline, suggesting that animals approached the vessel (e.g. to bow-ride) prior to being detected. To address this, we fitted the detection function to the observations beyond the spike and assumed that within it, detection probability was 1, effectively treating it like a strip transect. We then added the left-truncated observations back into the analysis as if they occurred in this strip. This treatment may have resulted in an underestimation of detection probability.

Figure 53: Distribution of the Beaufort covariate before (top row) and after (bottom row) observations were truncated to fit the SEFSC Pre-AMAPPS Problematic Species detection function.

Figure 54: Distribution of the VesselName covariate before (top row) and after (bottom row) observations were truncated to fit the SEFSC Pre-AMAPPS Problematic Species detection function.

3.2.2.2 SEFSC AMAPPS

After right-truncating observations greater than 5000 m, we fitted the detection function to the 284 observations that remained (Table 21). The selected detection function (Figure 55) used a hazard rate key function with Beaufort (Figure 56) as a covariate.

Table 21: Observations used to fit the SEFSC AMAPPS detection function.

ScientificName	n
Delphinus delphis	2
Stenella attenuata	10
Stenella clymene	3
Stenella coeruleoalba	11
Stenella frontalis	84
Stenella longirostris	1
Steno bredanensis	2
Tursiops truncatus	171
Total	**284**

Figure 55: SEFSC AMAPPS detection function and Q-Q plot showing its goodness of fit.

Statistical output for this detection function:

```
Summary for ds object
Number of observations :  284
Distance range         :  0  -  5000
AIC                    :  4678.464

Detection function:
 Hazard-rate key function

Detection function parameters
Scale coefficient(s):
            estimate         se
(Intercept)  7.8386611 0.3487749
Beaufort2-3 -0.6450433 0.3816484
Beaufort4   -1.3990617 0.4441169
Beaufort5   -1.8689041 0.5186901
```

```
Shape coefficient(s):
            estimate        se
(Intercept) 0.3878689 0.1380351


                       Estimate          SE         CV
Average p             0.3478259   0.03965009 0.1139941
N in covered region 816.5004271 101.68622285 0.1245391


Distance sampling Cramer-von Mises test (unweighted)
Test statistic = 0.107898   p = 0.547527
```
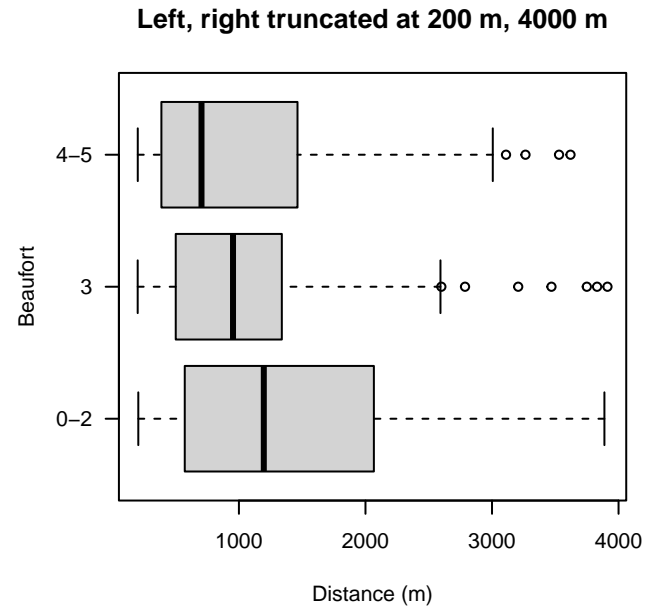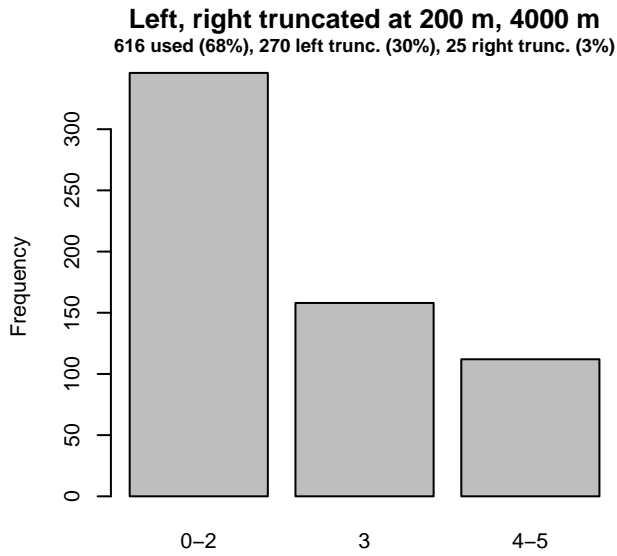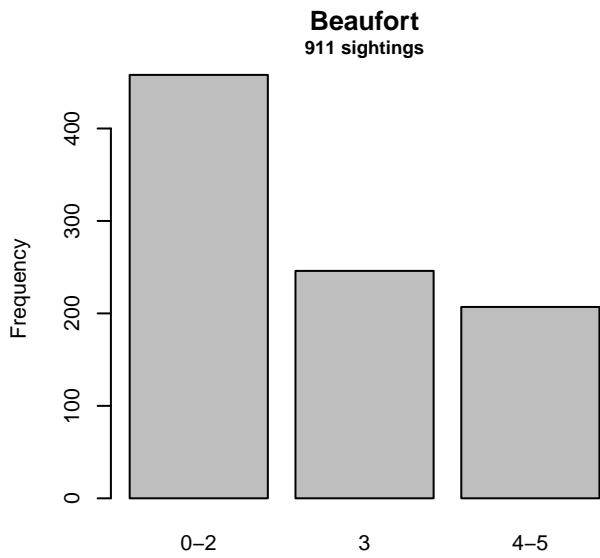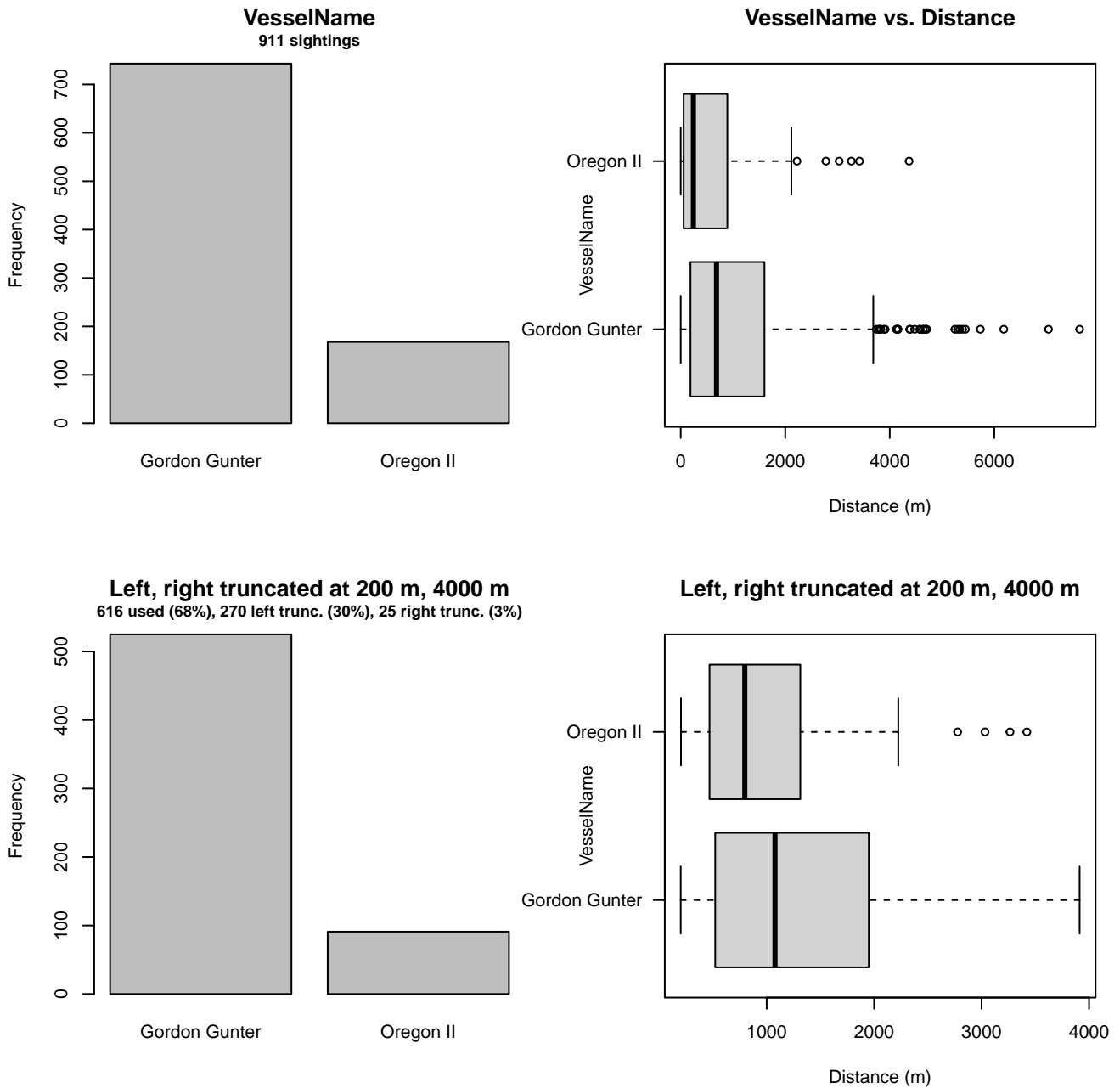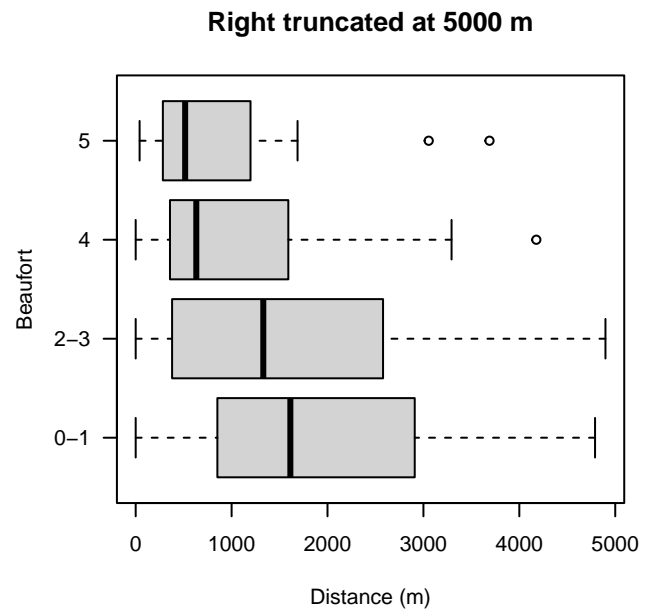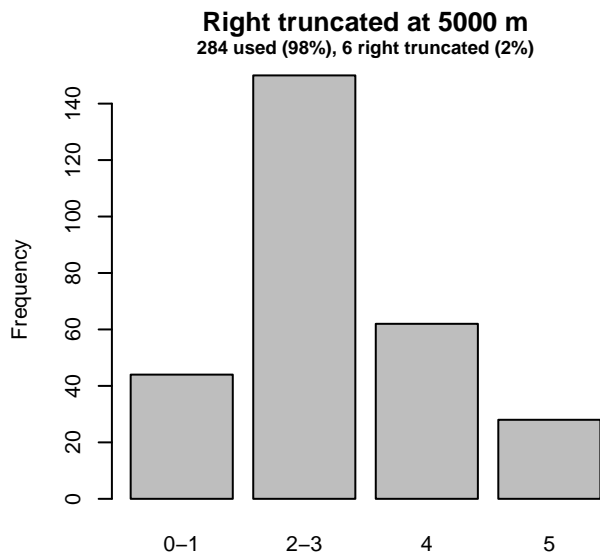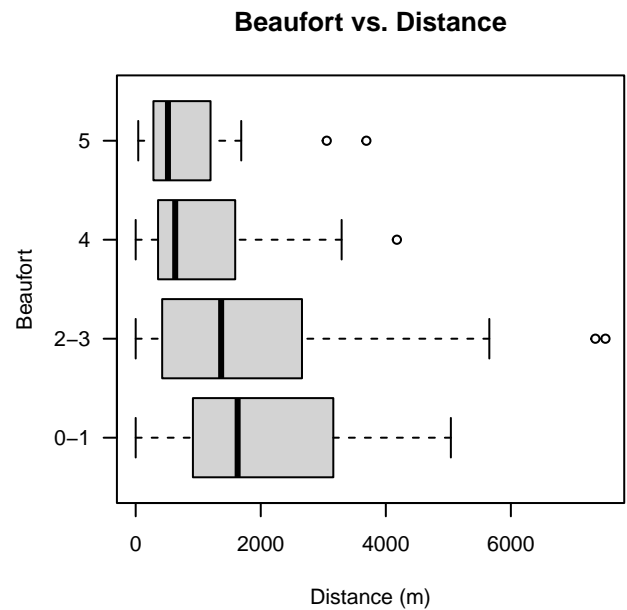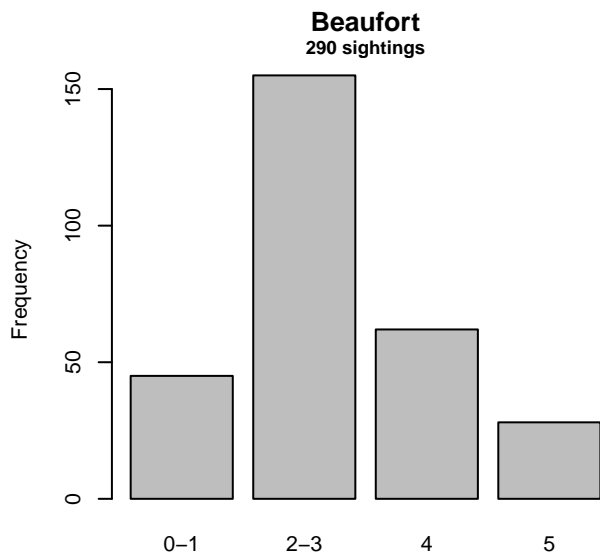

Figure 56: Distribution of the Beaufort covariate before (top row) and after (bottom row) observations were truncated to fit the SEFSC AMAPPS detection function.

3.2.2.3 NJ-DEP

After right-truncating observations greater than 3200 m, we fitted the detection function to the 175 observations that remained (Table 22). The selected detection function (Figure 57) used a hazard rate key function with no covariates.

Table 22: Observations used to fit the NJ-DEP detection function.

ScientificName	n
Delphinus delphis	19
Tursiops truncatus	156
Total	**175**
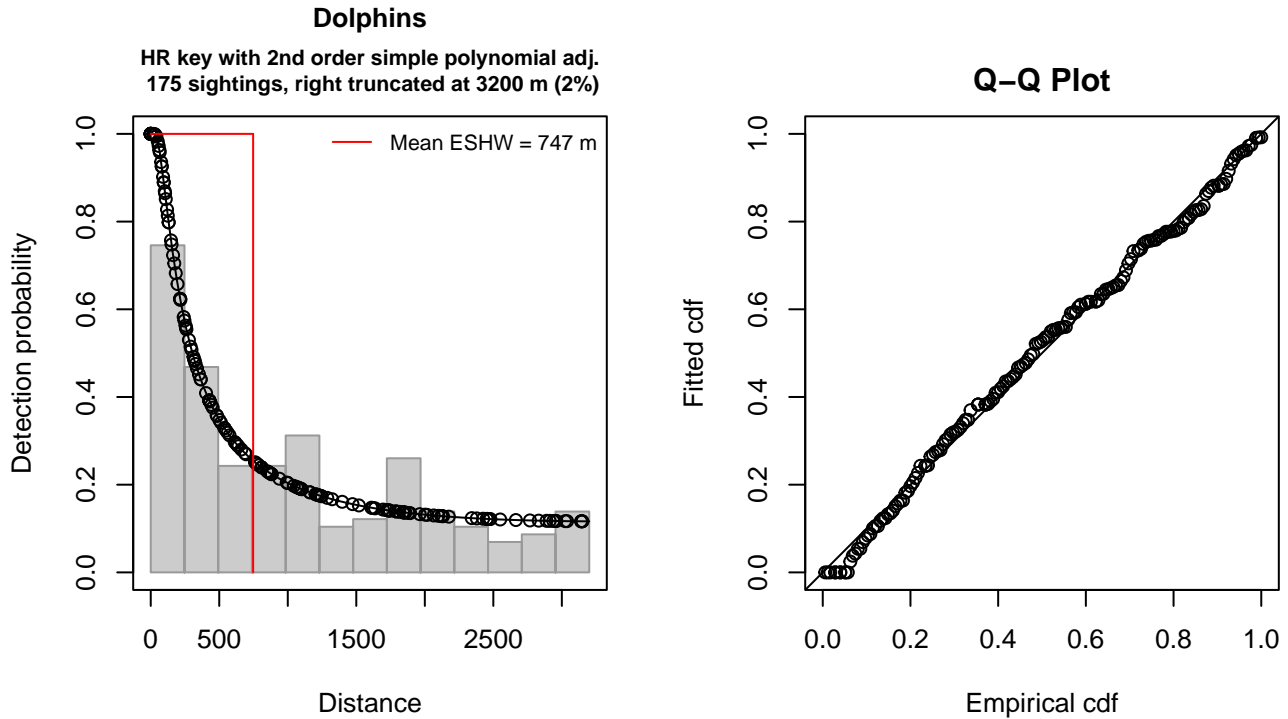
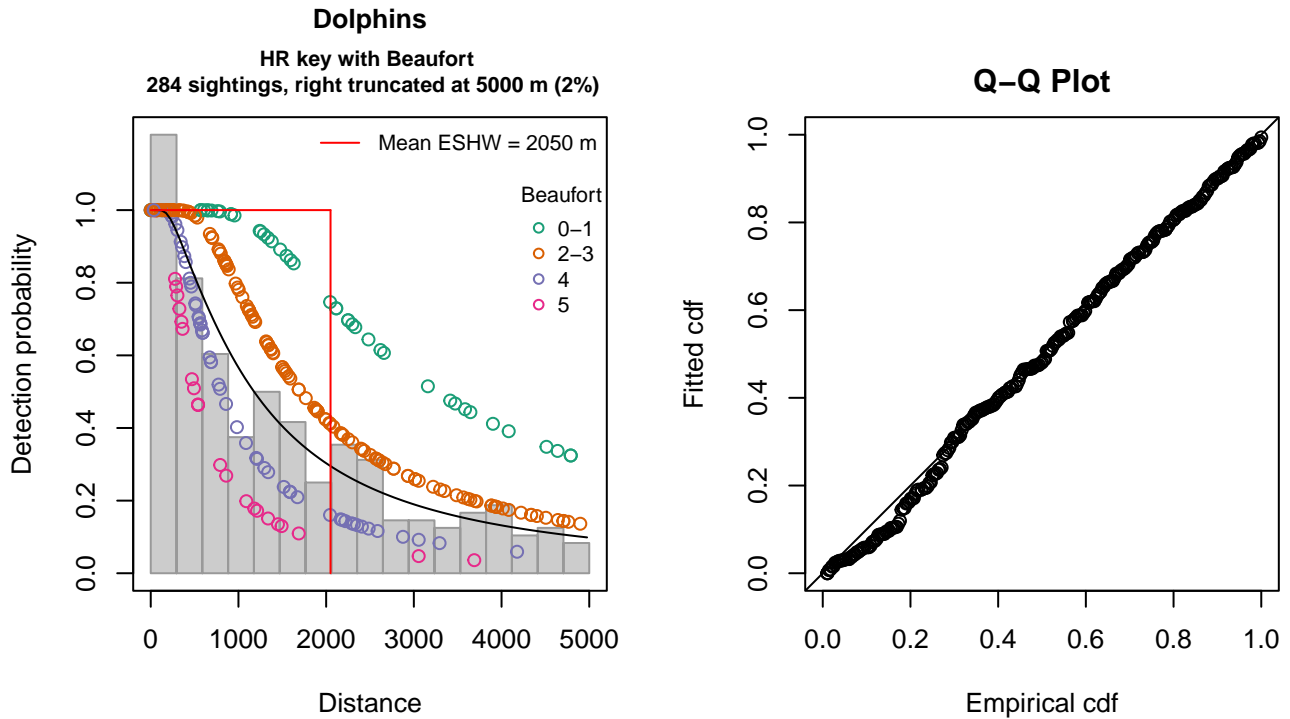Figure 57: NJ-DEP detection function and Q-Q plot showing its goodness of fit.

Statistical output for this detection function:

```
Summary for ds object
Number of observations :  175
Distance range         :  0  -  3200
AIC                    :  2750.547

Detection function:
 Hazard-rate key function with simple polynomial adjustment term of order 2

Detection function parameters
Scale coefficient(s):
            estimate        se
(Intercept) 5.340225 0.502875

Shape coefficient(s):
              estimate         se
(Intercept) 2.663565e-07 0.3025183
```

```
Adjustment term coefficient(s):
              estimate        se
poly, order 2 0.8448098 1.306568


Monotonicity constraints were enforced.
                     Estimate          SE         CV
Average p           0.2335197    0.05159473 0.2209438
N in covered region 749.4013460 172.84391894 0.2306427

Monotonicity constraints were enforced.

Distance sampling Cramer-von Mises test (unweighted)
Test statistic = 0.069450  p = 0.754942
```

3.2.2.4 Large Vessels

After right-truncating observations greater than 1100 m, we fitted the detection function to the 36 observations that remained (Table 23). The selected detection function (Figure 58) used a half normal key function with no covariates.

Table 23: Observations used to fit the Large Vessels detection function.

ScientificName	n
Lagenorhynchus acutus	36
Total	**36**
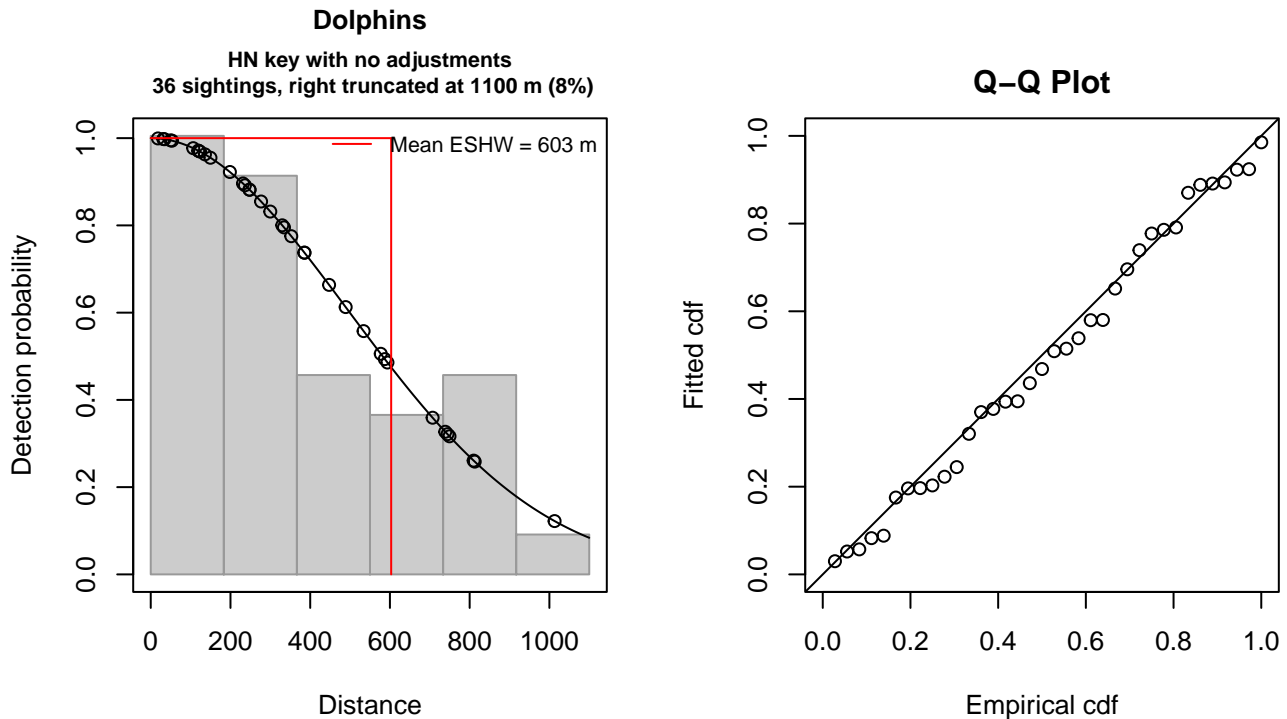
Figure 58: Large Vessels detection function and Q-Q plot showing its goodness of fit.

Statistical output for this detection function:

```
Summary for ds object
Number of observations :  36
Distance range         :  0  -  1100
```

```
AIC                      :    493.4472


Detection function:
 Half-normal key function


Detection function parameters
Scale coefficient(s):
          estimate        se
(Intercept) 6.202683 0.1646341


                   Estimate          SE        CV
Average p         0.5483057  0.07646146 0.1394504
N in covered region 65.6568085 11.74385160 0.1788672


Distance sampling Cramer-von Mises test (unweighted)
Test statistic = 0.026241  p = 0.986825
```

4 Bias Corrections

Density surface modeling methodology uses *distance sampling* (Buckland et al. 2001) to model the probability that an observer on a line transect survey will detect an animal given the perpendicular distance to it from the transect line. Distance sampling assumes that detection probability is 1 when perpendicular distance is 0. When this assumption is not met, detection probability is biased high, leading to an underestimation of density and abundance. This is known as the $g_0 < 1$ problem, where g_0 refers to the detection probability at distance 0. Modelers often try to address this problem by estimating g_0 empirically and dividing it into estimated density or abundance, thereby correcting those estimates to account for the animals that were presumed missed.

Two important sources of bias for visual surveys are known as *availability bias*, in which an animal was present on the transect line but impossible to detect, e.g. because it was under water, and *perception bias*, in which an animal was present and available but not noticed, e.g. because of its small size or cryptic coloration or behavior (Marsh and Sinclair 1989). Modelers often estimate the influence of these two sources of bias on detection probability independently, yielding two estimates of g_0, hereafter referred to as g_{0A} and g_{0P}, and multiply them together to obtain a final, combined estimate: $g_0 = g_{0A}.g_{0P}$.

Our overall approach was to perform this correction on a per-observation basis, to have the flexibility to account for many factors such as platform type, surveyor institution, group size, group composition (e.g. singleton, mother-calf pair, or surface active group), and geographic location (e.g. feeding grounds vs. calving grounds). The level of complexity of the corrections varied by species according to the amount of information available, with North Atlantic right whale having the most elaborate corrections, derived from a substantial set of publications documenting its behavior, and various lesser known odontocetes having corrections based only on platform type (aerial or shipboard), derived from comparatively sparse information. Here we document the corrections used for Atlantic white-sided dolphin.

4.1 Aerial Surveys

Reflecting the northerly distribution of the species, the only collaborating institution that reported sightings of Atlantic white-sided dolphins during aerial surveys that were suited to modeling small cetaceans was NOAA NEFSC (Table 1). Palka et al. (2021) developed perception bias corrections using two team, mark recapture distance sampling (MRDS) methodology (Burt et al. 2014) for aerial surveys conducted in 2010-2017 by NEFSC during the AMAPPS program. We applied this correction to all aerial sightings (all were from NEFSC), including those prior to the AMAPPS program and from the NARWSS program. Palka previously developed a correction for the pre-AMAPPS surveys (Palka 2006) but it utilized older methods and less data than the 2021 analysis, so we used the 2021 analysis instead.

No perception bias estimate was available for NARWSS, but that program used the same aircraft and many of the same observers as the AMAPPS program. However, it flew at a higher altitude and had a searching strategy designed to maximize detections of large whales, so it is possible the AMAPPS estimate undercorrected the NARWSS data (i.e. g_{0P} for NARWSS should have been less than g_{0P} for AMAPPS). If so, it is possible this led to an underestimation of density, as more than 80% sightings were reported by NARWSS.

For all aerial surveys, to account for the influence of large group sizes on perception bias, we followed Carretta et al. (2000) and set the perception bias correction factor for sightings of more than 25 animals to $g_{0P} = 0.994$.

We estimated availability bias corrections using the Laake et al. (1997) estimator and dive intervals reported by Palka et al. (2017) (Table 25). To estimate time in view, needed by the Laake estimator, we used results reported by Robertson et al. (2015), rescaled linearly for each survey program according to its target altitude and speed.

To address the influence of group size on availability bias, we applied the group availability estimator of McLellan et al. (2018) on a per-observation basis. Following Palka et al. (2021), who also used that method, we assumed that individuals in the group dived asynchronously. The resulting g_{0A} corrections ranged from about 0.53 to 1 (Figure 59), with the large majority of observations having a correction of 0.95 or higher, owing to large group sizes. We caution that the assumption of asynchronous diving can lead to an underestimation of density and abundance if diving is actually synchronous; see McLellan et al. (2018) for an exploration of this effect. However, if future research finds that this species conducts synchronous dives and characterizes the degree of synchronicity, the model can be updated to account for this knowledge.

Table 24: Perception bias corrections for Atlantic white-sided dolphin applied to aerial surveys.

Surveys	Group Size	g_{0P}	g_{0P} Source
All	≤ 25	0.570	Palka et al. (2021): NEFSC
All	> 25	0.994	Carretta et al. (2000)

Table 25: Surface and dive intervals for Atlantic white-sided dolphin used to estimate availability bias corrections.

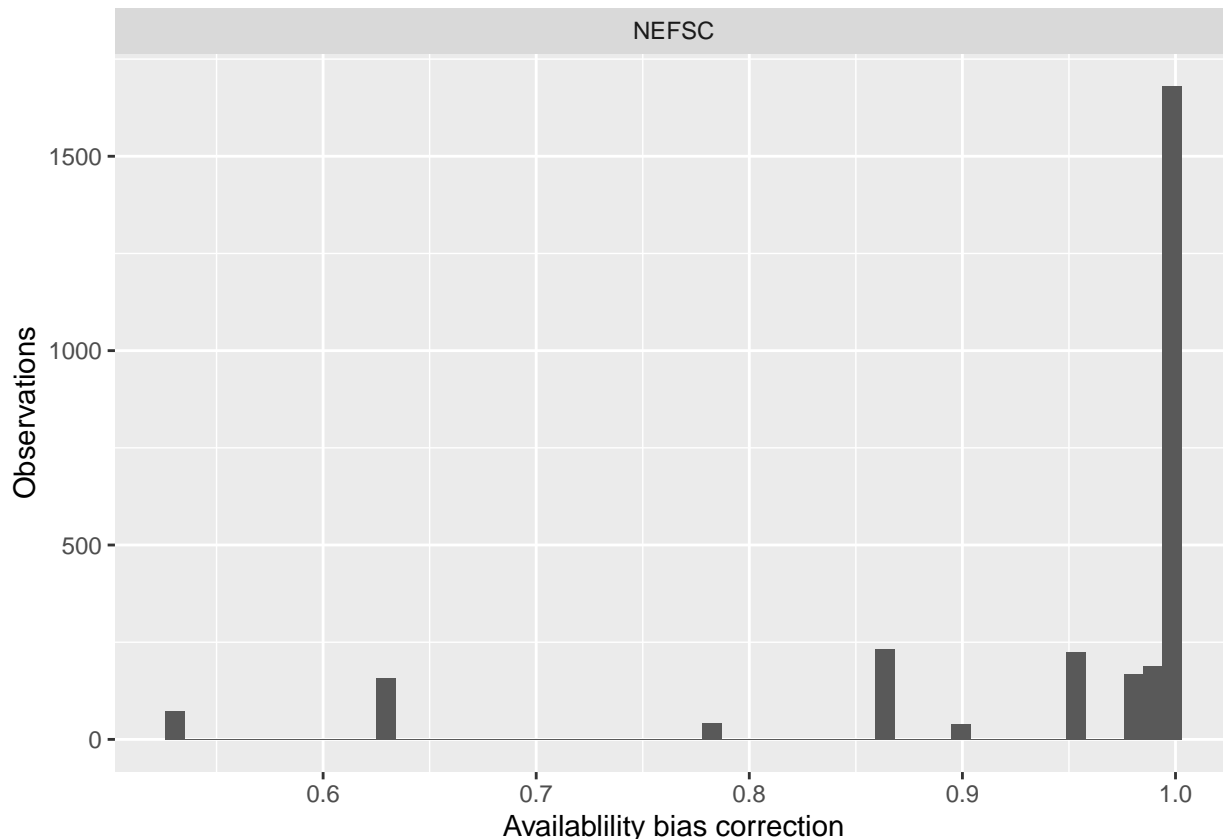| Surface Interval (s)	Dive Interval (s)	Source
4.8	38.8	Palka et al. (2017)

Figure 59: Availability bias corrections for Atlantic white-sided dolphin for aerial surveys, by institution.

4.2   Shipboard Surveys

Most of the shipboard surveys in our analysis used high-power (25x150), pedestal-mounted binoculars. Similar to aerial surveys, the only institution that reported sightings of Atlantic white-sided dolphins during high-power binocular surveys

was NOAA NEFSC[1]. Palka et al. (2021) developed perception bias corrections using two team, MRDS methodology (Burt et al. 2014) for high-power binocular surveys conducted in 2010-2017 by NEFSC during the AMAPPS program (Table 26). We also considered Palka and colleagues' earlier estimates (Palka 2006; Palka et al. 2017), but they utilized older methods and less data than the 2021 analysis, so we applied the Palka et al. (2021) estimates to all shipboard surveys that searched with high-power binoculars (all were from NEFSC).

Palka (2006) also developed a correction for an NEFSC shipboard survey (AJ 99-02) in which the primary team observers searched by naked eye. We applied this estimate to that survey as well as to the MCR Song of the Whale surveys, which also searched by naked eye but did not have a program-specific estimate. We caution that the platform height for the MCR surveys was substantially (~9m) lower than the NEFSC survey, and the target survey speed was slower (6 knots for MCR vs. 10 knots for NEFSC)

For all surveys, to account for the influence of large group sizes on perception bias, we followed Barlow and Forney (2007) and set the perception bias correction factor for sightings of more than 20 animals to $g_{0P} = 0.97$. Given that the dive interval of this species (Table 25) was short relative to the amount of time a given patch of water remained in view to shipboard observers, we assumed that no availability bias correction was needed ($g_{0A} = 1$), following Palka et al. (2021).

Table 26: Perception and availability bias corrections for Atlantic white-sided dolphin applied to shipboard surveys.

Surveys	Searching Method	Group Size	g_{0P}	g_{0P} Source	g_{0A}	g_{0A} Source
NEFSC	Binoculars	≤ 20	0.52	Palka et al. (2021): NEFSC	1	Assumed
NEFSC, MCR	Naked eye	≤ 20	0.27	Palka et al. (2006)	1	Assumed
All	All	> 20	0.97	Barlow and Forney (2007)	1	Assumed

5 Density Model

In the North Atlantic, white-sided dolphins are found primarily in temperate and sub-polar waters of the continental shelf (Hayes et al. 2022). Along the U.S. eastern seaboard, they are most frequently found in the Gulf of Maine but appear to range as far south as Virginia or North Carolina in winter (Hayes et al. 2022), although strandings data suggest they rarely occur there. Byrd et al. (2014) reported only 14 strandings of white-sided dolphins in North Carolina during 1997-2008 but 23 strandings of humpback whales, a population an order of magnitude smaller that is known to regularly overwinter in coastal Virginia and North Carolina (Aschettino et al. 2018). In Byrd's analysis, 13 of the 14 white-sided dolphin strandings occurred in March and April, while the 14th occurred in February. On 4 May 2008, a 17-year old male white-sided dolphin stranded near Myrtle Beach, South Carolina (Powell et al. 2012), but this individual was in ill health and was regarded an out-of-range anomaly (Hayes et al. 2022).

More recently, Thorne et al. (2022) tested stranding records of odontocetes reported along the eastern U.S. from 1996 to 2020 for evidence of distribution shifts. They reported that Atlantic white-sided dolphin showed strong evidence of a poleward (i.e. northward) shift in distribution, and noted that while the species historically occurred at or near Cape Hatteras, North Carolina, their results suggested the trailing edge of the species' distribution had shifted north as waters warmed over the period.

The southernmost sighting available to our analysis was reported by observers on R/V Song of the Whale on 17 April 2019 southeast of Cape Lookout, North Carolina, in the Gulf Stream (Figure 1). The confidence in this sighting was rated by observers as "possible", the lowest level of confidence in that survey's protocol. Given this ucertainty, the species' preference for cooler waters, the low level of strandings this far south, and the evidence that the trailing edge has moved north from Cape Hatteras, we consider the identification of this sighting doubtful, and if correct it would be an extralimital anomaly. The next northernmost sighting was reported by the AMAPPS GU 14-02 shipboard survey on 29 March 2014 on the continental slope due east of Assateague Island, Virginia. This appeared to be a valid identification. All other sightings of white sided dolphins reported by our collaborators were north of Hudson Canyon.

Barring unusual circumstances, our modeling approach was to exclude from models ecoregions where a species is known to be absent, to avoid unnecessarily inflating the model with zero-abundance segments, especially if covariate values there might be similar to regions where the species is present. Therefore, given the preponderance of evidence that the species does not inhabit waters south of Cape Hatteras, we split the study area there, where the Gulf Stream departs the continental shelf,

---

[1]Table 6-6 of Palka et al. (2021) lists white-sided dolphin sightings for SEFSC during spring, but this refers to sightings made during the 2014 R/V Gordon Gunter cruise (GU 14-02) conducted by NEFSC personnel in a region traditionally covered by NEFSC, as documented by Palka et al. (2014). Accordingly, we tallied these sightings as being from NEFSC rather than SEFSC. We suspect Palka et al. (2021) tallied them as being from SEFSC because the survey was conducted on R/V Gordon Gunter, a vessel traditionally used by SEFSC but not NEFSC.

and fitted our density model only to the northern region, referred to as "North of Gulf Stream" in this report. For the "South of Gulf Stream" region, we assumed density was zero.

The surveys incorporated into our model, spanning 1998-2020 (see Section 1), reported nearly 2900 sightings in the "North of Gulf Stream" region (Figure 60). Palka et al. (1997), in a paper summarizing the status of the species in U.S. and Canadian Atlantic waters, reported that spatiotemporal patterns in sightings and strandings indicate seasonal shifts in the species' distribution, suggesting a more northerly distribution in summer and southerly in winter, but did not report evidence of specific, large-scale migrations that would warrant defining multiple seasons under our modeling methodology. Accordingly, we fitted a single, year-round model for the "North of Gulf Stream" region.

When ranked by REML score (Wood 2011), the highest ranked candidate models with climatological covariates outranked those with contemporaneous covariates, and explained 1% more deviance. However, when predicted across the study period, the climatological-covariate models yielded unreasonably large densities across the northern center and edge of the Scotian Shelf, where surveying was very sparse (Figure 60), particularly in non-summer months. To avoid that likely-aberrant seasonal extrapolation, we selected the top-ranked contemporaneous-covariate model, which included seven covariates (Table 27).

Relationships with bathymetric covariates indicated a positive effect on density at seafloor depths greater than 40 meters with a strong peak at the 125 m isobath, and avoidance of enclosed inshore waters having low fetch (Figure 63). Consistent with this, the relationship with primary productivity (VGPM) dropped strongly at the high end of the sampled range, corresponding to conditions close to shore. The relationships with surface temperature and salinity indicated a preference for the cold, fresher shelf waters north of Cape Hatteras, with steep declines in density shown for temperatures greater than 21 °C and salinities greater than 33 PSU. Finally, the model indicated higher densities close to surface temperature fronts.

5.1 Final Model

Atlantic white-sided dolphin
1998-2020, Year_Round (Jan-Dec)
North of Gulf Stream

767995 km
169357 segments
1895 with sightings
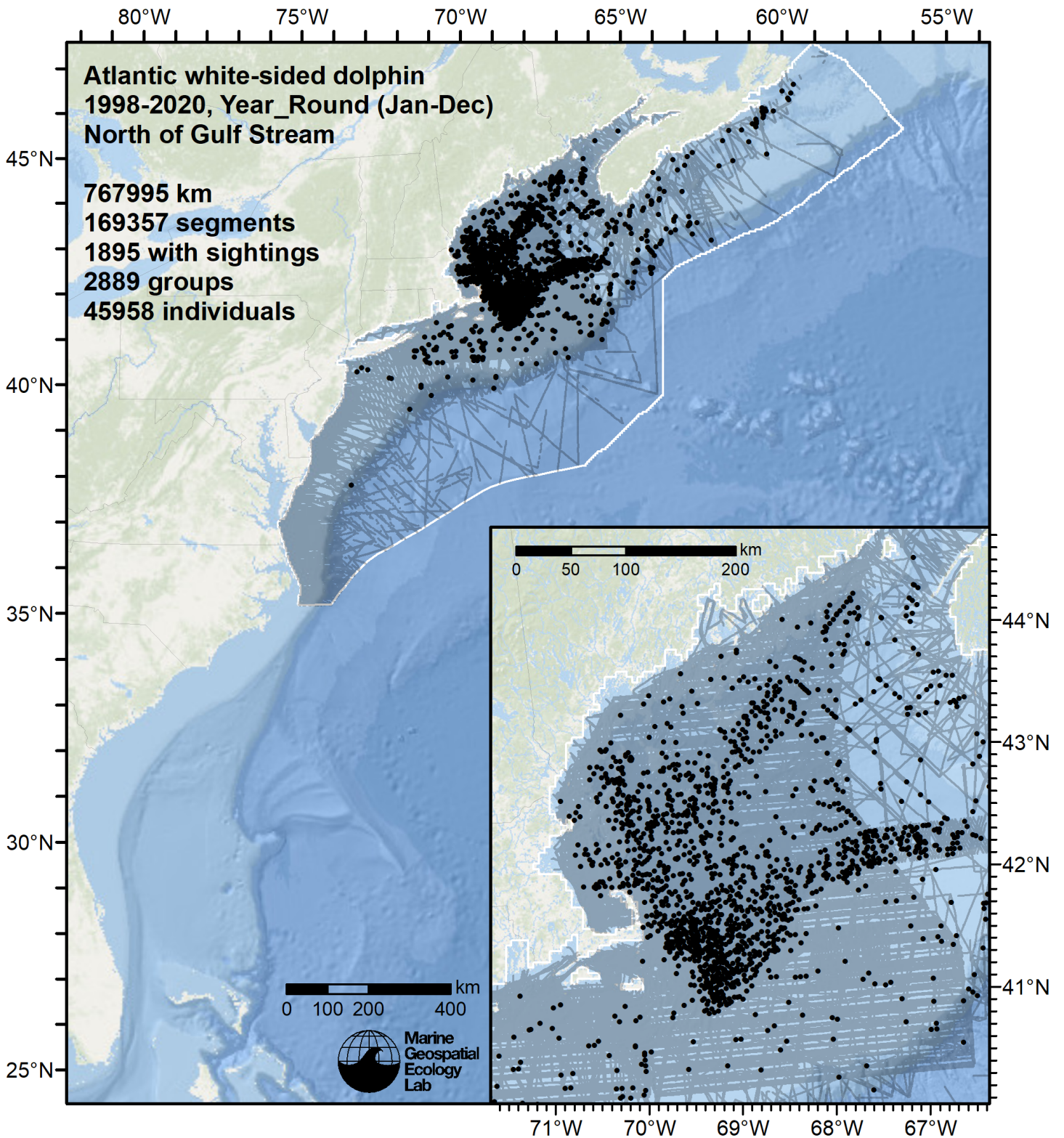**2889 groups**
45958 individuals

Figure 60: Survey segments used to fit the model for the region North of Gulf Stream. Black points indicate segments with observations.
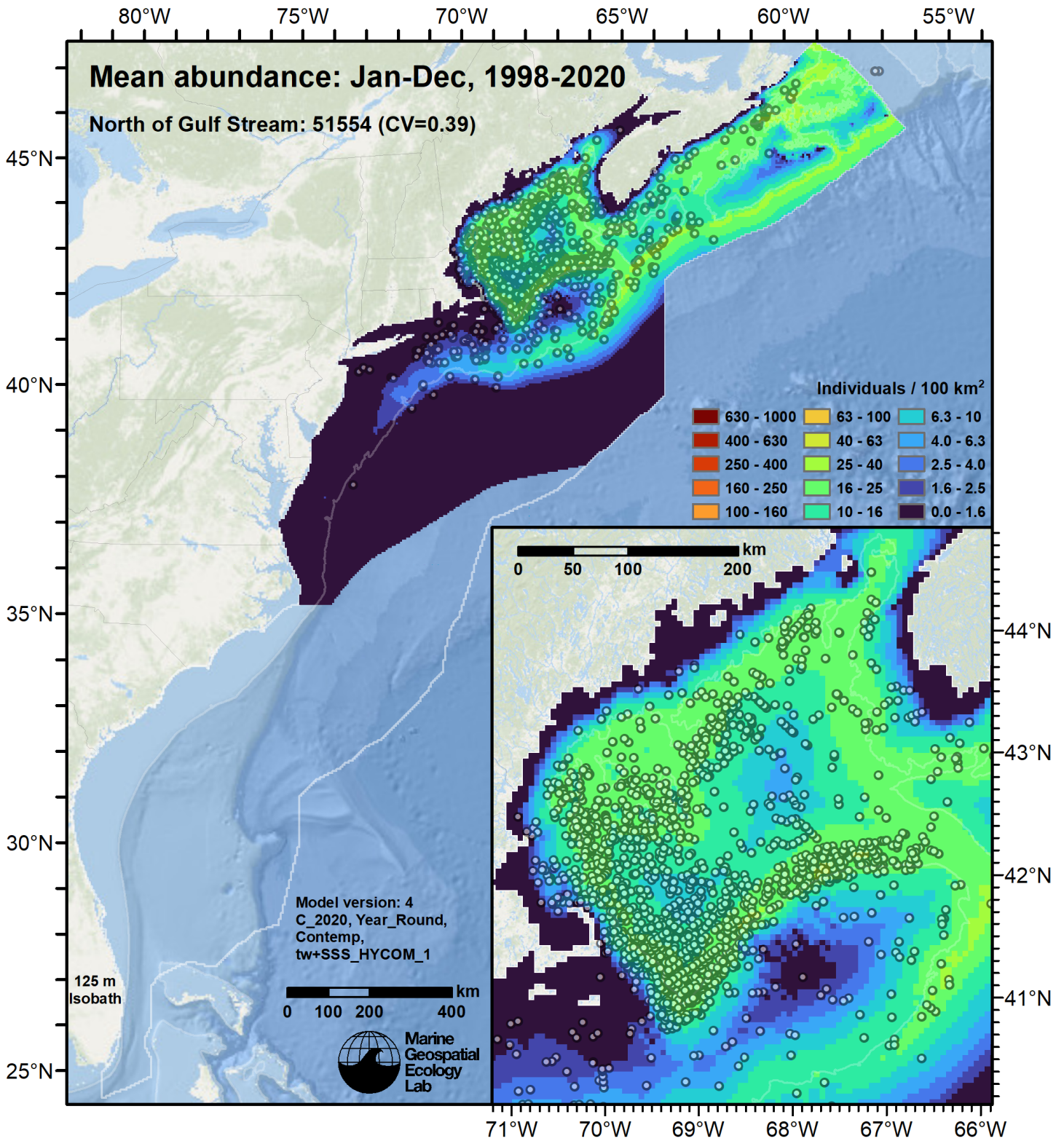
Figure 61: Atlantic white-sided dolphin mean density for the indicated period, as predicted by the model for the region North of Gulf Stream. Open circles indicate segments with observations. Mean total abundance and its coefficient of variation (CV) are given in the subtitle. Variance was estimated with the analytic approach given by Miller et al. (2022), Appendix S1, and accounts both for uncertainty in model parameter estimates and for seasonal and interannual variability in dynamic covariates.
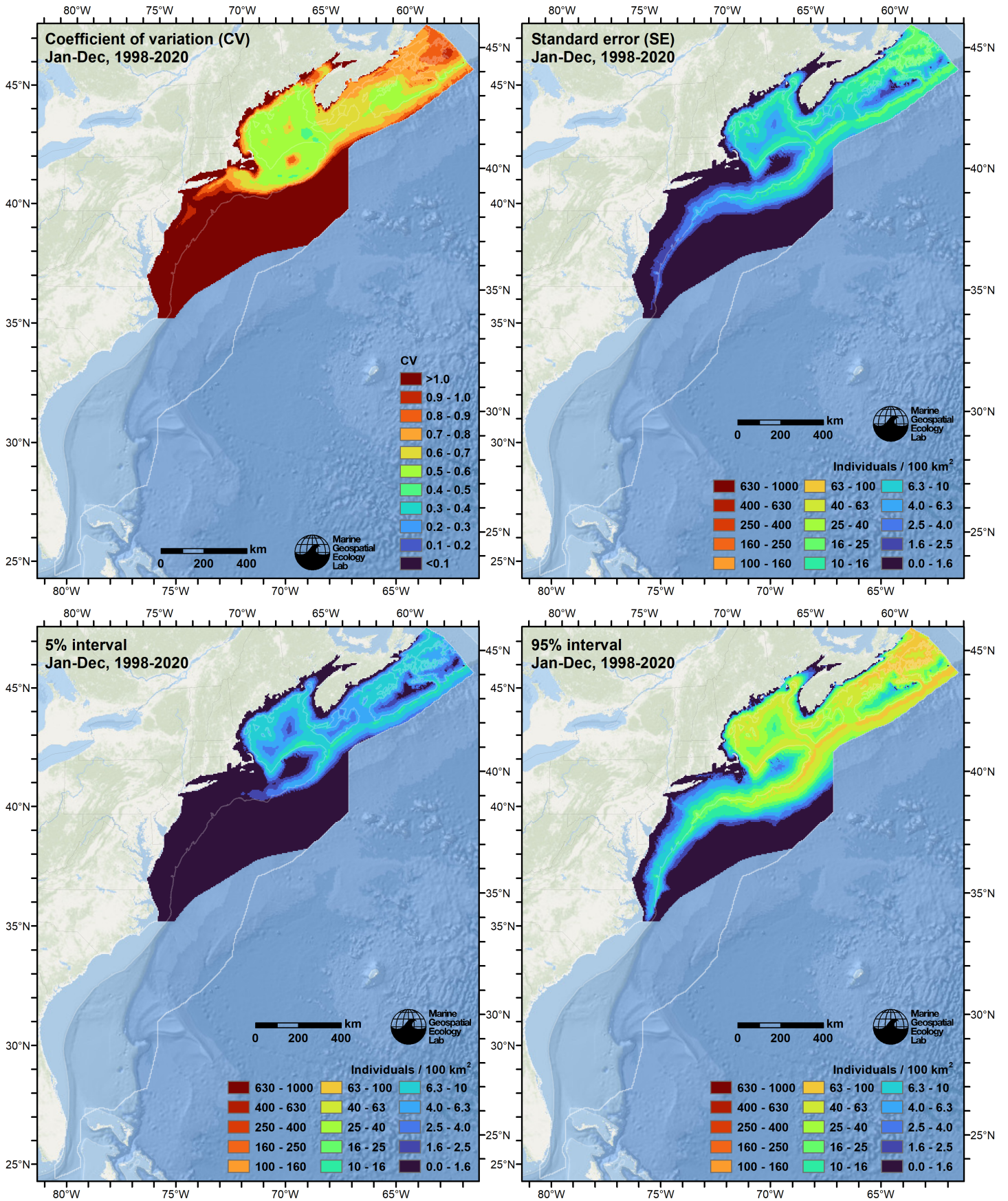
Figure 62: Uncertainty statistics for the Atlantic white-sided dolphin mean density surface (Figure 61) predicted by the model for the region North of Gulf Stream. Variance was estimated with the analytic approach given by Miller et al. (2022), Appendix S1, and accounts both for uncertainty in model parameter estimates and for seasonal and interannual variability in dynamic covariates.

Statistical output for this model:


```
Family: Tweedie(p=1.444)
Link function: log


Formula:
IndividualsCorrected ~ offset(log(SegmentArea)) + s(Fetch_50km,
    bs = "ts") + s(log10(pmax(5, pmin(Depth, 3000)))), bs = "ts") +
    s(pmax(-100, pmin(I(DistTo125m/1000), 100)), bs = "ts") +
    s(pmax(3, pmin(SST_CMC, 29)), bs = "ts") + s(pmax(31, pmin(SSS_HYCOM,
    36)), bs = "ts") + s(pmin(I(DistToFront063/1000), 75), bs = "ts") +
    s(pmax(300, pmin(PP_VGPM, 4000)), bs = "ts")


Parametric coefficients:
            Estimate Std. Error t value Pr(>|t|)
(Intercept) -19.5628     0.2044   -95.7   <2e-16 ***
---
Signif. codes:  0 '***' 0.001 '**' 0.01 '*' 0.05 '.' 0.1 ' ' 1


Approximate significance of smooth terms:
                                              edf Ref.df      F p-value
s(Fetch_50km)                              0.8783      9  0.763 0.00473 **
s(log10(pmax(5, pmin(Depth, 3000))))       4.8218      9  9.587 < 2e-16 ***
s(pmax(-100, pmin(I(DistTo125m/1000), 100))) 5.1775    9 11.506 < 2e-16 ***
s(pmax(3, pmin(SST_CMC, 29)))              7.1213      9 24.312 < 2e-16 ***
s(pmax(31, pmin(SSS_HYCOM, 36)))           5.5520      9 23.280 < 2e-16 ***
s(pmin(I(DistToFront063/1000), 75))        1.0692      9  2.554 1.4e-06 ***
s(pmax(300, pmin(PP_VGPM, 4000)))          7.4133      9 11.654 < 2e-16 ***
---
Signif. codes:  0 '***' 0.001 '**' 0.01 '*' 0.05 '.' 0.1 ' ' 1


R-sq.(adj) =  0.00947   Deviance explained = 28.1%
-REML =  17590  Scale est. = 65.37     n = 169357


Method: REML   Optimizer: outer newton
full convergence after 14 iterations.
Gradient range [-0.00925201,0.004527502]
(score 17590.17 & scale 65.36989).
Hessian positive definite, eigenvalue range [0.3729097,6016.725].
Model rank =  64 / 64


Basis dimension (k) checking results. Low p-value (k-index<1) may
indicate that k is too low, especially if edf is close to k'.


                                              k'    edf k-index p-value
s(Fetch_50km)                              9.000 0.878    0.79   0.175
s(log10(pmax(5, pmin(Depth, 3000))))       9.000 4.822    0.75   0.010 **
s(pmax(-100, pmin(I(DistTo125m/1000), 100))) 9.000 5.178  0.77   0.040 *
s(pmax(3, pmin(SST_CMC, 29)))              9.000 7.121    0.76   0.005 **
s(pmax(31, pmin(SSS_HYCOM, 36)))           9.000 5.552    0.74  <2e-16 ***
s(pmin(I(DistToFront063/1000), 75))        9.000 1.069    0.80   0.685
s(pmax(300, pmin(PP_VGPM, 4000)))          9.000 7.413    0.79   0.255
---
Signif. codes:  0 '***' 0.001 '**' 0.01 '*' 0.05 '.' 0.1 ' ' 1
```

(a) Seafloor depth (m)

(b) Distance to 125m isobath (km)

(c) Distance to SST front (km)

(d) Fetch (km) (max 50 km)

(e) Net primary productivity (mg C m^{-2} day^{-1}) (VGPM)

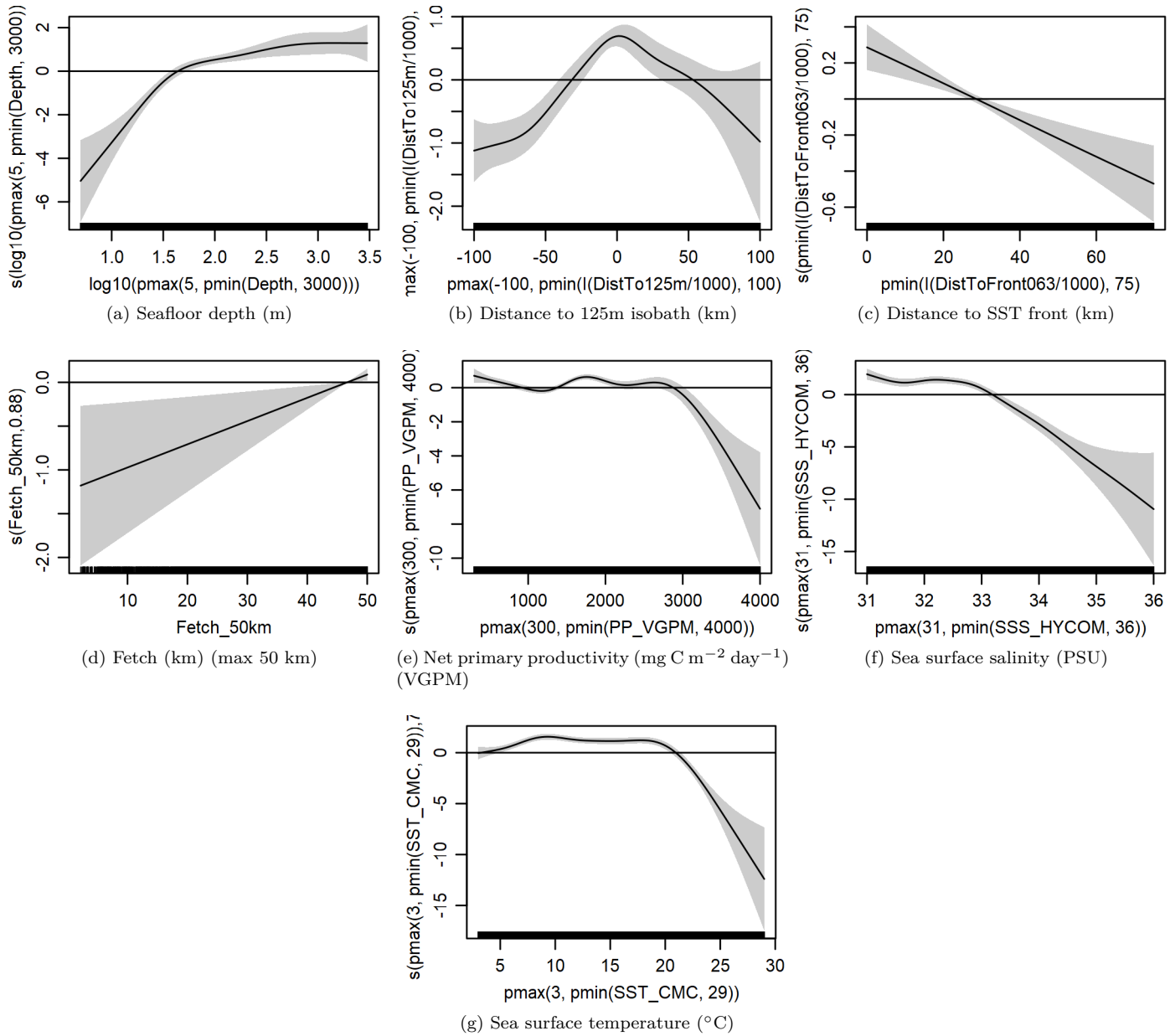(f) Sea surface salinity (PSU)

(g) Sea surface temperature (°C)

Figure 63: Functional plots for the final model for the region North of Gulf Stream. Transforms and other treatments are indicated in axis labels. *log10* indicates the covariate was $\log_{10}$ transformed. *pmax* and *pmin* indicate the covariate's minimum and maximum values, respectively, were Winsorized to the values shown. Winsorization was used to prevent runaway extrapolations during prediction when covariates exceeded sampled ranges, or for ecological reasons, depending on the covariate. */1000* indicates meters were transformed to kilometers for interpretation convenience.

Table 27: Covariates used in the final model for the region North of Gulf Stream.

Covariate	Description
Depth	Depth (m) of the seafloor, from SRTM30_PLUS (Becker et al. (2009))
DistTo125m	Distance (km) to the 125m isobath, derived from SRTM30_PLUS (Becker et al. (2009))
DistToFront063	Monthly mean distance (km) to the closest sea surface temperature front detected in daily GHRSST Level 4 CMC0.2deg and CMC0.1deg images (Brasnett (2008); Canada Meteorological Center (2012); Meissner et al. (2016); Canada Meteorological Center (2016)) with MGET's implementation of the Canny edge detector (Roberts et al. (2010); Canny (1986))

Table 27: Covariates used in the final model for the region North of Gulf Stream. *(continued)*

| Covariate	Description
Fetch_50km	Fetch (km): mean distance to shore averaged over 16 radial directions, limited to a maximum of 50 km
PP_VGPM	Monthly mean net primary productivity (mg C m^{-2} day^{-1}) from the Vertically Generalized Production Model (VGPM) (Behrenfeld and Falkowski (1997))
SSS_HYCOM	Monthly mean sea surface salinity (PSU) from the HYCOM GOFS 3.1 1/12° ocean model (Chassignet et al. (2009))
SST_CMC	Monthly mean sea surface temperature (°C) from GHRSST Level 4 CMC0.2deg and CMC0.1deg (Brasnett (2008); Canada Meteorological Center (2012); Meissner et al. (2016); Canada Meteorological Center (2016))

5.2 Diagnostic Plots
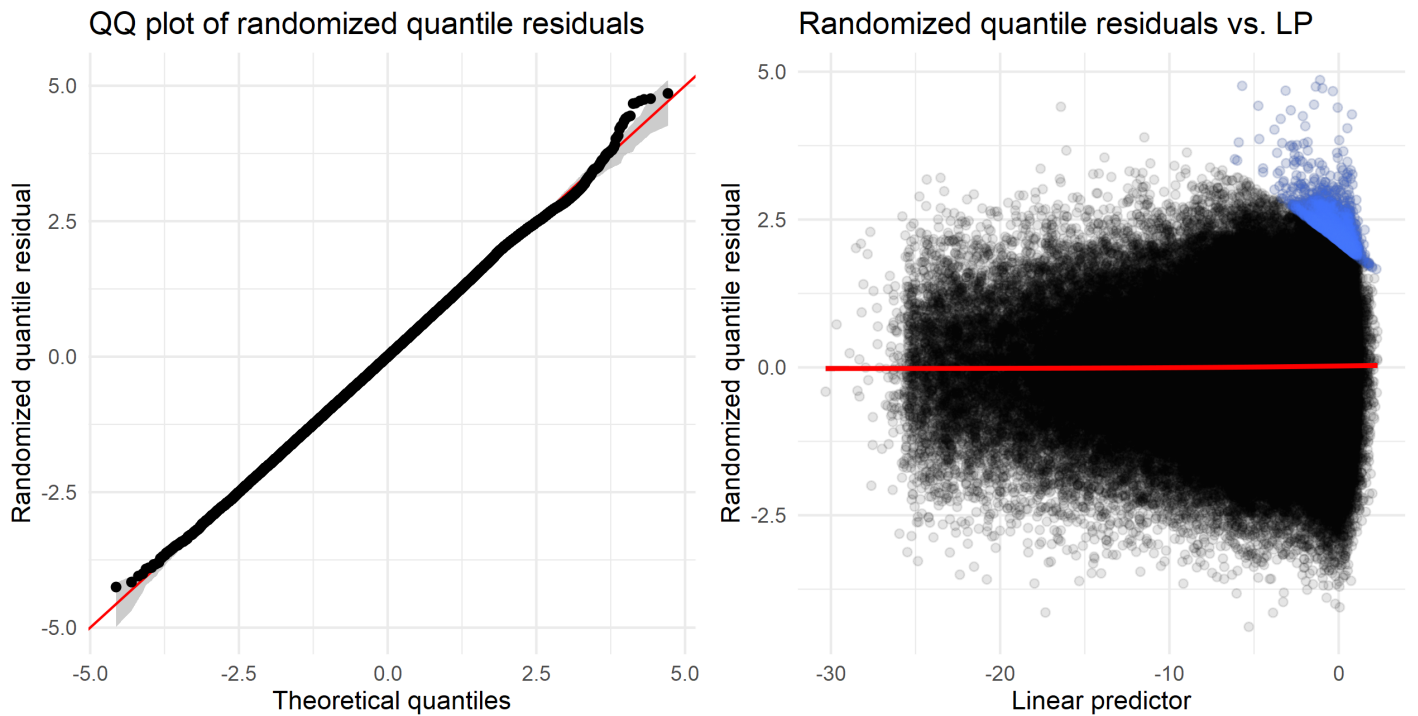
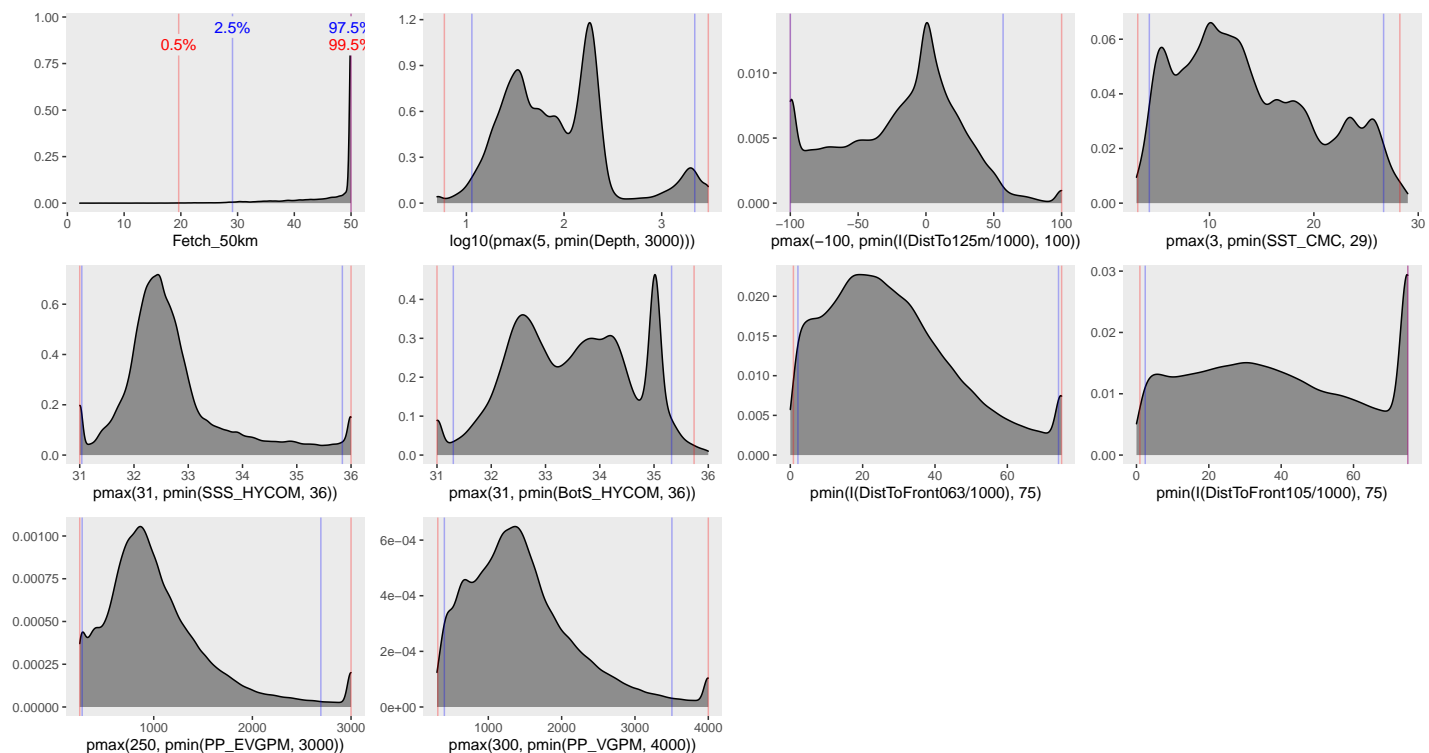Figure 64: Residual plots for the final model for the region North of Gulf Stream.

Figure 65: Density histograms showing the distributions of the covariates considered during the final model selection step. The final model may have included only a subset of the covariates shown here (see Figure 63), and additional covariates may have been considered in preceding selection steps. Red and blue lines enclose 99% and 95% of the distributions, respectively. Transforms and other treatments are indicated in axis labels. *log10* indicates the covariate was $\log_{10}$ transformed. *pmax* and *pmin* indicate the covariate's minimum and maximum values, respectively, were Winsorized to the values shown. Winsorization was used to prevent runaway extrapolations during prediction when covariates exceeded sampled ranges, or for ecological reasons, depending on the covariate. */1000* indicates meters were transformed to kilometers for interpretation convenience.
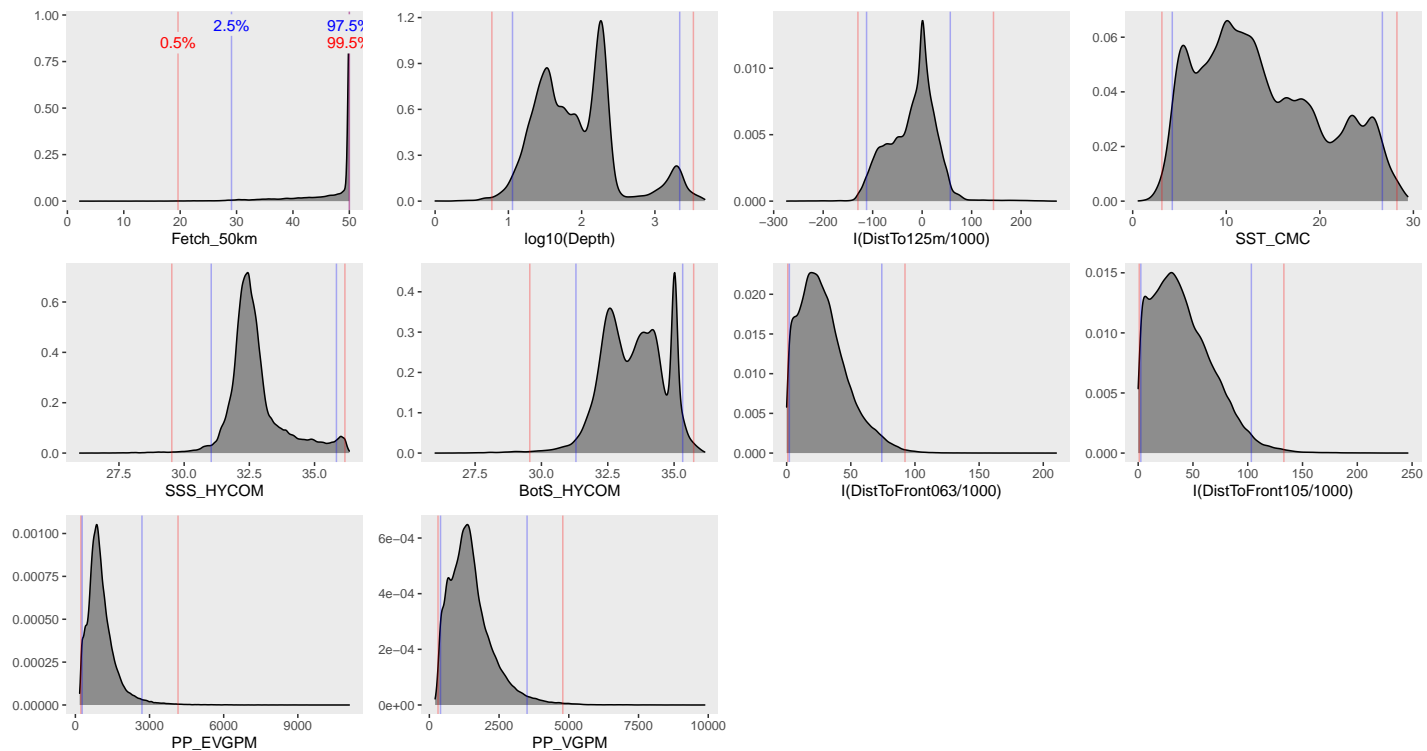
Figure 66: Density histograms shown in Figure 65 replotted without Winsorization, to show the full range of sampling represented by survey segments.
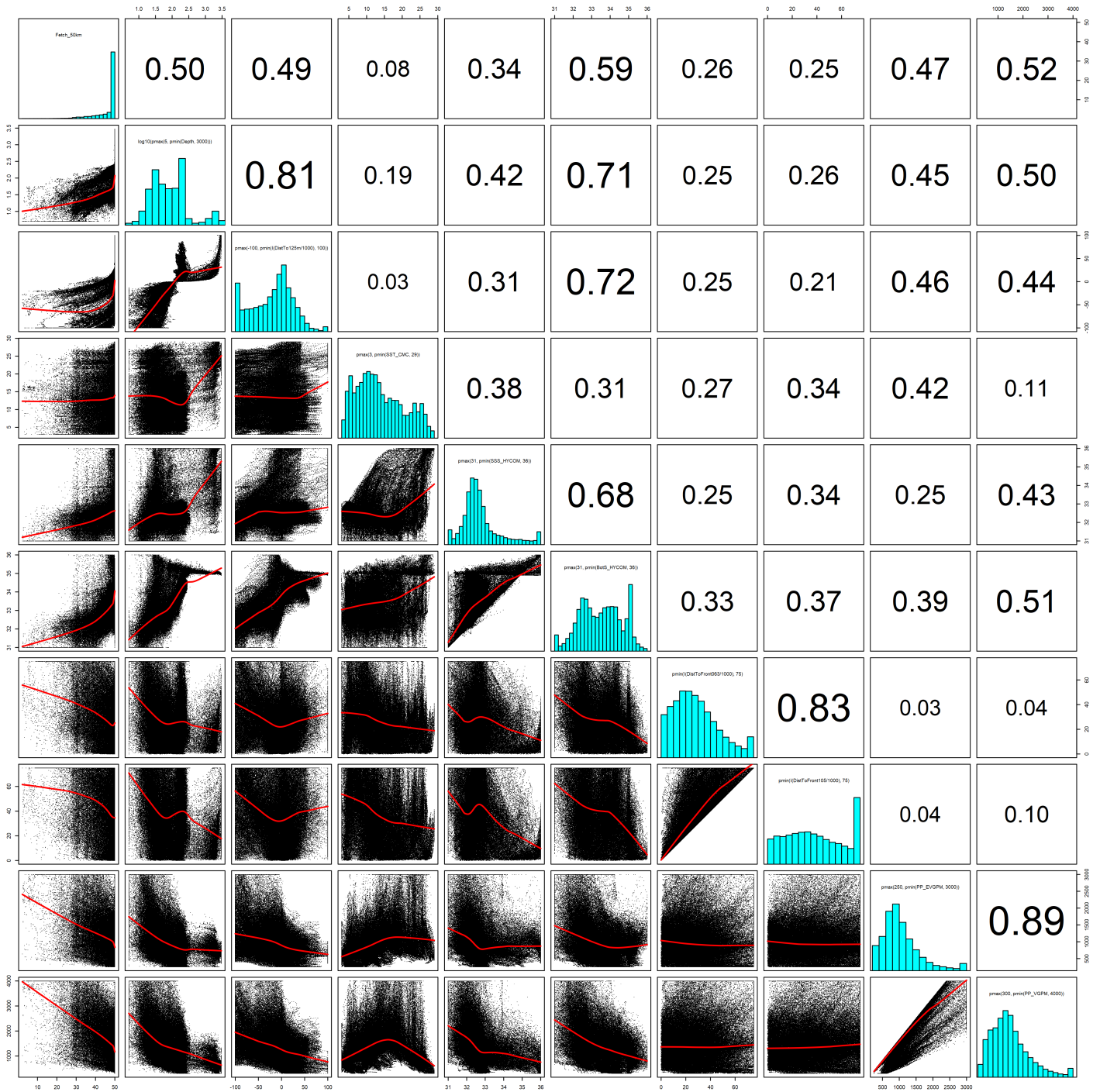
Figure 67: Scatterplot matrix of the covariates considered during the final model selection step. The final model may have included only a subset of the covariates shown here (see Figure 63), and additional covariates may have been considered in preceding selection steps. Covariates are transformed and Winsorized as shown in Figure 65. This plot is used to check simple correlations between covariates (via pairwise Pearson coefficients above the diagonal) and visually inspect for concurvity (via scatterplots and red lowess curves below the diagonal).
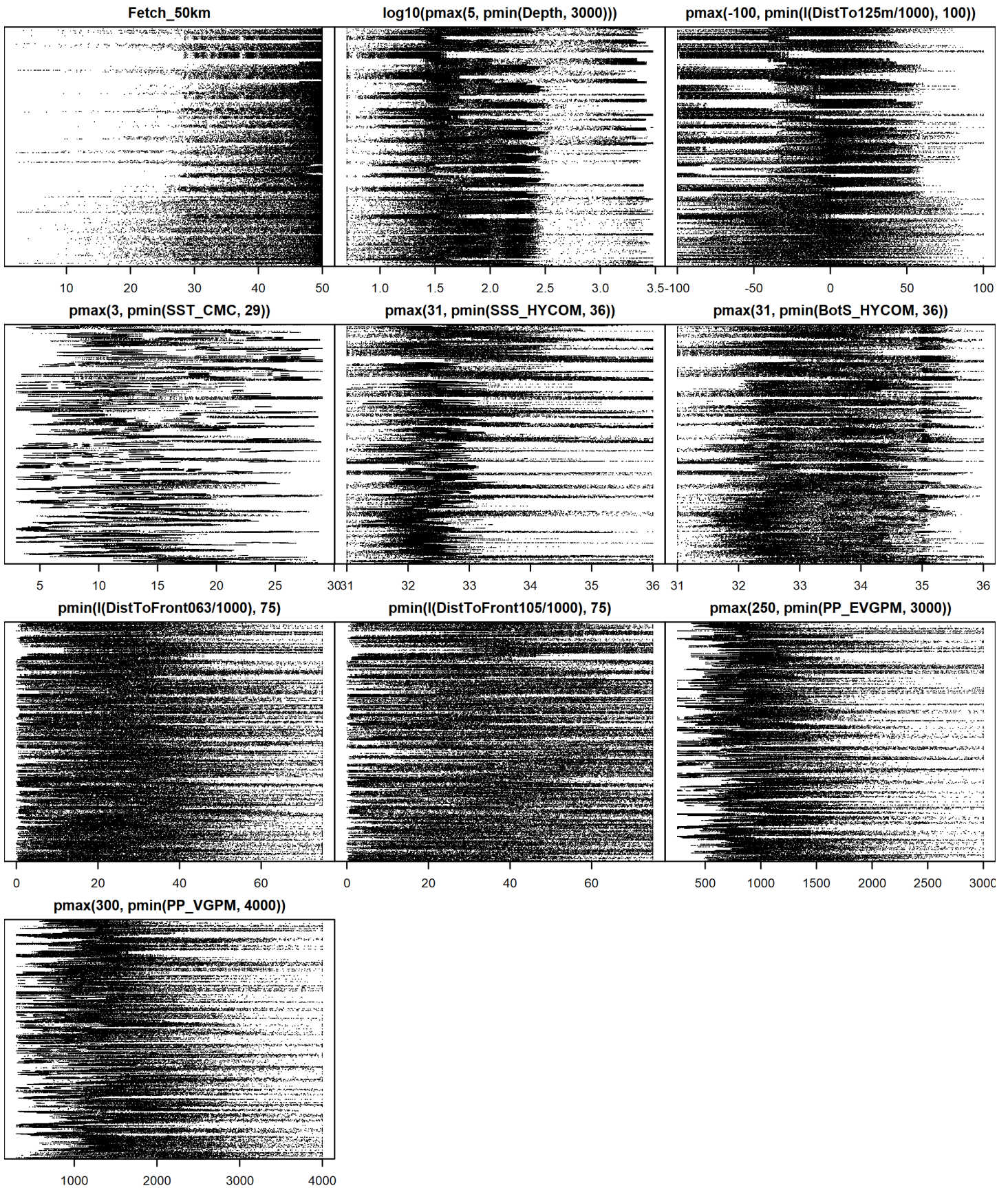
Figure 68: Dotplot of the covariates considered during the final model selection step. The final model may have included only a subset of the covariates shown here (see Figure 63), and additional covariates may have been considered in preceding selection steps. Covariates are transformed and Winsorized as shown in Figure 65. This plot is used to check for suspicious patterns and outliers in the data. Points are ordered vertically by segment ID, sequentially in time.

5.3 Extrapolation Diagnostics

5.3.1 Univariate Extrapolation

(a) Depth covariate

(b) DistTo125m covariate
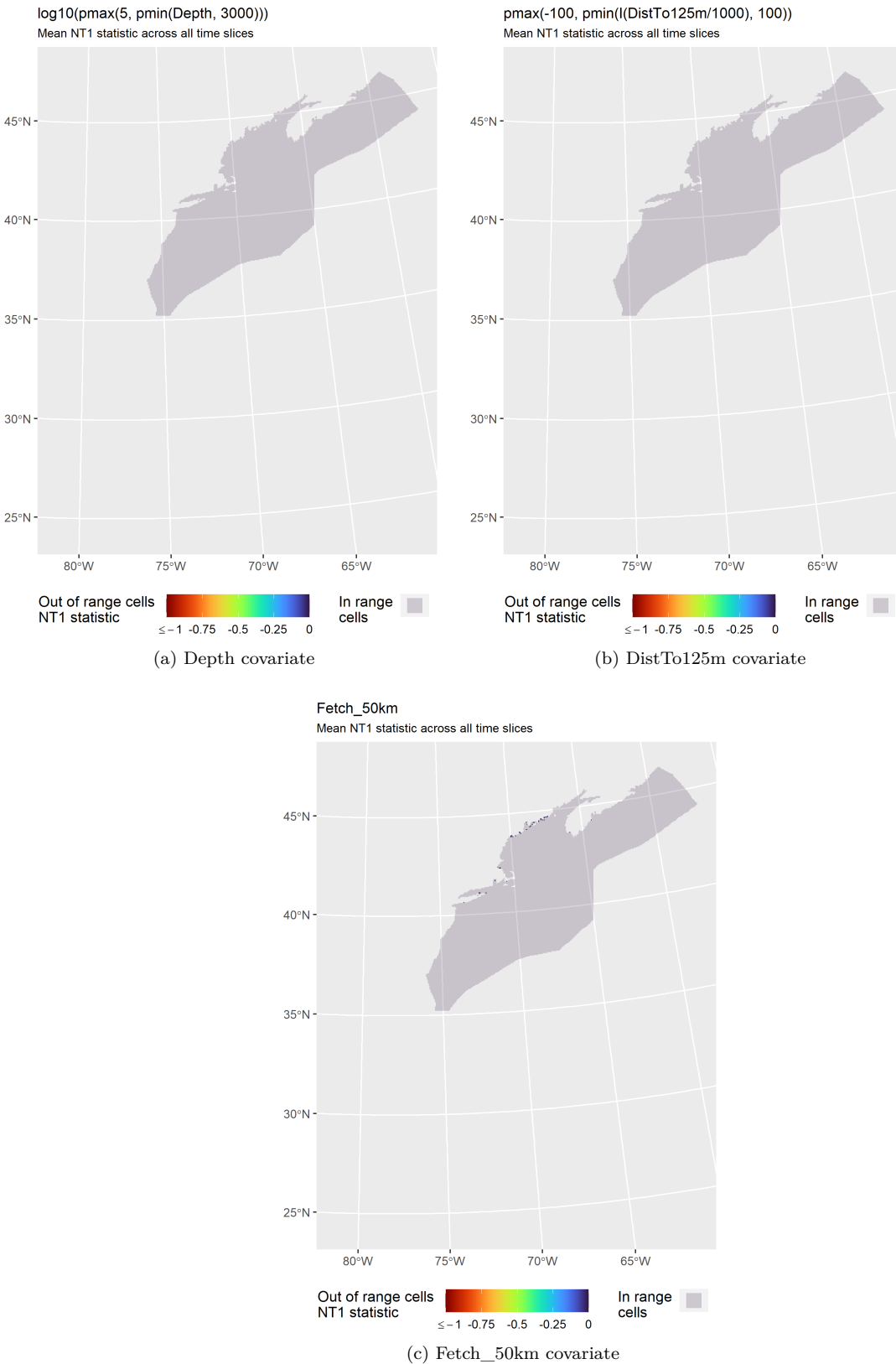

(c) Fetch_50km covariate

Figure 69: NT1 statistic (Mesgaran et al. (2014)) for static covariates used in the model for the region North of Gulf Stream. Areas outside the sampled range of a covariate appear in color, indicating univariate extrapolation of that covariate occurred there. Areas within the sampled range appear in gray, indicating it did not occur.
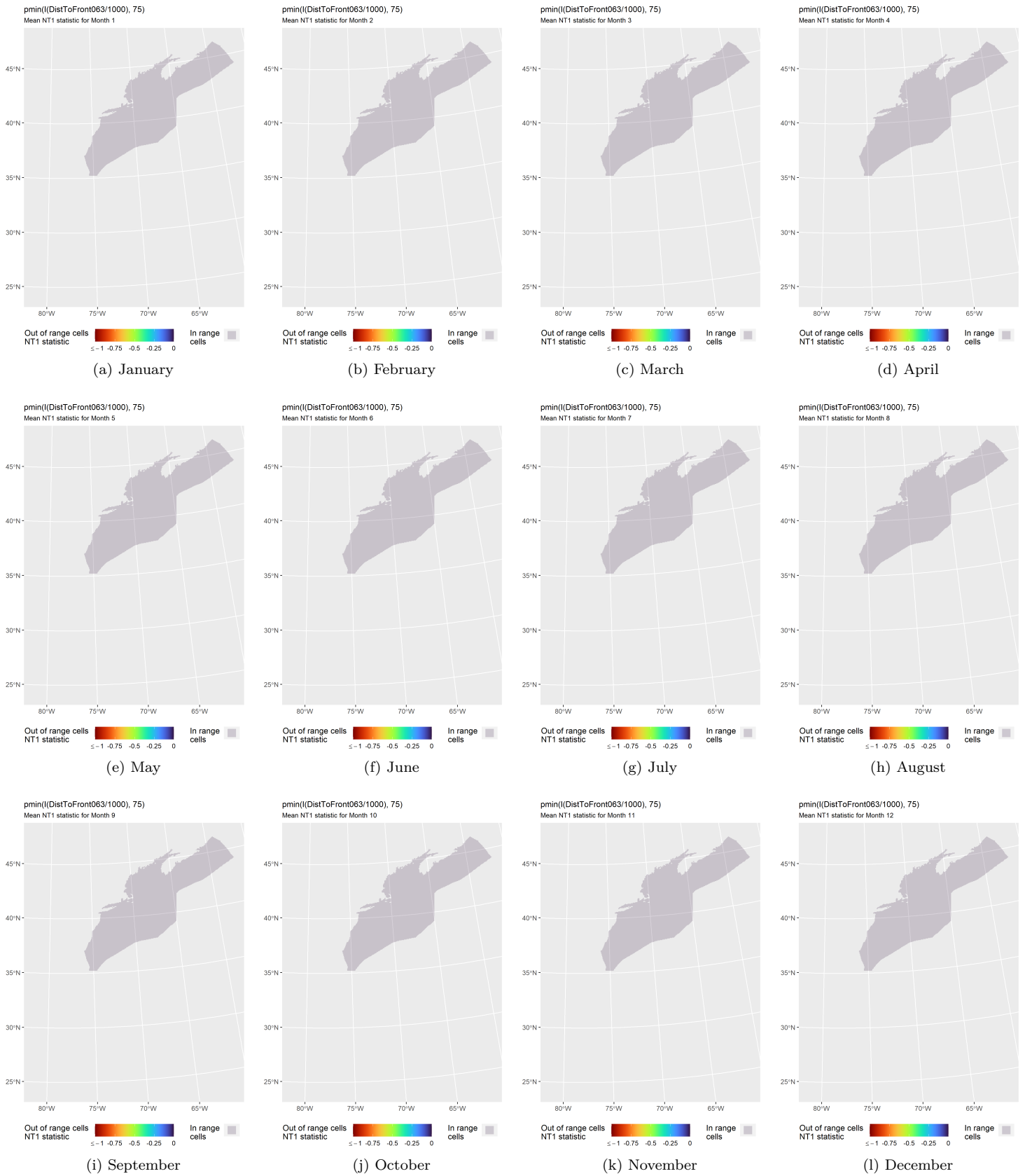
Figure 70: NT1 statistic (Mesgaran et al. (2014)) for the DistToFront063 covariate in the model for the region North of Gulf Stream. Areas outside the sampled range of a covariate appear in color, indicating univariate extrapolation of that covariate occurred there during the month. Areas within the sampled range appear in gray, indicating it did not occur.
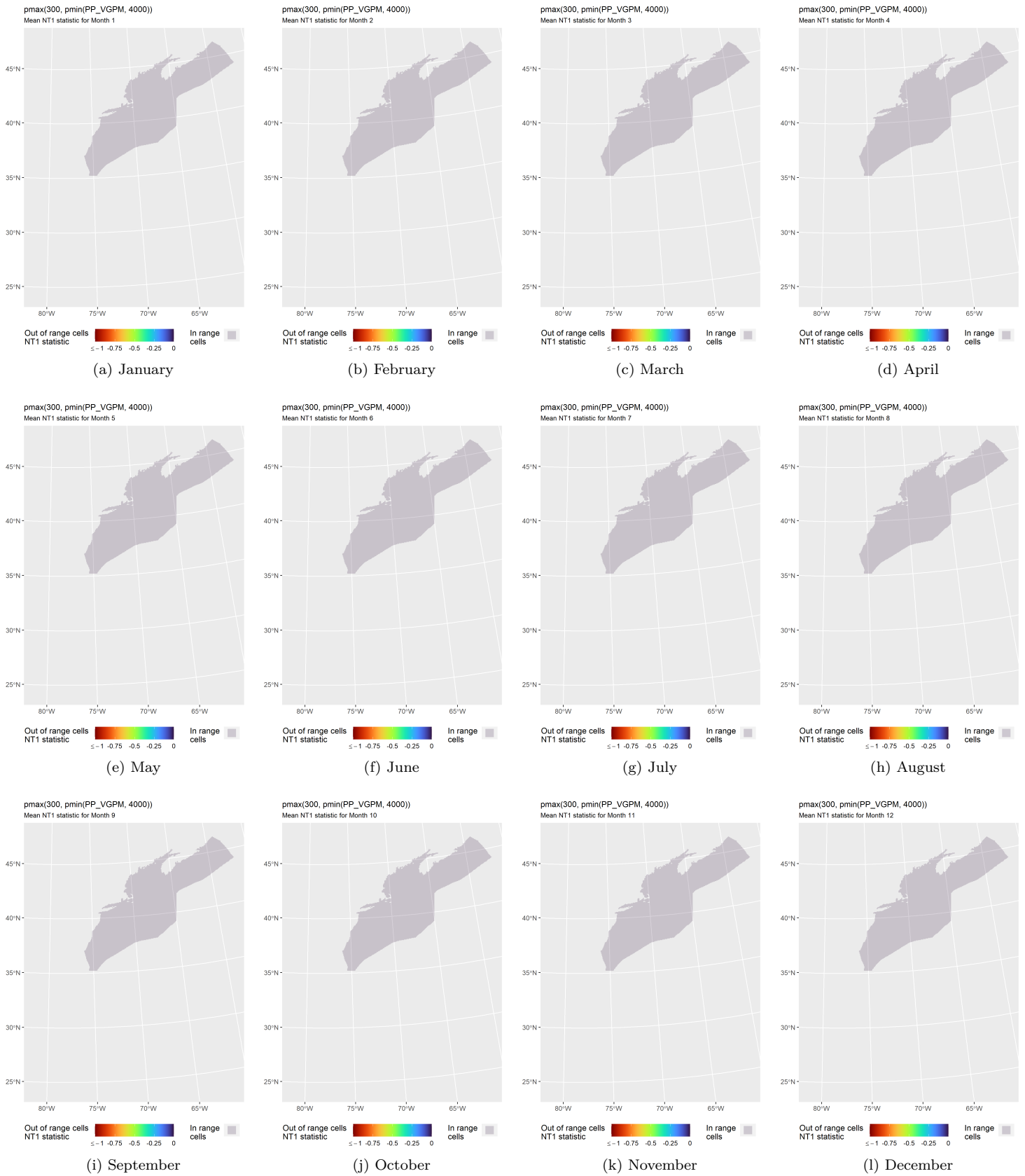
Figure 71: NT1 statistic (Mesgaran et al. (2014)) for the PP_VGPM covariate in the model for the region North of Gulf Stream. Areas outside the sampled range of a covariate appear in color, indicating univariate extrapolation of that covariate occurred there during the month. Areas within the sampled range appear in gray, indicating it did not occur.

Figure 72: NT1 statistic (Mesgaran et al. (2014)) for the SSS_HYCOM covariate in the model for the region North of Gulf Stream. Areas outside the sampled range of a covariate appear in color, indicating univariate extrapolation of that covariate occurred there during the month. Areas within the sampled range appear in gray, indicating it did not occur.
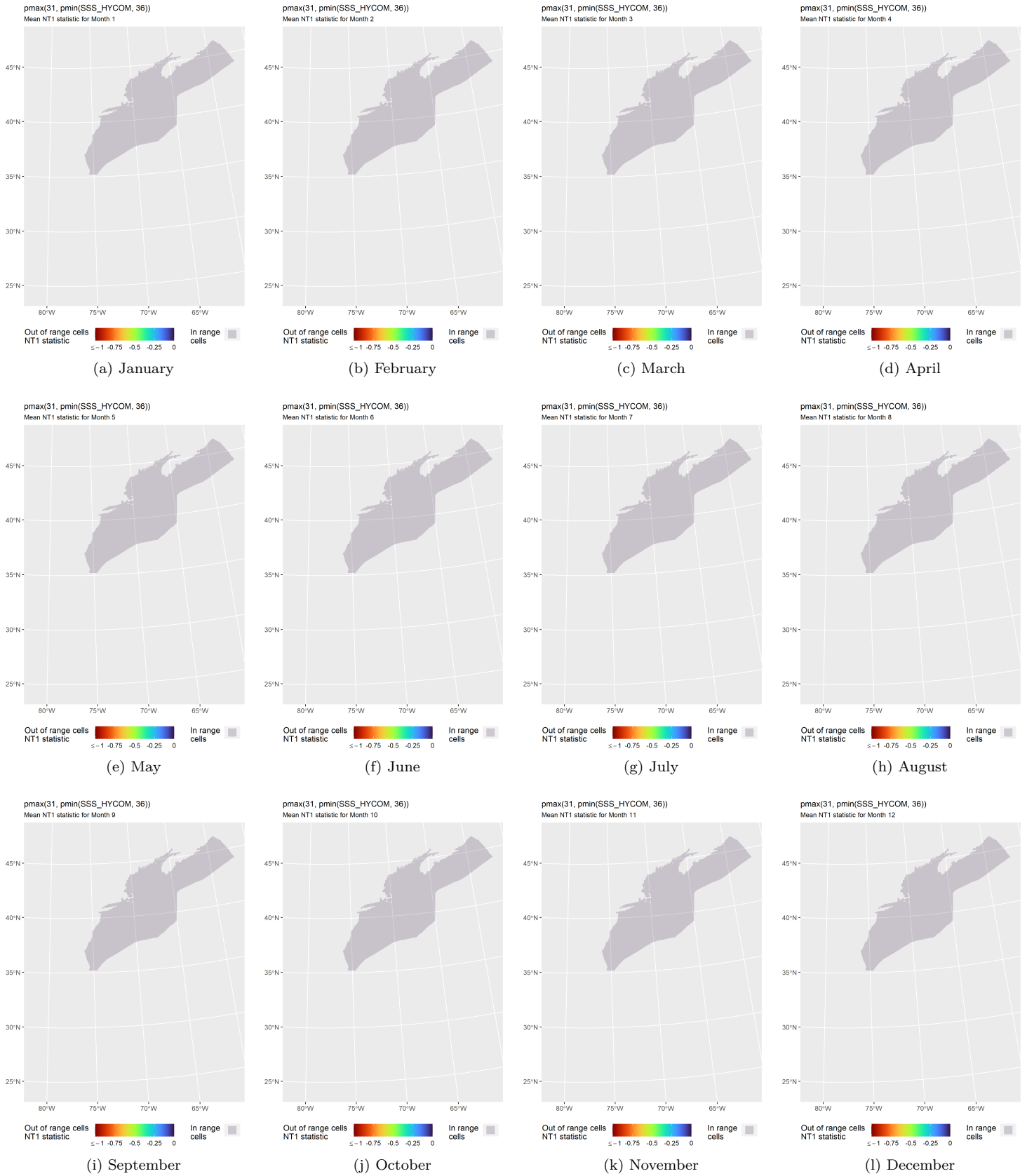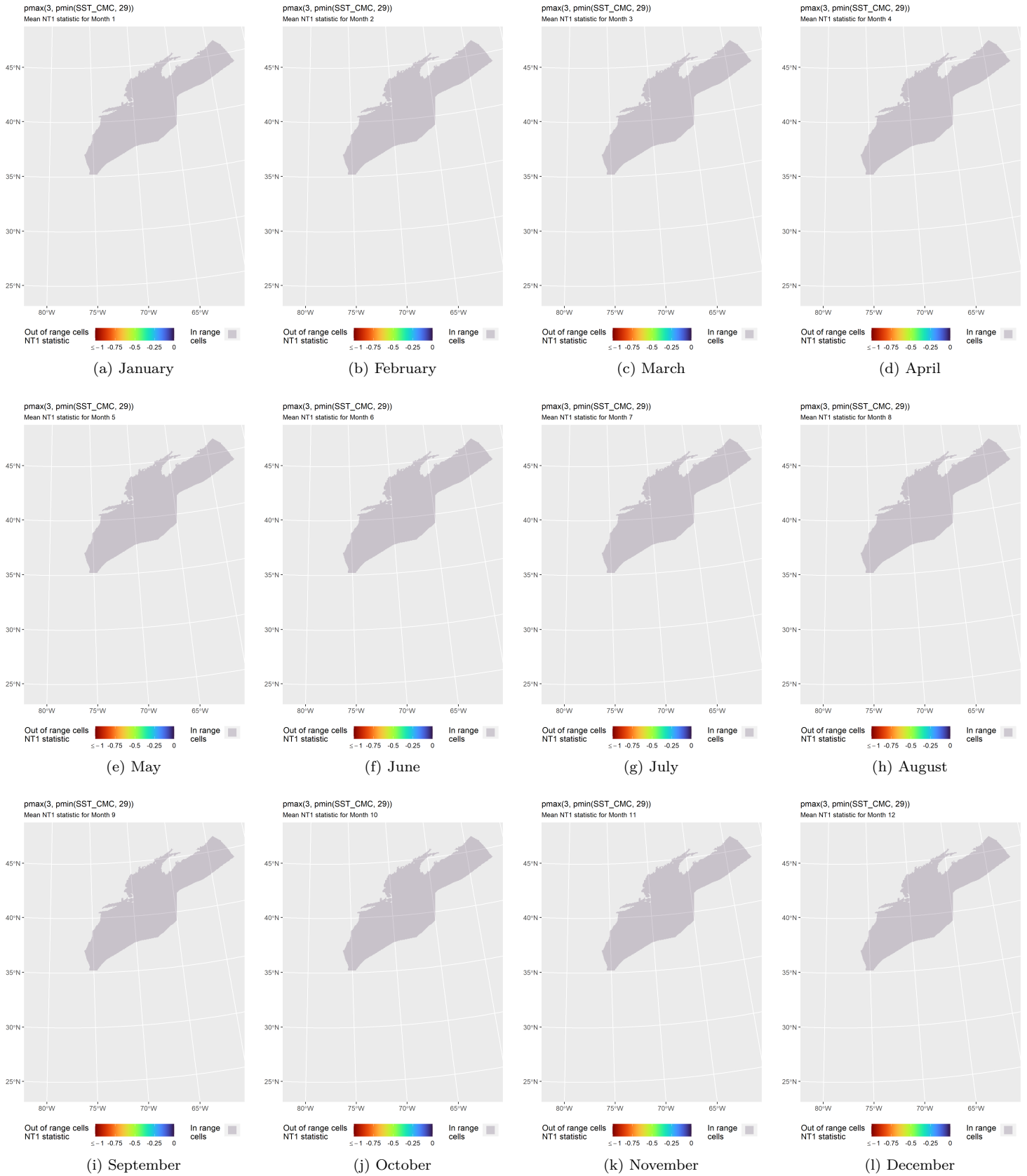
Figure 73: NT1 statistic (Mesgaran et al. (2014)) for the SST_CMC covariate in the model for the region North of Gulf Stream. Areas outside the sampled range of a covariate appear in color, indicating univariate extrapolation of that covariate occurred there during the month. Areas within the sampled range appear in gray, indicating it did not occur.
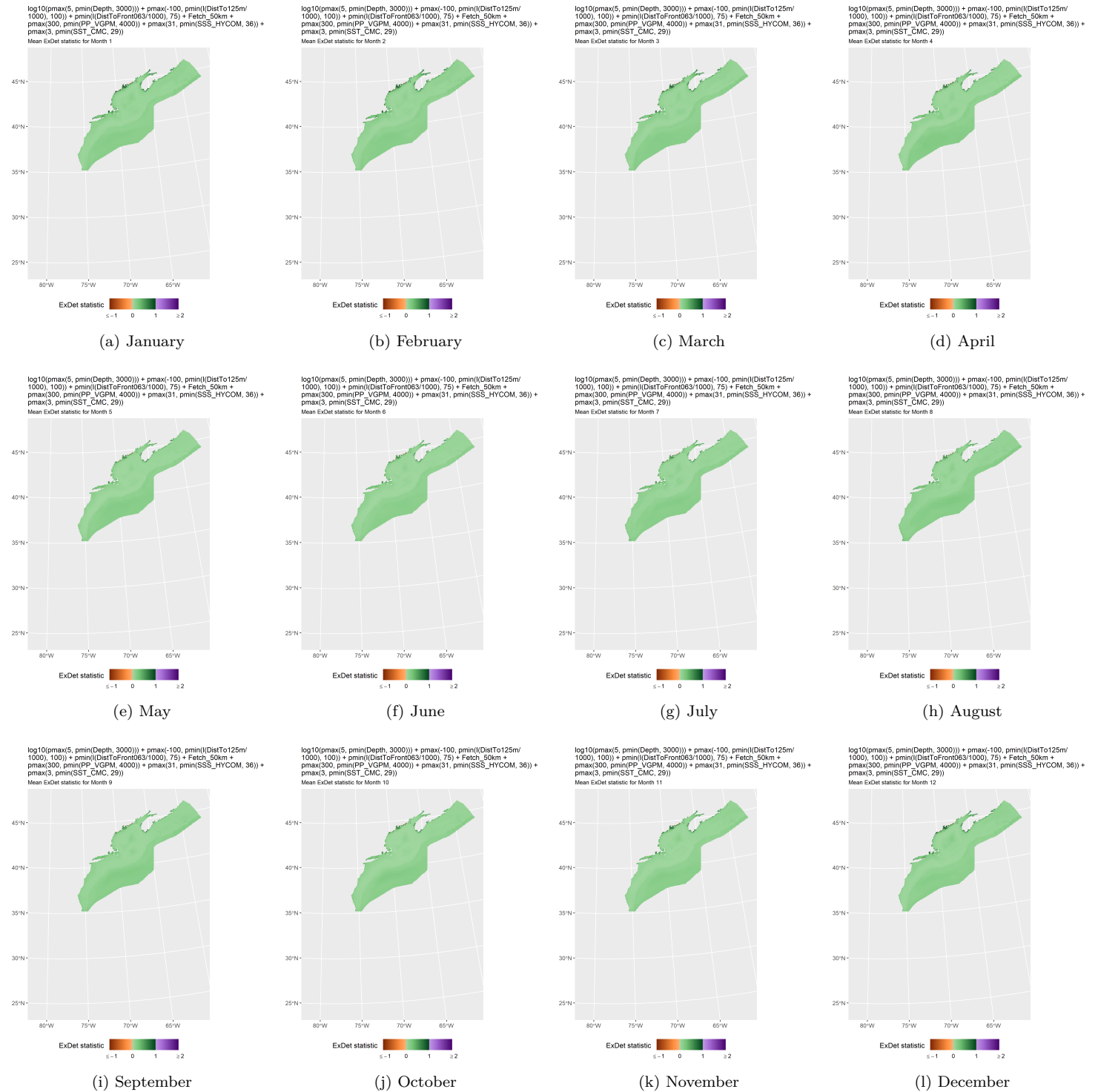
5.3.2 Multivariate Extrapolation

Figure 74: ExDet statistic (Mesgaran et al. (2014)) for all of the covariates used in the model for the region North of Gulf Stream. Areas in orange (ExDet < 0) required univariate extrapolation of one or more covariates (see previous section). Areas in purple (ExDet > 1), did not require univariate extrapolation but did require multivariate extrapolation, by virtue of having novel combinations of covariates not represented in the survey data, according to the NT2 statistic (Mesgaran et al. (2014)). Areas in green ($0 \geq \text{ExDet} \leq 1$) did not require either type of extrapolation.

6 Predictions

Based on our evaluation of this model in the context of what is known of this species (see Section 7), we summarized its predictions into monthly climatological density and uncertainty surfaces, shown in the maps below.
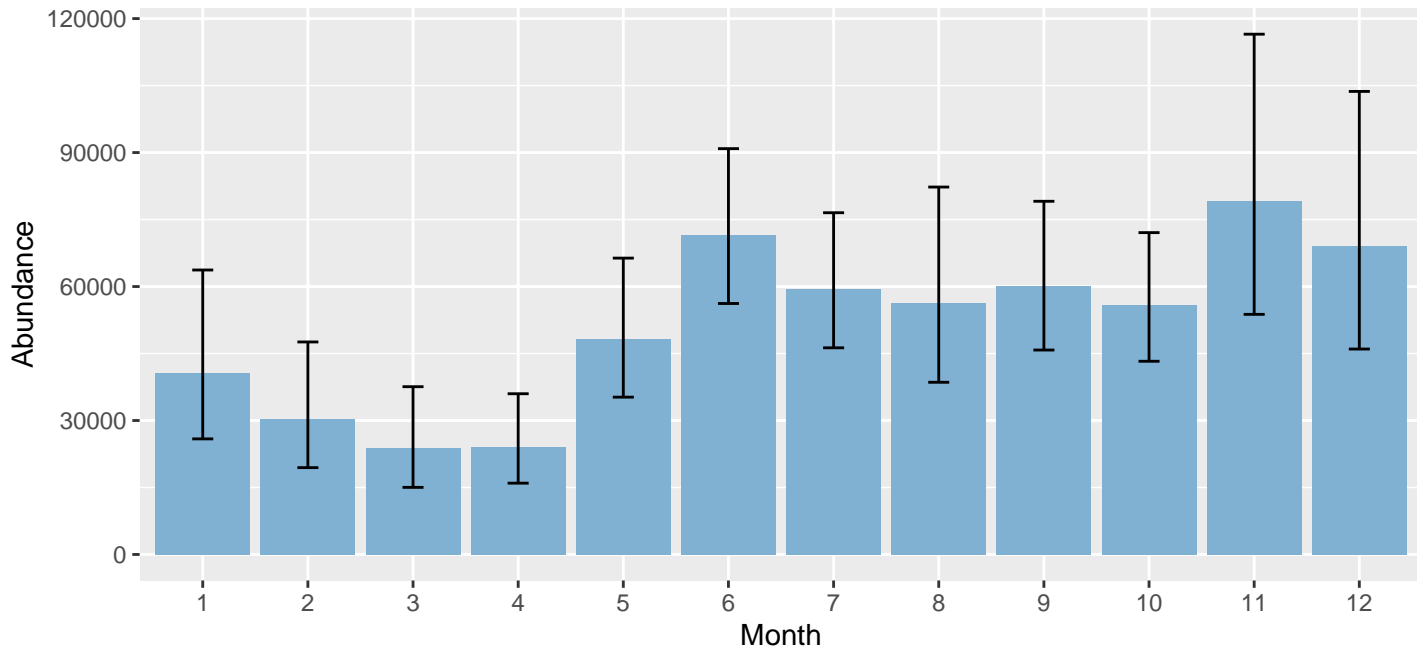
6.1 Summarized Predictions

Figure 75: Mean monthly abundance for the prediction area for 1998-2020. Error bars are a 95% interval, made with a log-normal approximation using the prediction's CV. The CV was estimated with the analytic approach given by Miller et al. (2022), Appendix S1, and accounts both for uncertainty in model parameter estimates and for temporal variability in dynamic covariates.

Table 28: Mean monthly abundance and density for the prediction area for 1998-2020. CV and intervals estimated as described for the previous figure.

Month	Abundance	CV	95% Interval	Area (km^2)	Density (individuals / 100 km^2)
1	40,607	0.233	25,886 - 63,700	1,272,925	3.19
2	30,422	0.231	19,447 - 47,591	1,272,925	2.39
3	23,758	0.237	15,024 - 37,567	1,272,925	1.87
4	23,977	0.210	15,972 - 35,993	1,272,925	1.88
5	48,350	0.163	35,227 - 66,363	1,272,925	3.80
6	71,466	0.123	56,202 - 90,875	1,272,925	5.61
7	59,507	0.129	46,273 - 76,526	1,272,925	4.67
8	56,328	0.195	38,563 - 82,277	1,272,925	4.43
9	60,171	0.140	45,778 - 79,089	1,272,925	4.73
10	55,843	0.131	43,266 - 72,076	1,272,925	4.39
11	79,149	0.199	53,771 - 116,505	1,272,925	6.22
12	69,066	0.210	46,004 - 103,690	1,272,925	5.43

Figure 76: Survey effort and observations (top left), predicted density with observations (top right), predicted density without observations (bottom right), and coefficient of variation of predicted density (bottom left), for the month of January for the given era. Variance was estimated with the analytic approach given by Miller et al. (2022), Appendix S1, and accounts both for uncertainty in model parameter estimates and for temporal variability in dynamic covariates.
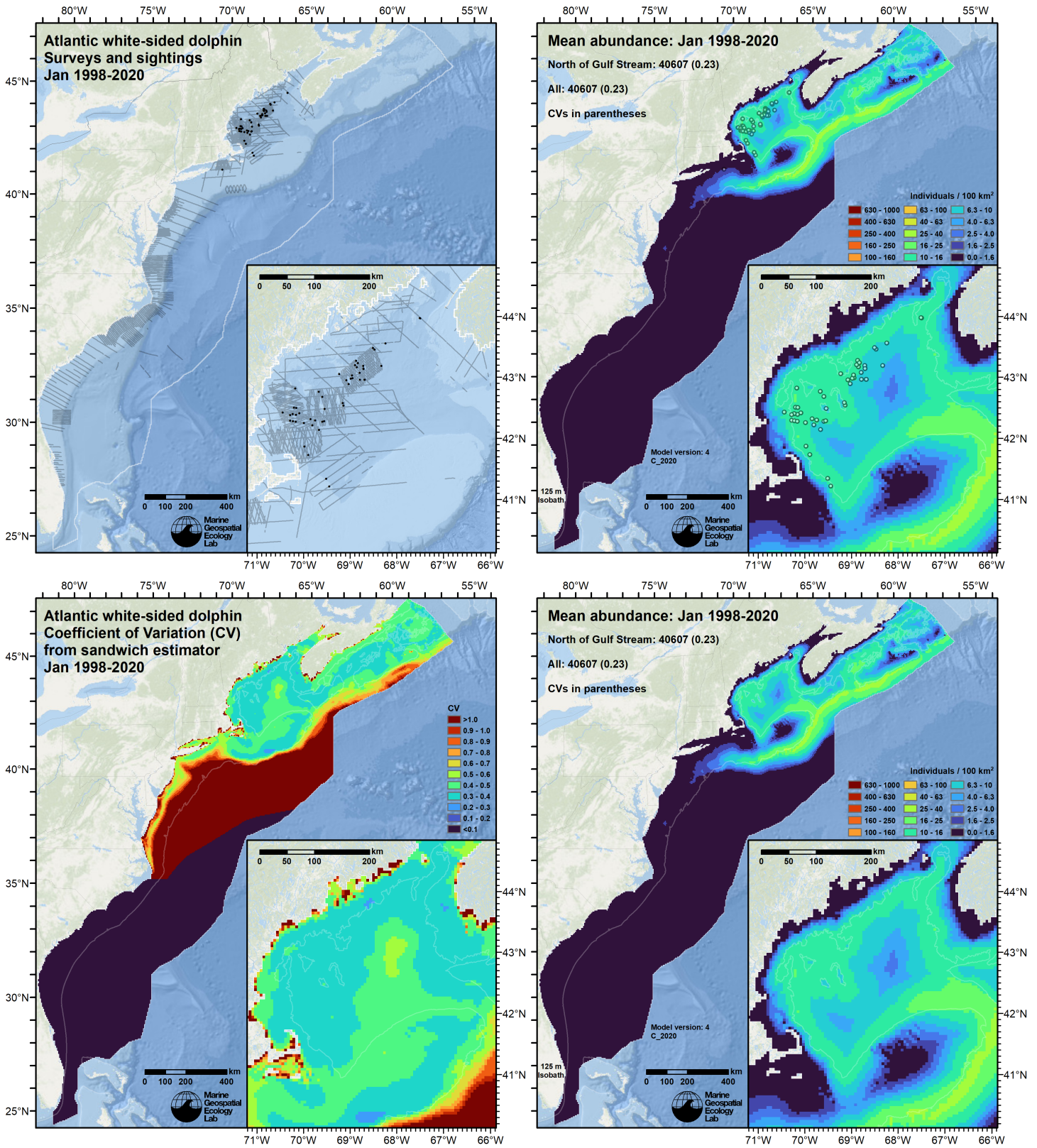
Figure 77: Survey effort and observations (top left), predicted density with observations (top right), predicted density without observations (bottom right), and coefficient of variation of predicted density (bottom left), for the month of February for the given era. Variance was estimated with the analytic approach given by Miller et al. (2022), Appendix S1, and accounts both for uncertainty in model parameter estimates and for temporal variability in dynamic covariates.
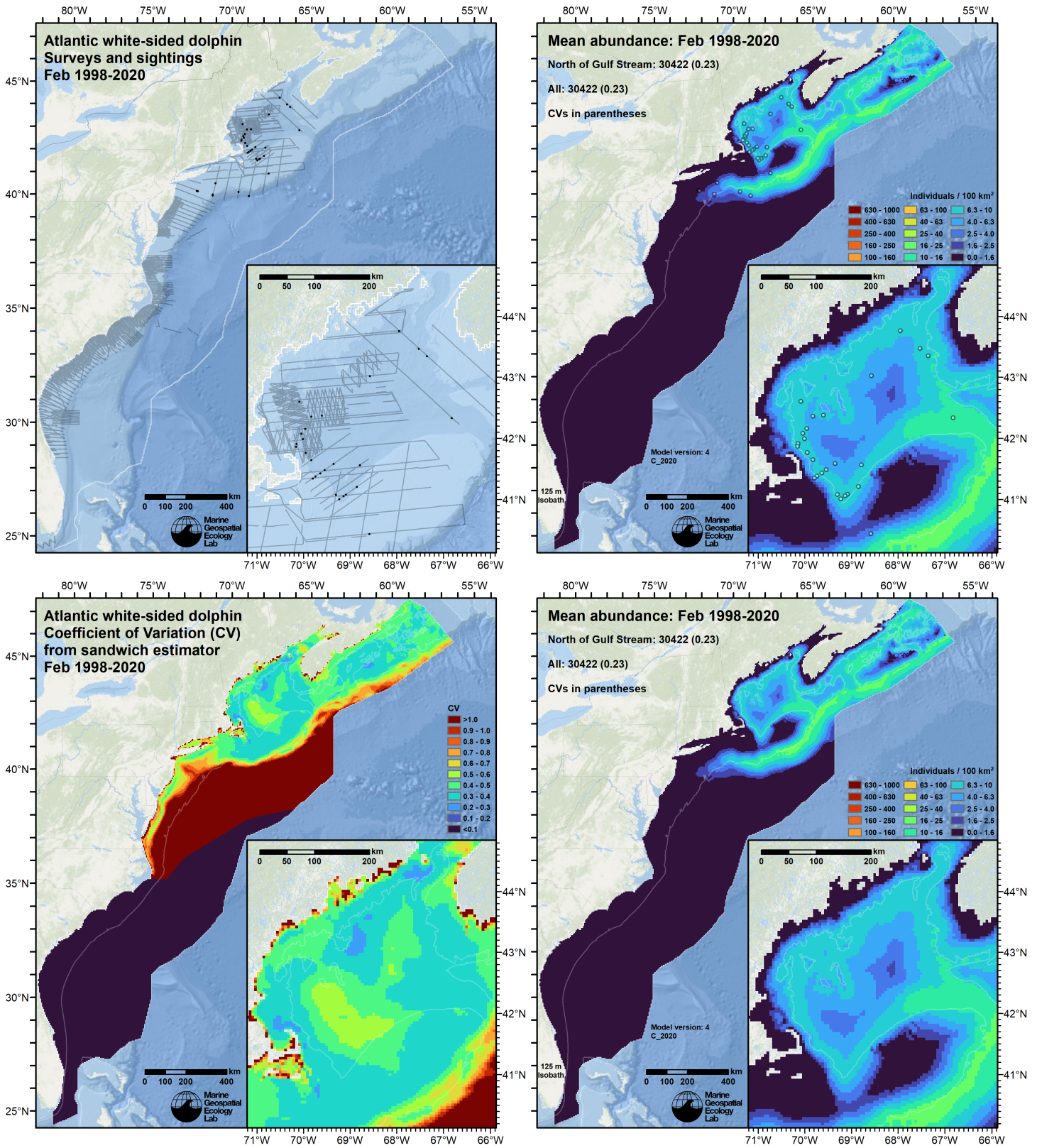
Figure 78: Survey effort and observations (top left), predicted density with observations (top right), predicted density without observations (bottom right), and coefficient of variation of predicted density (bottom left), for the month of March for the given era. Variance was estimated with the analytic approach given by Miller et al. (2022), Appendix S1, and accounts both for uncertainty in model parameter estimates and for temporal variability in dynamic covariates.
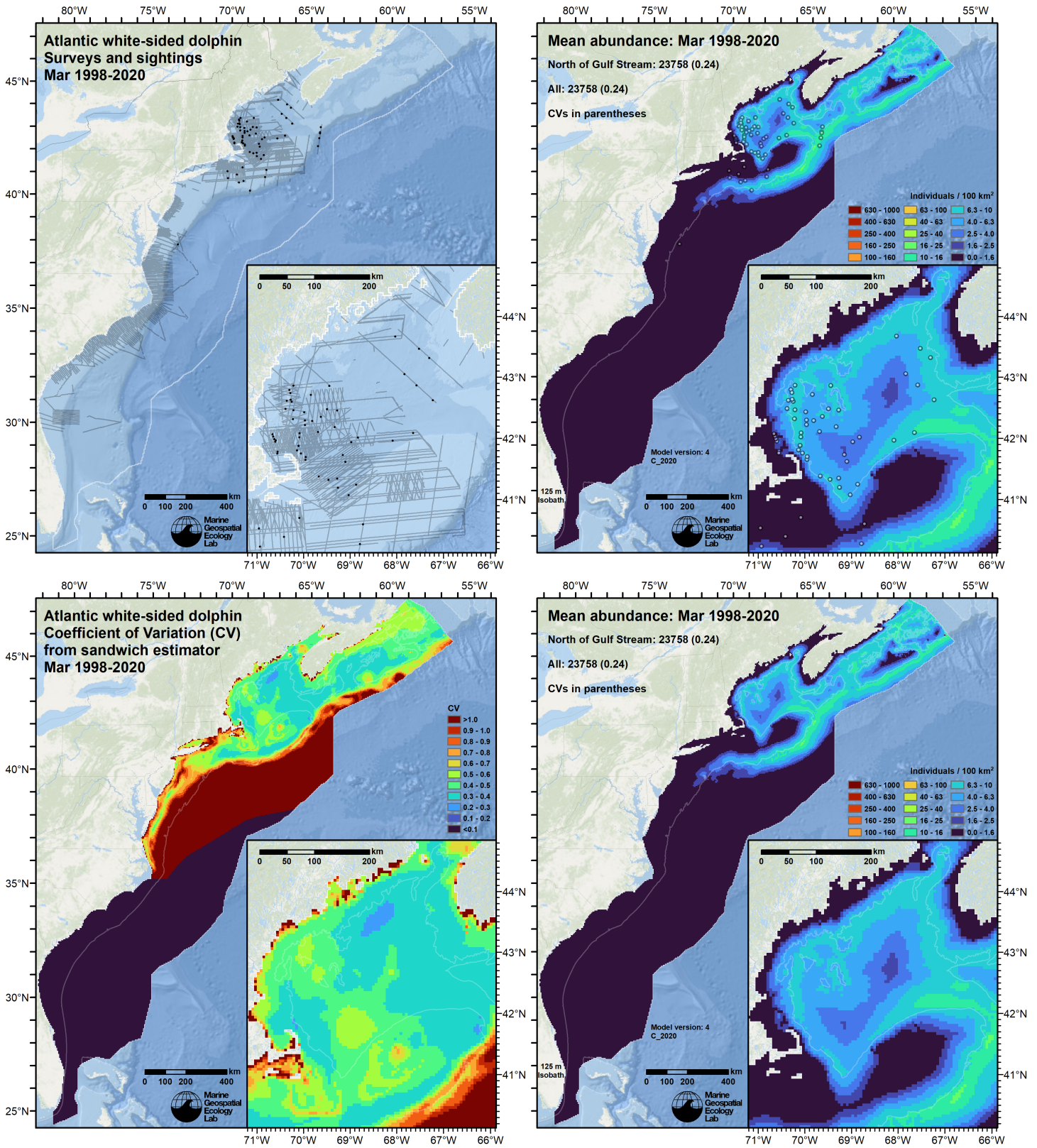
Figure 79: Survey effort and observations (top left), predicted density with observations (top right), predicted density without observations (bottom right), and coefficient of variation of predicted density (bottom left), for the month of April for the given era. Variance was estimated with the analytic approach given by Miller et al. (2022), Appendix S1, and accounts both for uncertainty in model parameter estimates and for temporal variability in dynamic covariates.

Figure 80: Survey effort and observations (top left), predicted density with observations (top right), predicted density without observations (bottom right), and coefficient of variation of predicted density (bottom left), for the month of May for the given era. Variance was estimated with the analytic approach given by Miller et al. (2022), Appendix S1, and accounts both for uncertainty in model parameter estimates and for temporal variability in dynamic covariates.
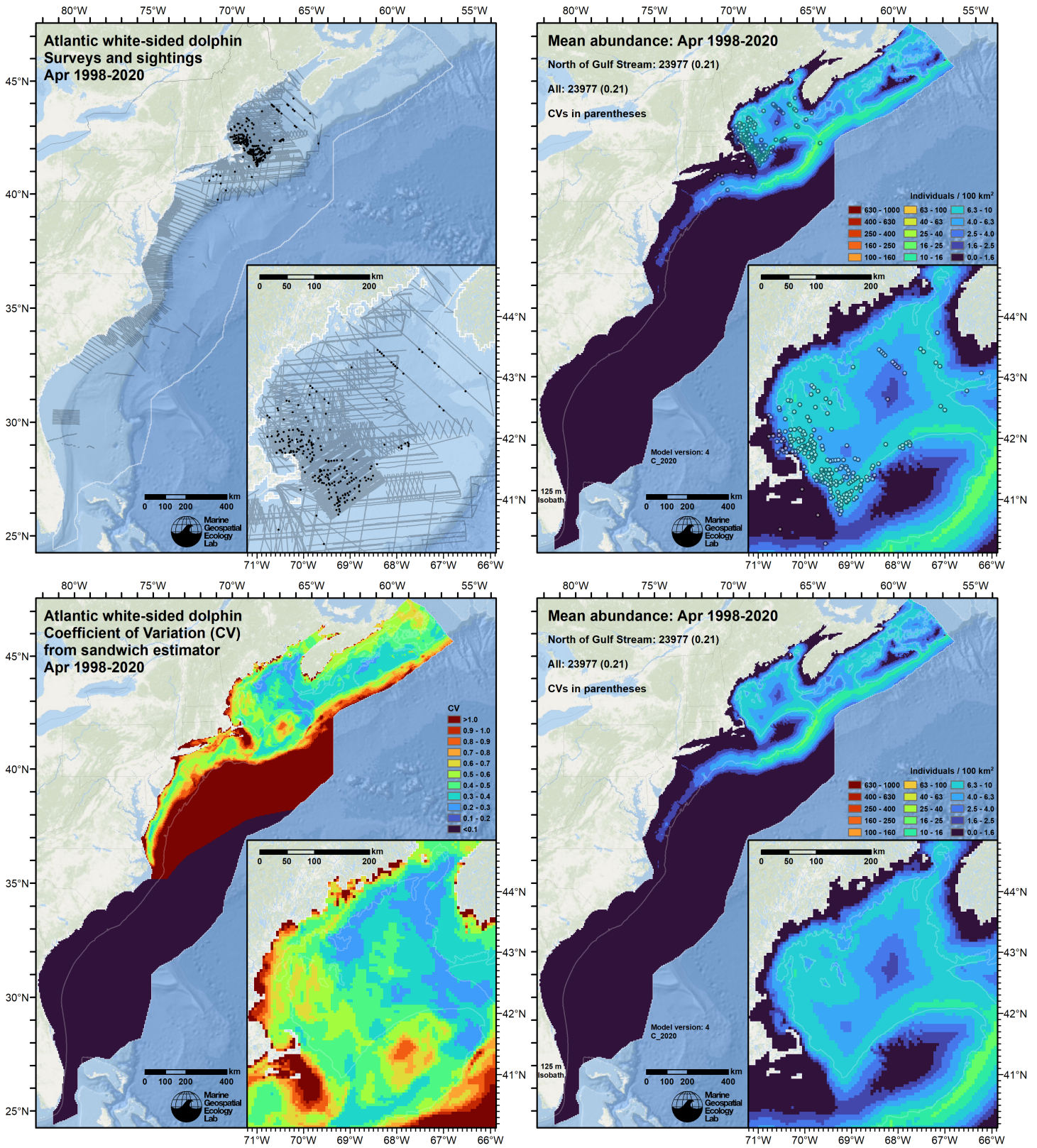
Figure 81: Survey effort and observations (top left), predicted density with observations (top right), predicted density without observations (bottom right), and coefficient of variation of predicted density (bottom left), for the month of June for the given era. Variance was estimated with the analytic approach given by Miller et al. (2022), Appendix S1, and accounts both for uncertainty in model parameter estimates and for temporal variability in dynamic covariates.
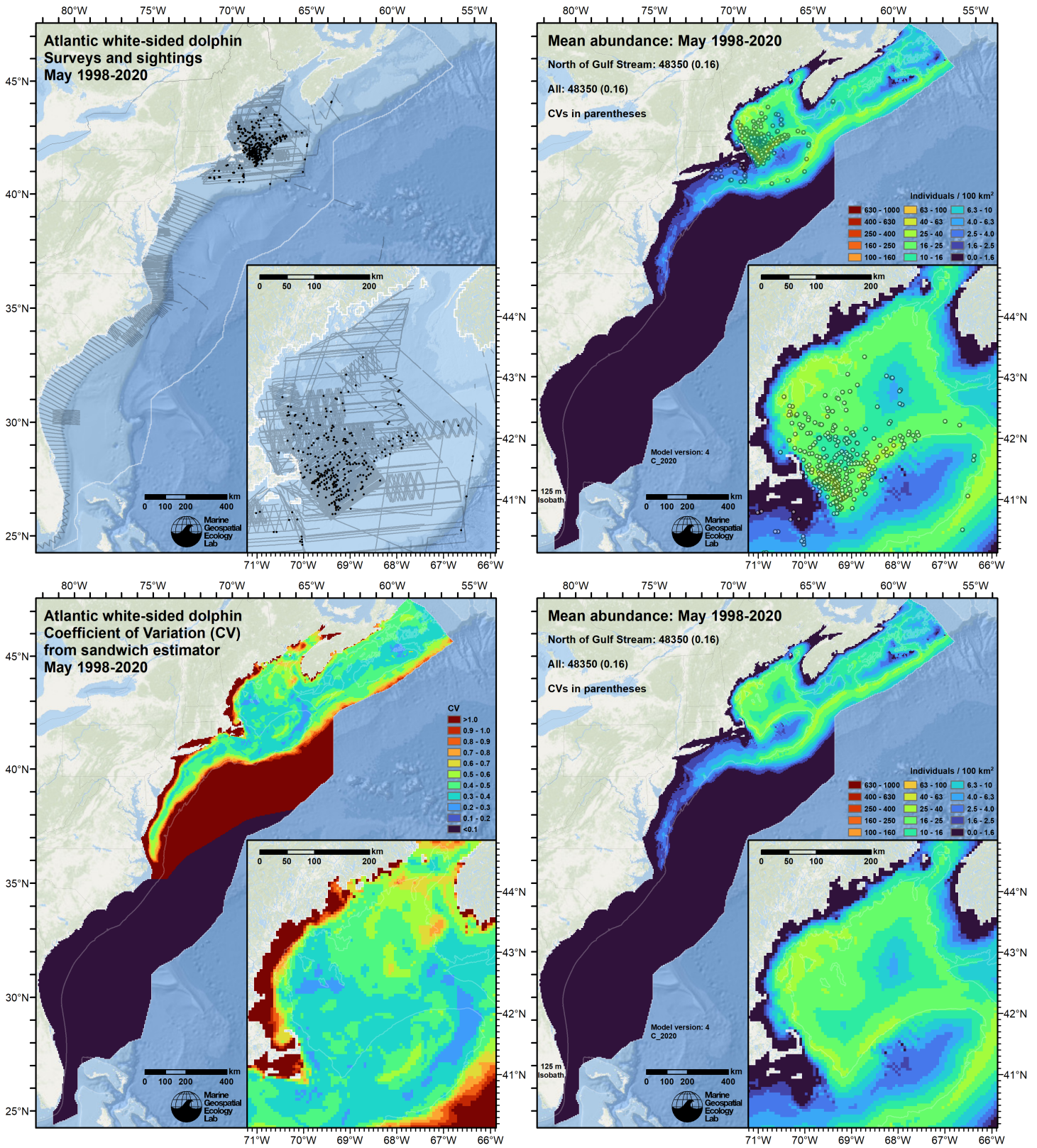
Figure 82: Survey effort and observations (top left), predicted density with observations (top right), predicted density without observations (bottom right), and coefficient of variation of predicted density (bottom left), for the month of July for the given era. Variance was estimated with the analytic approach given by Miller et al. (2022), Appendix S1, and accounts both for uncertainty in model parameter estimates and for temporal variability in dynamic covariates.
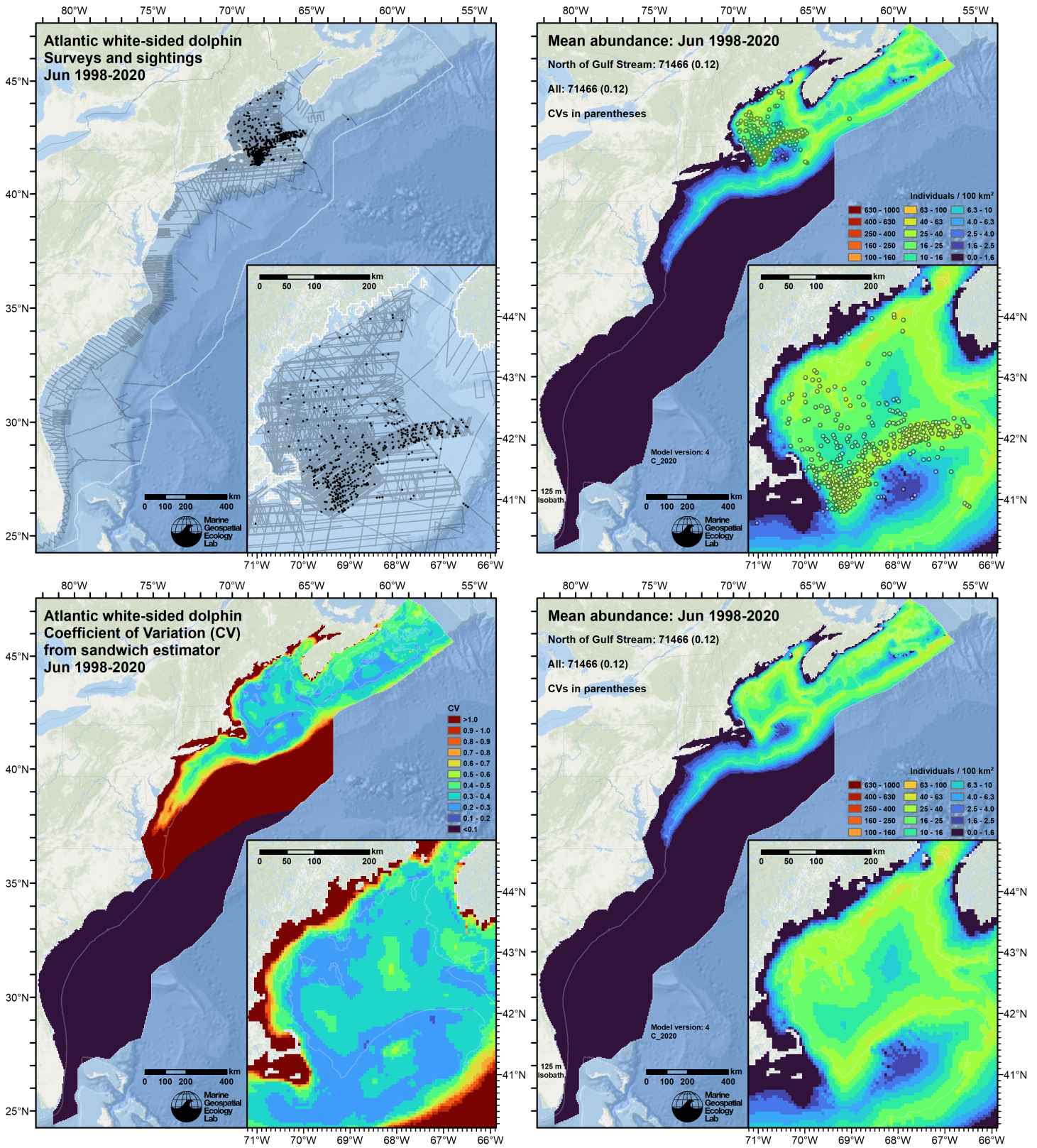
Figure 83: Survey effort and observations (top left), predicted density with observations (top right), predicted density without observations (bottom right), and coefficient of variation of predicted density (bottom left), for the month of August for the given era. Variance was estimated with the analytic approach given by Miller et al. (2022), Appendix S1, and accounts both for uncertainty in model parameter estimates and for temporal variability in dynamic covariates.
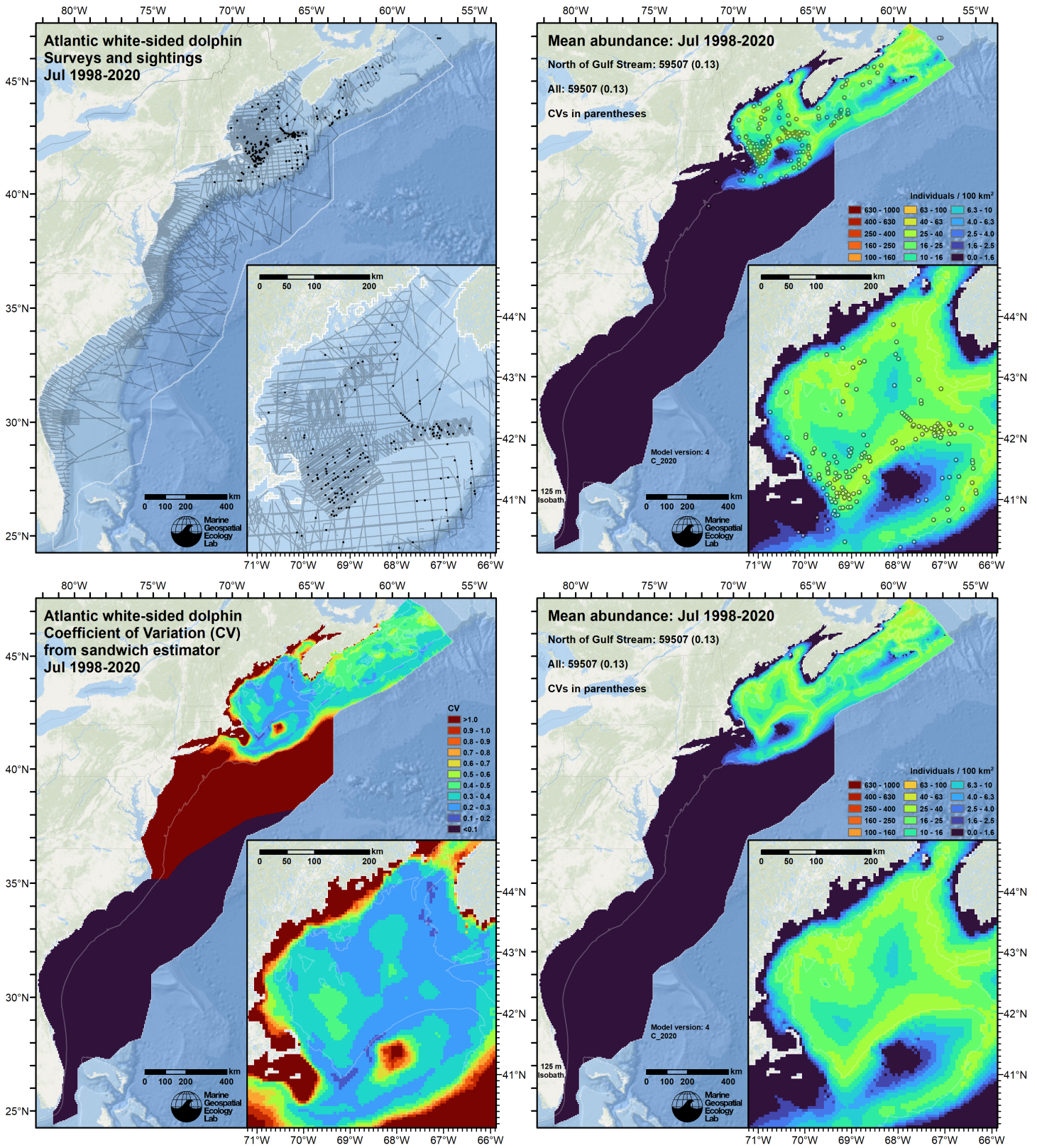
Figure 84: Survey effort and observations (top left), predicted density with observations (top right), predicted density without observations (bottom right), and coefficient of variation of predicted density (bottom left), for the month of September for the given era. Variance was estimated with the analytic approach given by Miller et al. (2022), Appendix S1, and accounts both for uncertainty in model parameter estimates and for temporal variability in dynamic covariates.
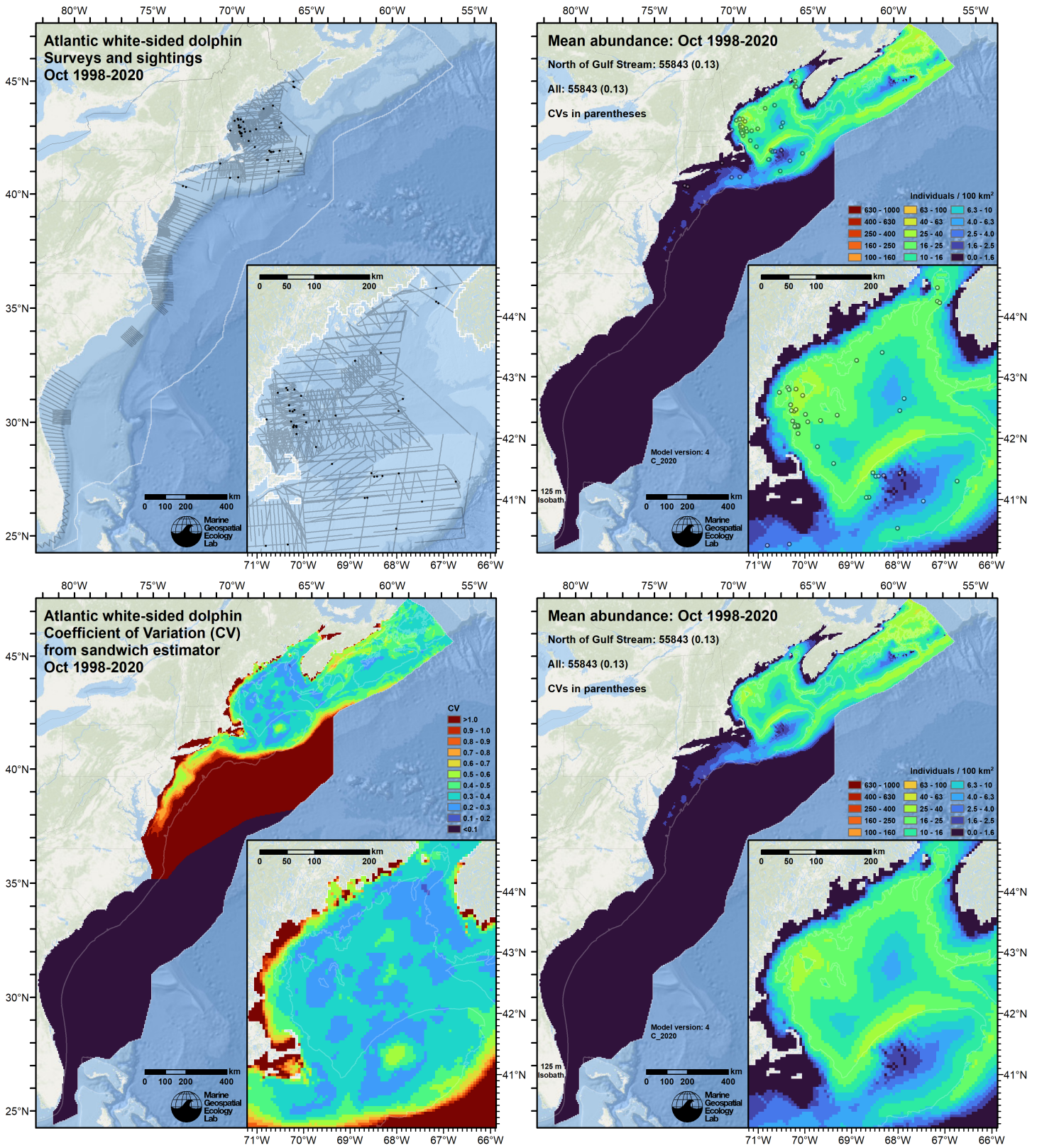
Figure 85: Survey effort and observations (top left), predicted density with observations (top right), predicted density without observations (bottom right), and coefficient of variation of predicted density (bottom left), for the month of October for the given era. Variance was estimated with the analytic approach given by Miller et al. (2022), Appendix S1, and accounts both for uncertainty in model parameter estimates and for temporal variability in dynamic covariates.
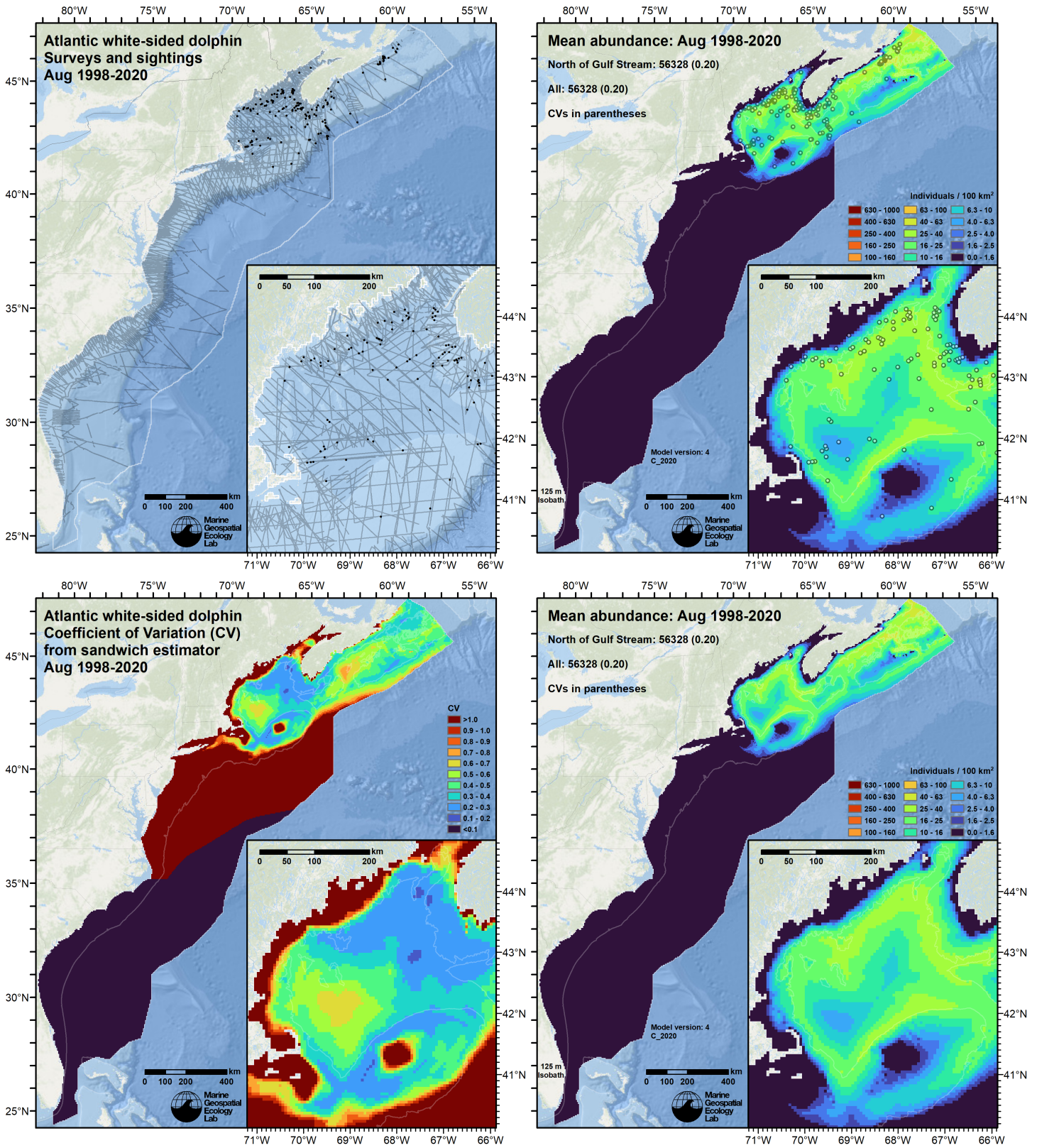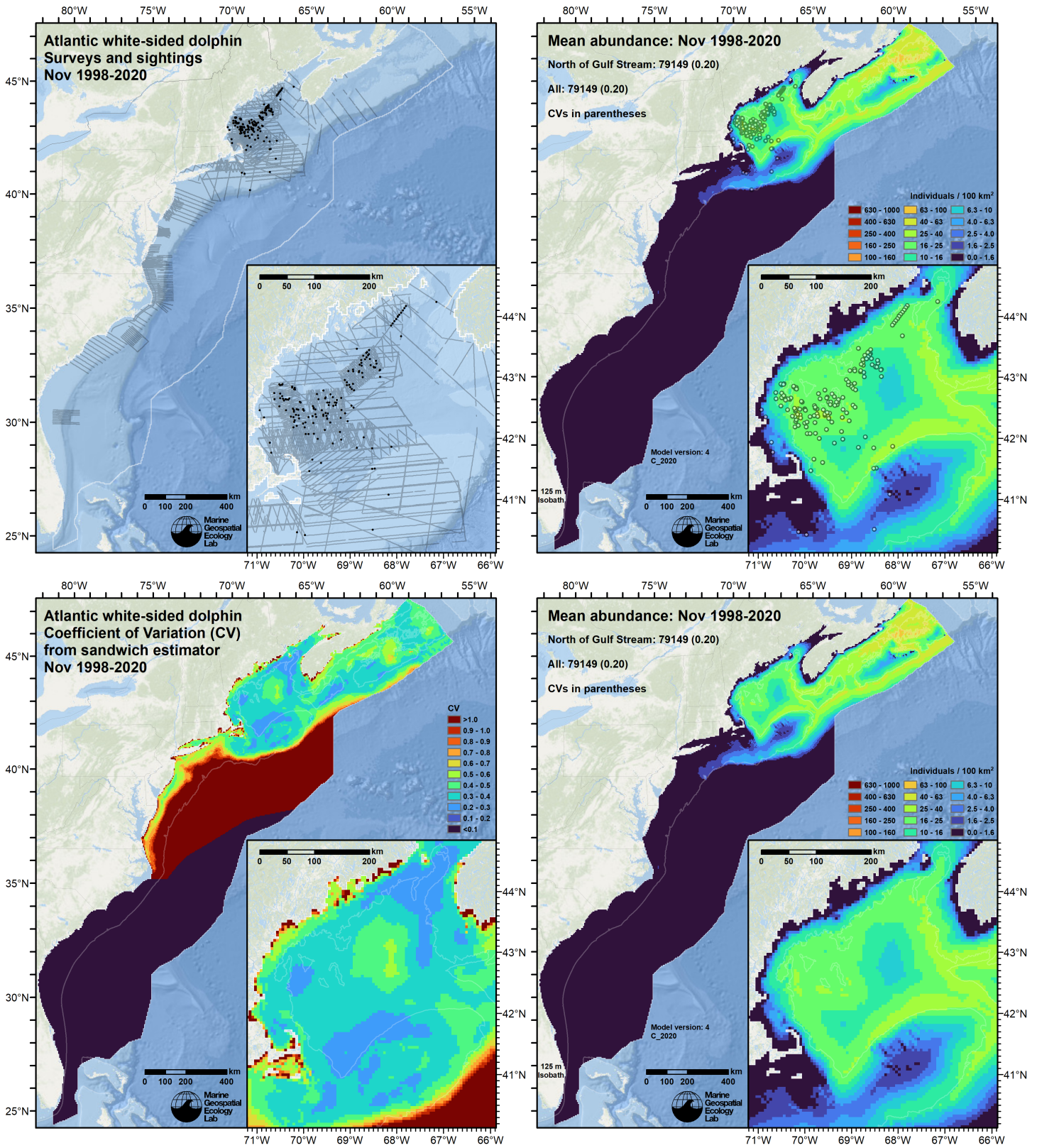
Figure 86: Survey effort and observations (top left), predicted density with observations (top right), predicted density without observations (bottom right), and coefficient of variation of predicted density (bottom left), for the month of November for the given era. Variance was estimated with the analytic approach given by Miller et al. (2022), Appendix S1, and accounts both for uncertainty in model parameter estimates and for temporal variability in dynamic covariates.
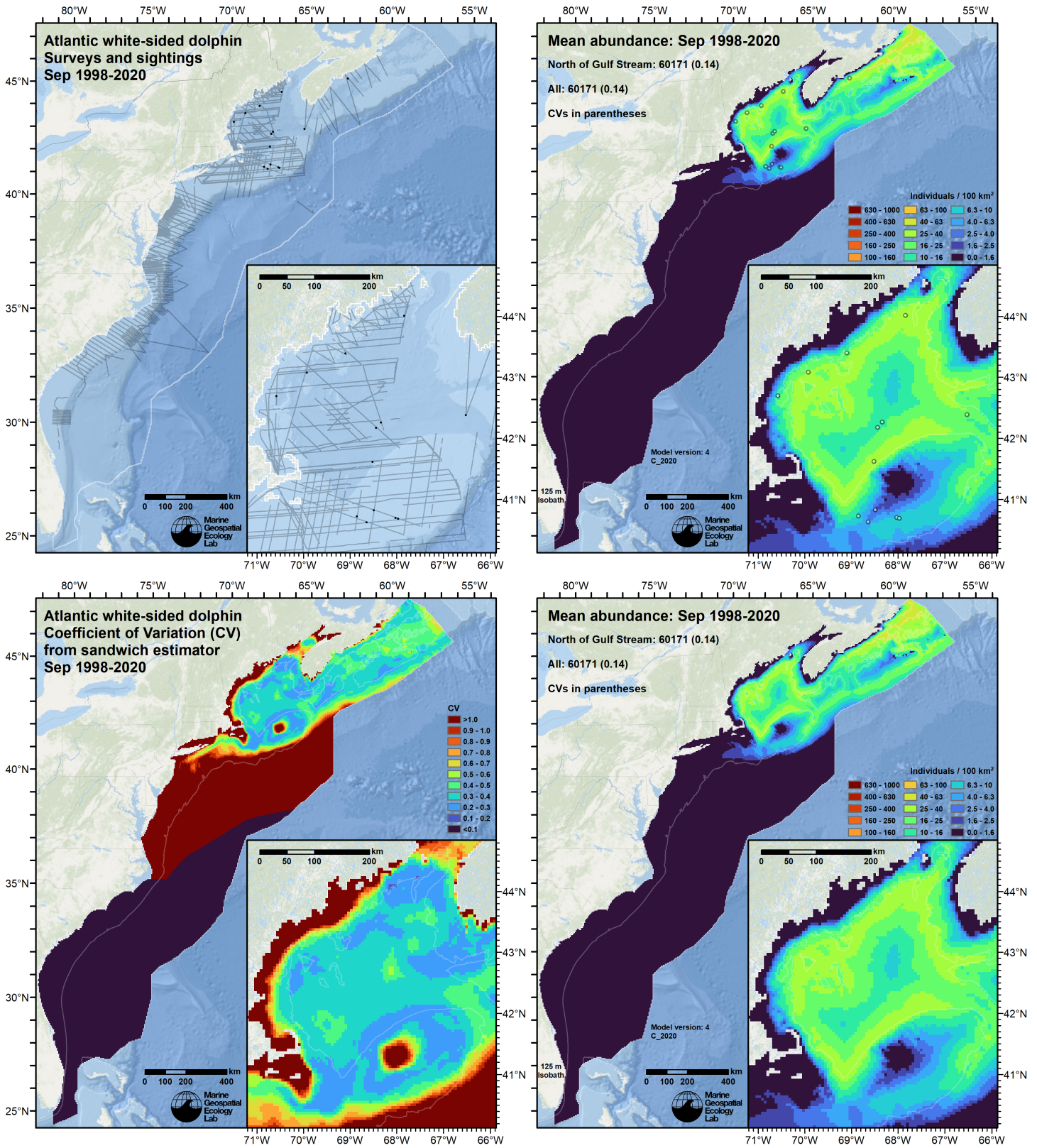
Figure 87: Survey effort and observations (top left), predicted density with observations (top right), predicted density without observations (bottom right), and coefficient of variation of predicted density (bottom left), for the month of December for the given era. Variance was estimated with the analytic approach given by Miller et al. (2022), Appendix S1, and accounts both for uncertainty in model parameter estimates and for temporal variability in dynamic covariates.
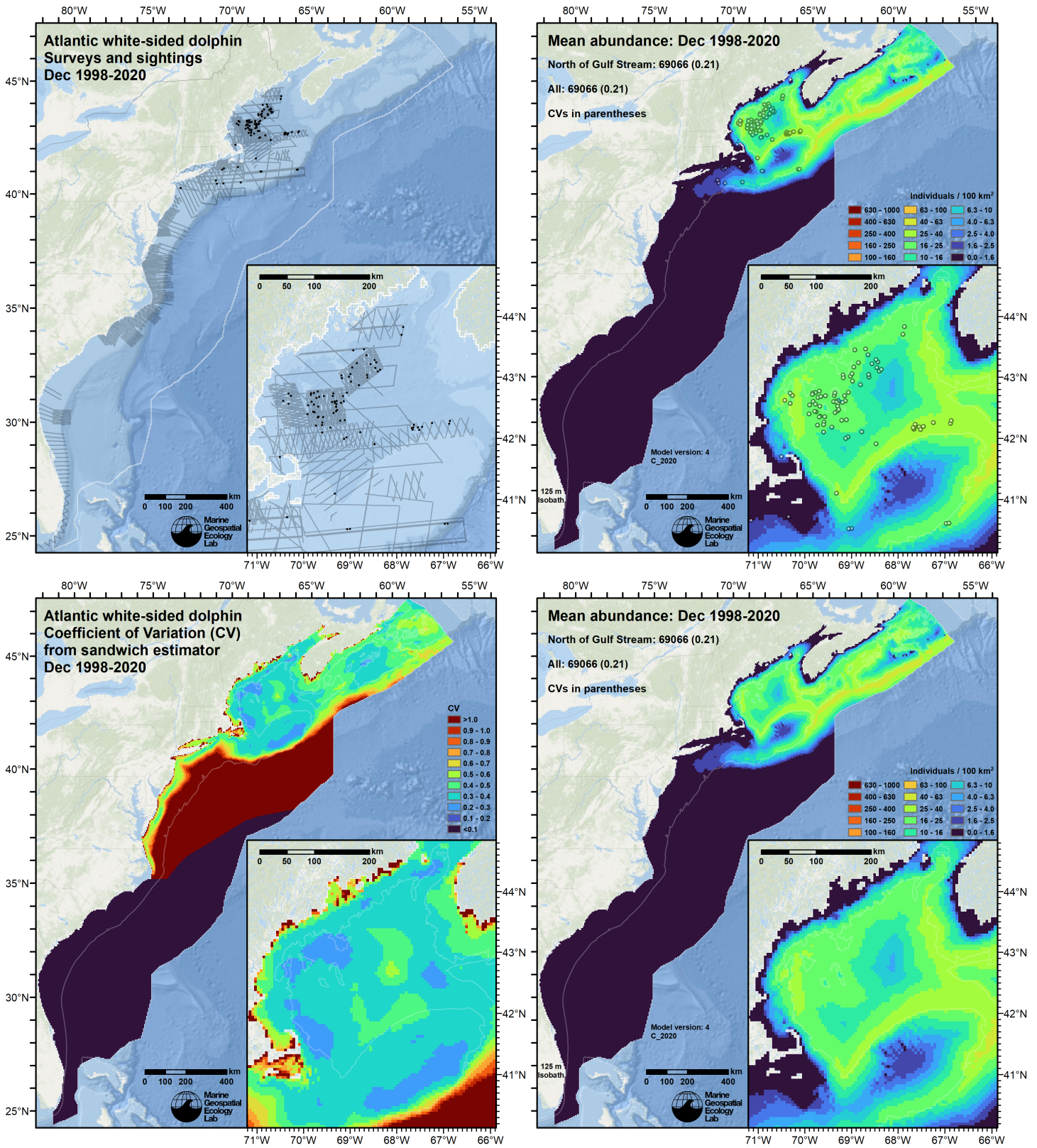
6.2 Abundance Comparisons

6.2.1 NOAA Stock Assessment Report

Table 29: Comparison of regional abundance estimates from the 2021 NOAA Stock Assessment Report (SAR) (Hayes et al. (2022)) to estimates from this density model extracted from roughly comparable zones (Figure 88 below). The SAR estimates were based on a single year of surveying, while the model estimates were taken from the multi-year mean density surfaces we provide to model users (Section 6.1).

2021 Stock Assessment Report			Density Model		
Month/Year	Area	N_{est}	Period	Zone	Abundance
Jun-Sep 2016	Central Virginia to Maine[a]	31,912	Jun-Sep 1998-2020	NEFSC	19,305
Jun-Aug 2016	Florida to central Virginia[b]	0	Jun-Aug 1998-2020	SEFSC	211
Aug-Sep 2016	Bay of Fundy to Gulf of St. Lawrence[c]	61,321	Jun-Sep 1998-2020	Canada[d]	42,202
Jun-Sep 2016	Total	93,233	Jun-Sep 1998-2020	Total	61,718

[a] Estimate originally from Palka (2020), denoted in the SAR as "US part of Gulf of Maine population".

[b] The SAR did not provide an estimate for this area.

[c] Estimate originally from Lawson and Gosselin (2018), denoted in the SAR as "Canadian part of Gulf of Maine and all of Gulf of St. Lawrence population". Sightings were reported throughout the Scotian Shelf and Gulf of St. Lawrence (see Figure 1 of the 2021 SAR).

[d] Our Canada zone is roughly comparable to the SAR's "Bay of Fundy/Scotian Shelf" area but does not include the Gulf of St. Lawrence.
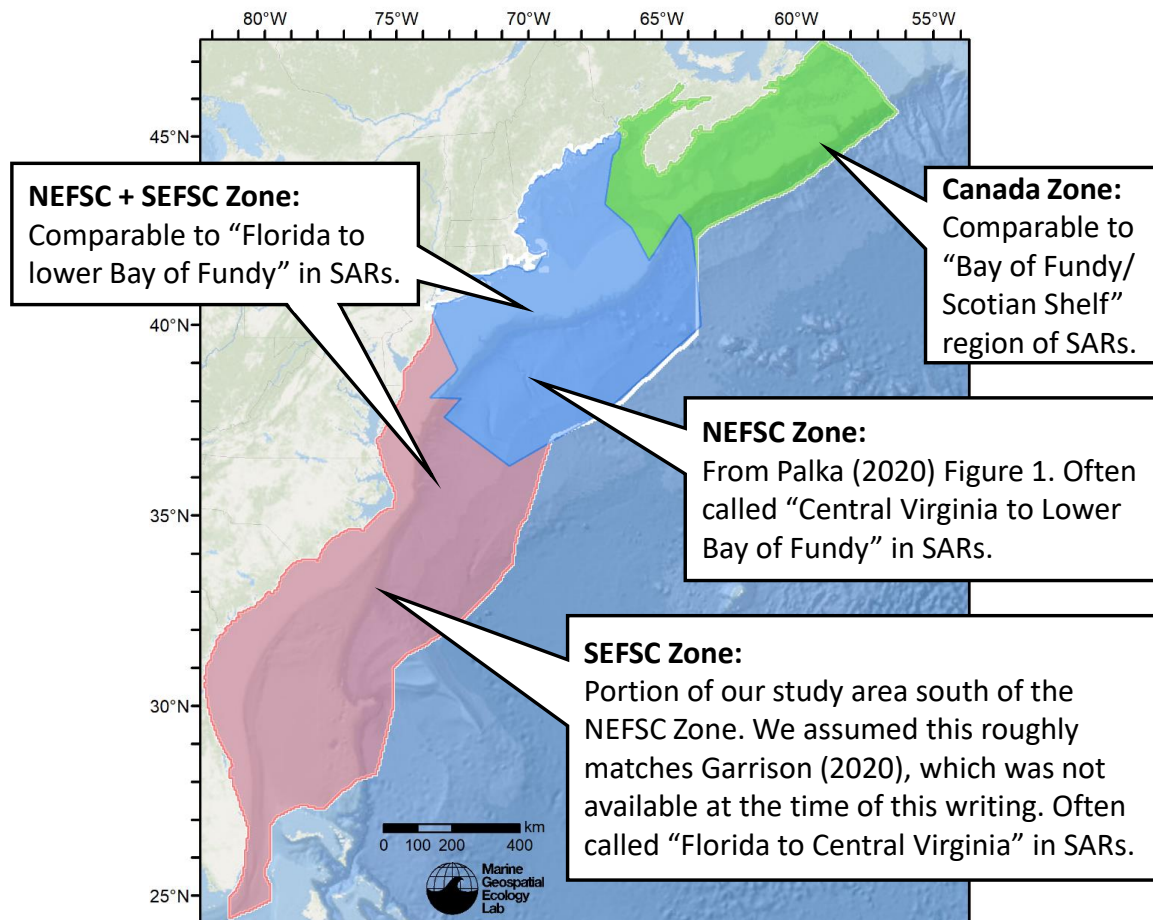

Figure 88: Zones for which we extracted abundance estimates from the density model for comparison to estimates from the NOAA Stock Assessment Report.
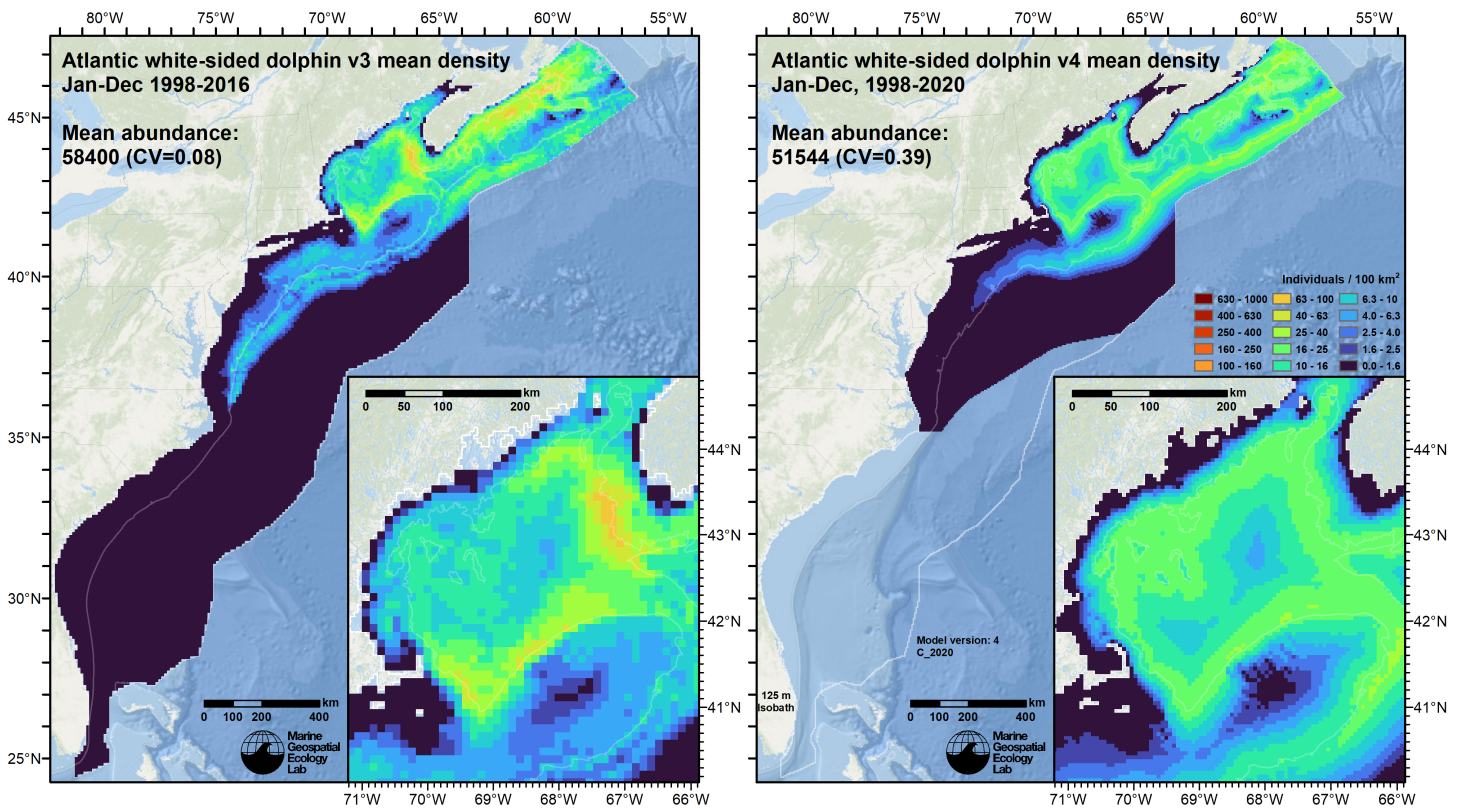
6.2.2 Previous Density Model

Figure 89: Comparison of the mean density predictions from the previous model (left) released by Roberts et al. (2018) to those from this model (right).

7 Discussion

When summarized across the modeled period (1998-2020), mean monthly density maps (Figures 76-87) generally agreed with the overall distribution and seasonal pattern described in the literature. Hayes et al. (2022) stated that for Georges Bank and various parts of the Gulf of Maine, white-sided dolphin numbers are low from January to May, high from June through September, and intermediate from October through December. Our model's monthly abundance totals roughly agree with this pattern (Figure 75). Although our abundance totals for November and December appear to deviate from that description, the peak contributions come from areas beyond Georges Bank and the Gulf of Maine: from the northern half of the Scotian Shelf in November (Figure 86) and the Scotian Shelf edge in December (Figure 87). Surveying on the Scotian Shelf was very sparse outside of summer and we urge caution with these predictions of high density in late autumn, as they represent a temporal extrapolation.

Hayes et al. (2022) stated "sightings south of Georges Bank, particularly around Hudson Canyon, occur year-round but at low densities". Our mean monthly density maps largely agree with this depiction. Our model also predicts low densities south of Hudson Canyon in April through June and absence in other months, which is generally consistent with the temporal pattern in the strandings analyzed by Byrd et al. (2014), who reported that all but one stranding in North Carolina during 1997-2008 occurred in March and April, and with the and the report of Powell et al. (2012), who documented a single stranding in South Carolina in May 2008.

Mean monthly abundance predicted by our model for the prediction region ranged from a low of 23,758 in March to a high of 71,466 in June, with a second peak of 79,149 in November, driven by the high Scotian Shelf densties discussed above (Figure 75; Table 28). Our model's mean predicted abundance for summer (June-September) of 61,718 was substantially lower than the estimate of 93,233 from the most recent NOAA Stock Assessment Report (SAR) (Hayes et al. 2022) (Table 29), but was not directly comparable because the SAR's "Bay of Fundy to Gulf of St. Lawrence" region extended substantially beyond our prediction area, which did not include the Gulf of St. Lawrence (Figure 88). However, the SAR's "Central Virginia to Maine" region was comparable to our "Canada" zone, and there our model's mean abundance was 40% lower than the SAR's estimate. We therefore advise caution when utilizing our model predictions to assess the potential impacts of threats to the species.

It is possible this difference is traceable to interannual variability; the SAR was based on a single year of surveying, while our analysis on multiple years of surveys conducted over two decades. Hayes et al. (2022) recounted that, historically, a "gap" appeared to exist between the Gulf of Maine and Gulf of St. Lawrence populations, in which relatively few sightings were recorded between the two regions (i.e. along the Scotian Shelf). Hayes et al. (2022) stated that this gap has been less obvious since 2007 and speculated that an increasing number of animals distributed further northward could be due to climate change in the Gulf of Maine. This hypothesis is consistent with the findings of Thorne et al. (2022), who concluded in an analysis of stranding records that there was strong statistical evidence of a poleward (i.e. northward) shift in distribution. Our model's monthly predictions (Figures 76-87) do not show an obvious gap or reduction in density on the Scotian Shelf relative to the Gulf of Maine. Given this, one way to interpret the difference between our summer abundance prediction and that of the SAR is that our model reflected the purported northerly shift that has occurred over time, while the SAR was based on one year in which the population did not move as far north.

Given the general match between the model's predictions and what has been reported in the literature, the differences discussed above notwithstanding, we elected to offer density predictions for this species at monthly temporal resolution.

Compared to the previous model (version 3), this model (version 4) predicted 12% lower total abundance, with the bulk of the decrease occurring off the southern tip of Nova Scotia and along its coastal waters to the northeast (Figure 89). Lower abundance was also predicted south of Hudson Canyon. We consider these changes to be in better agreement with the literature and therefore be an improvement over the previous model. However, it is also possible to interpret them as suggestive of a northward shift in the species' distribution, perhaps with some portion of the population moving beyond the study area. This interpretation requires more investigation with an approach specifically designed to test for it, ideally by including surveys conducted by DFO (Lawson and Gosselin 2009, 2018), and additional data gathered in the years beyond 2020.

The substantially larger CV in this model compared to the previous version is due to this model using contemporaneous covariates and fully accounting for the temporal variability in predictions as well as the error in model parameter estimates via the method of Miller et al. (2022), while the previous version used climatological covariates and only accounted for the error in model parameter estimates, resulting in an underestimate of variance. The CV estimated for the new model is thus an improvement, by virtue if it accounting for additional important sources of variance.

References

Aschettino JM, Engelhaupt D, Engelhaupt A, Richlen M, DiMatteo A (2018) Mid-Atlantic Humpback Whale Monitoring, Virginia Beach, Virginia: 2017/18 Annual Progress Report.

Atlas R, Hoffman RN, Ardizzone J, Leidner SM, Jusem JC, Smith DK, Gombos D (2011) A Cross-calibrated, Multiplatform Ocean Surface Wind Velocity Product for Meteorological and Oceanographic Applications. Bulletin of the American Meteorological Society 92:157–174. doi: 10.1175/2010BAMS2946.1

Barco SG, Burt L, DePerte A, Digiovanni R Jr. (2015) Marine Mammal and Sea Turtle Sightings in the Vicinity of the Maryland Wind Energy Area July 2013-June 2015, VAQF Scientific Report #2015-06. Virginia Aquarium & Marine Science Center Foundation, Virginia Beach, VA

Barlow J, Forney KA (2007) Abundance and population density of cetaceans in the California Current ecosystem. Fishery Bulletin 105:509–526.

Becker JJ, Sandwell DT, Smith WHF, Braud J, Binder B, Depner J, Fabre D, Factor J, Ingalls S, Kim S-H, Ladner R, Marks K, Nelson S, Pharaoh A, Trimmer R, Von Rosenberg J, Wallace G, Weatherall P (2009) Global Bathymetry and Elevation Data at 30 Arc Seconds Resolution: SRTM30_PLUS. Marine Geodesy 32:355–371. doi: 10.1080/01490410903297766

Behrenfeld MJ, Falkowski PG (1997) Photosynthetic rates derived from satellite-based chlorophyll concentration. Limnology and oceanography 42:1–20. doi: 10.4319/lo.1997.42.1.0001

Brasnett B (2008) The impact of satellite retrievals in a global sea-surface-temperature analysis. Quarterly Journal of the Royal Meteorological Society 134:1745–1760. doi: 10.1002/qj.319

Breiman L (2001) Random Forests. Machine Learning 45:5–32. doi: 10.1023/A:1010933404324

Buckland ST, Anderson DR, Burnham KP, Laake JL, Borchers DL, Thomas L (2001) Introduction to Distance Sampling: Estimating Abundance of Biological Populations. Oxford University Press, Oxford, UK

Burt ML, Borchers DL, Jenkins KJ, Marques TA (2014) Using mark-recapture distance sampling methods on line transect surveys. Methods in Ecology and Evolution 5:1180–1191. doi: 10.1111/2041-210X.12294

Byrd BL, Harms CA, Hohn AA, McLellan WA, Lovewell GN, Moore KT, Altman KM, Rosel PE, Barco SG, Thayer VG, Friedlaender A (2014) Strandings as indicators of marine mammal biodiversity and human interactions off the coast of North Carolina. Fishery Bulletin 112:1–23. doi: 10.7755/FB.112.1.1

Canada Meteorological Center (2012) GHRSST Level 4 CMC0.2deg Global Foundation Sea Surface Temperature Analysis Version 2.0. PODAAC, CA, USA. doi: 10.5067/GHCMC-4FM02

Canada Meteorological Center (2016) GHRSST Level 4 CMC0.1deg Global Foundation Sea Surface Temperature Analysis Version 3.0. PODAAC, CA, USA. doi: 10.5067/GHCMC-4FM03

Canny JF (1986) A computational approach to edge detection. IEEE Transactions on Pattern Analysis and Machine Intelligence 8:679–698. doi: 10.1016/B978-0-08-051581-6.50024-6

Carretta JV, Lowry MS, Stinchcomb CE, Lynn MS, E. CR (2000) Distribution and abundance of marine mammals at San Clemente Island and surrounding offshore waters: Results from aerial and ground surveys in 1998 and 1999. NOAA Administrative Report LJ-00-02. NOAA National Marine Fisheries Service, Southwest Fisheries Center, La Jolla, CA

Chassignet E, Hurlburt H, Metzger EJ, Smedstad O, Cummings J, Halliwell G, Bleck R, Baraille R, Wallcraft A, Lozano C, Tolman H, Srinivasan A, Hankin S, Cornillon P, Weisberg R, Barth A, He R, Werner F, Wilkin J (2009) US GODAE: Global Ocean Prediction with the HYbrid Coordinate Ocean Model (HYCOM). Oceanog 22:64–75. doi: 10.5670/oceanog.2009.39

Cole T, Gerrior P, Merrick RL (2007) Methodologies of the NOAA National Marine Fisheries Service Aerial Survey Program for Right Whales (Eubalaena glacialis) in the Northeast U.S., 1998-2006. U.S. Department of Commerce, Woods Hole, MA

Cotter MP (2019) Aerial Surveys for Protected Marine Species in the Norfolk Canyon Region: 2018–2019 Final Report. HDR, Inc., Virginia Beach, VA

Foley HJ, Paxton CGM, McAlarney RJ, Pabst DA, Read AJ (2019) Occurrence, Distribution, and Density of Protected Species in the Jacksonville, Florida, Atlantic Fleet Training and Testing (AFTT) Study Area. Duke University Marine Lab, Beaufort, NC

Garnesson P, Mangin A, Fanton d'Andon O, Demaria J, Bretagnon M (2019) The CMEMS GlobColour chlorophyll *a* product based on satellite observation: Multi-sensor merging and flagging strategies. Ocean Science 15:819–830. doi: 10.5194/os-15-819-2019

Garrison LP (2020) Abundance of cetaceans along the southeast U.S. East coast from a summer 2016 vessel survey. PRD Contribution # PRD-2020-04. NOAA National Marine Fisheries Service, Southeast Fisheries Science Center, Miami, FL

Garrison LP, Martinez A, Maze-Foley K (2010) Habitat and abundance of cetaceans in Atlantic Ocean continental slope waters off the eastern USA. Journal of Cetacean Research and Management 11:267–277.

Geo-Marine, Inc. (2010) New Jersey Department of Environmental Protection Baseline Studies Final Report Volume III: Marine Mammal and Sea Turtle Studies. Geo-Marine, Inc., Plano, TX

Hayes SA, Josephson E, Maze-Foley K, Rosel PE, Wallace J, Brossard A, Chavez-Rosales S, Cole TVN, Garrison LP, Hatch J, Henry A, Horstman SC, Litz J, Lyssikatos MC, Mullin KD, Murray K, Orphanides C, Ortega-Ortiz J, Pace RM, Palka DL, Powell J, Rappucci G, Soldevilla M, Wenzel FW (2022) US Atlantic and Gulf of Mexico Marine Mammal Stock Assessments 2021. NOAA National Marine Fisheries Service, Northeast Fisheries Science Center, Woods Hole, MA

Hothorn T, Hornik K, Zeileis A (2006) Unbiased Recursive Partitioning: A Conditional Inference Framework. Journal of Computational and Graphical Statistics 15:651–674. doi: 10.1198/106186006X133933

Laake JL, Calambokidis J, Osmek SD, Rugh DJ (1997) Probability of Detecting Harbor Porpoise From Aerial Surveys: Estimating g(0). Journal of Wildlife Management 61:63–75. doi: 10.2307/3802415

Lawson JW, Gosselin J-F (2009) Distribution and preliminary abundance estimates for cetaceans seen during Canada's Marine Megafauna Survey-A component of the 2007 TNASS. Department of Fisheries and Oceans, St. John's, NL, Canada

Lawson JW, Gosselin J-F (2018) Estimates of cetacean abundance from the 2016 NAISS aerial surveys of eastern Canadian waters, with a comparison to estimates from the 2007 TNASS. NAMMCO SC/25/AE/09. In: Proceedings of the NAMMCO 25th Scientific Committee (SC). North Atlantic Marine Mammal Commission, Bergen-Tromsø, Norway,

Lehodey P, Senina I, Murtugudde R (2008) A spatial ecosystem and populations dynamics model (SEAPODYM)–Modeling of tuna and tuna-like populations. Progress in Oceanography 78:304–318. doi: 10.1016/j.pocean.2008.06.004

Lehodey P, Conchon A, Senina I, Domokos R, Calmettes B, Jouanno J, Hernandez O, Kloser R (2015) Optimization of a micronekton model with acoustic data. ICES Journal of Marine Science 72:1399–1412. doi: 10.1093/icesjms/fsu233

Mallette SD, Lockhart GG, McAlarney RJ, Cummings EW, McLellan WA, Pabst DA, Barco SG (2014) Documenting Whale Migration off Virginia's Coast for Use in Marine Spatial Planning: Aerial and Vessel Surveys in the Proximity of the Virginia Wind Energy Area (VA WEA), VAQF Scientific Report 2014-08. Virginia Aquarium & Marine Science Center Foundation, Virginia Beach, VA

Mallette SD, Lockhart GG, McAlarney RJ, Cummings EW, McLellan WA, Pabst DA, Barco SG (2015) Documenting Whale Migration off Virginia's Coast for Use in Marine Spatial Planning: Aerial Surveys in the Proximity of the Virginia Wind Energy Area (VA WEA) Survey/Reporting Period: May 2014 - December 2014, VAQF Scientific Report 2015-02. Virginia Aquarium & Marine Science Center Foundation, Virginia Beach, VA

Mallette SD, McAlarney RJ, Lockhart GG, Cummings EW, Pabst DA, McLellan WA, Barco SG (2017) Aerial Survey Baseline Monitoring in the Continental Shelf Region of the VACAPES OPAREA: 2016 Annual Progress Report. Virginia Aquarium & Marine Science Center Foundation, Virginia Beach, VA

Marsh H, Sinclair DF (1989) Correcting for Visibility Bias in Strip Transect Aerial Surveys of Aquatic Fauna. The Journal of Wildlife Management 53:1017. doi: 10.2307/3809604

McAlarney R, Cummings E, McLellan W, Pabst A (2018) Aerial Surveys for Protected Marine Species in the Norfolk Canyon Region: 2017 Annual Progress Report. University of North Carolina Wilmington, Wilmington, NC

McLellan WA, McAlarney RJ, Cummings EW, Read AJ, Paxton CGM, Bell JT, Pabst DA (2018) Distribution and abundance of beaked whales (Family Ziphiidae) Off Cape Hatteras, North Carolina, U.S.A. Marine Mammal Science. doi: 10.1111/mms.12500

Meissner T, Wentz FJ, Scott J, Vazquez-Cuervo J (2016) Sensitivity of Ocean Surface Salinity Measurements From Spaceborne L-Band Radiometers to Ancillary Sea Surface Temperature. IEEE Trans Geosci Remote Sensing 54:7105–7111. doi: 10.1109/TGRS.2016.2596100

Mesgaran MB, Cousens RD, Webber BL (2014) Here be dragons: A tool for quantifying novelty due to covariate range and correlation change when projecting species distribution models. Diversity Distrib 20:1147–1159. doi: 10.1111/ddi.12209

Miller DL, Becker EA, Forney KA, Roberts JJ, Cañadas A, Schick RS (2022) Estimating uncertainty in density surface models. PeerJ 10:e13950. doi: 10.7717/peerj.13950

Mullin KD, Fulling GL (2003) Abundance of cetaceans in the southern U.S. North Atlantic Ocean during summer 1998. Fishery Bulletin 101:603–613.

Palka D (2020) Cetacean Abundance in the US Northwestern Atlantic Ocean Summer 2016. Northeast Fish Sci Cent Ref Doc. 20-05. NOAA National Marine Fisheries Service, Northeast Fisheries Science Center, Woods Hole, MA

Palka D, Read A, Potter C (1997) Summary of knowledge of white-sided dolphins (Lagenorhynchus acutus) from US and Canadian Atlantic Waters. Rep Int Whal Commn 47:729–734.

Palka D, Aichinger Dias L, Broughton E, Chavez-Rosales S, Cholewiak D, Davis G, DeAngelis A, Garrison L, Haas H, Hatch J, Hyde K, Jech M, Josephson E, Mueller-Brennan L, Orphanides C, Pegg N, Sasso C, Sigourney D, Soldevilla M, Walsh H (2021) Atlantic Marine Assessment Program for Protected Species: FY15 – FY19 (OCS Study BOEM 2021-051). U.S. Deptartment of the Interior, Bureau of Ocean Energy Management, Washington, DC

Palka DL (2006) Summer abundance estimates of cetaceans in US North Atlantic navy operating areas (NEFSC Reference Document 06-03). U.S. Department of Commerce, Northeast Fisheries Science Center, Woods Hole, MA

Palka DL, Cholewiak D, Broughton E, Jech M, Force M, Guida V, Lowe M, Lawson G (2014) Shipboard habitat survey during March – April 2014: Northeast Fisheries Science Center. NOAA National Marine Fisheries Service, Northeast Fisheries Science Center, Woods Hole, MA

Palka DL, Chavez-Rosales S, Josephson E, Cholewiak D, Haas HL, Garrison L, Jones M, Sigourney D, Waring G, Jech M, Broughton E, Soldevilla M, Davis G, DeAngelis A, Sasso CR, Winton MV, Smolowitz RJ, Fay G, LaBrecque E, Leiness JB, Dettloff K, Warden M, Murray K, Orphanides C (2017) Atlantic Marine Assessment Program for Protected Species: 2010-2014 (OCS Study BOEM 2017-071). U.S. Deptartment of the Interior, Bureau of Ocean Energy Management, Washington, DC

Perkins NJ, Schisterman EF (2006) The Inconsistency of "Optimal" Cutpoints Obtained using Two Criteria based on the Receiver Operating Characteristic Curve. American Journal of Epidemiology 670–675.

Powell JWB, Rotstein DS, McFee WE (2012) First Records of the Melon-Headed Whale (Peponocephala electra) and the Atlantic White-Sided Dolphin (Lagenorhynchus acutus) in South Carolina. Southeastern Naturalist 11:23–34. doi: 10.1656/058.011.0102

Read AJ, Barco S, Bell J, Borchers DL, Burt ML, Cummings EW, Dunn J, Fougeres EM, Hazen L, Hodge LEW, Laura A-M, McAlarney RJ, Peter N, Pabst DA, Paxton CGM, Schneider SZ, Urian KW, Waples DM, McLellan WA (2014)

Occurrence, distribution and abundance of cetaceans in Onslow Bay, North Carolina, USA. Journal of Cetacean Research and Management 14:23–35.

Roberts JJ, Best BD, Dunn DC, Treml EA, Halpin PN (2010) Marine Geospatial Ecology Tools: An integrated framework for ecological geoprocessing with ArcGIS, Python, R, MATLAB, and C++. Environmental Modelling & Software 25:1197–1207. doi: 10.1016/j.envsoft.2010.03.029

Roberts JJ, Best BD, Mannocci L, Fujioka E, Halpin PN, Palka DL, Garrison LP, Mullin KD, Cole TVN, Khan CB, McLellan WA, Pabst DA, Lockhart GG (2016) Habitat-based cetacean density models for the U.S. Atlantic and Gulf of Mexico. Scientific Reports 6:22615. doi: 10.1038/srep22615

Roberts JJ, Mannocci L, Schick RS, Halpin PN (2018) Final Project Report: Marine Species Density Data Gap Assessments and Update for the AFTT Study Area, 2017-2018 (Opt. Year 2), Document Version 1.2. Duke University Marine Geospatial Ecology Lab, Durham, NC

Roberts JJ, Yack TM, Halpin PN (2023) Marine mammal density models for the U.S. Navy Atlantic Fleet Training and Testing (AFTT) study area for the Phase IV Navy Marine Species Density Database (NMSDD), Document Version 1.3. Duke University Marine Geospatial Ecology Lab, Durham, NC

Robertson FC, Koski WR, Brandon JR, Thomas TA, Trites AW (2015) Correction factors account for the availability of bowhead whales exposed to seismic operations in the Beaufort Sea. Journal of Cetacean Research and Management 15:35–44.

Ryan C, Boisseau O, Cucknell A, Romagosa M, Moscrop A, McLanaghan R (2013) Final report for trans-Atlantic research passages between the UK and USA via the Azores and Iceland, conducted from R/V Song of the Whale 26 March to 28 September 2012. Marine Conservation Research International, Essex, UK

Silsbe GM, Behrenfeld MJ, Halsey KH, Milligan AJ, Westberry TK (2016) The CAFE model: A net production model for global ocean phytoplankton. Global Biogeochemical Cycles 30:1756–1777. doi: 10.1002/2016GB005521

Thorne LH, Heywood EI, Hirtle NO (2022) Rapid restructuring of the odontocete community in an ocean warming hotspot. Global Change Biology gcb.16382. doi: 10.1111/gcb.16382

Torres LG, Mclellan WA, Meagher E, Pabst DA (2005) Seasonal distribution and relative abundance of bottlenose dolphins, Tursiops truncatus, along the US mid-Atlantic coast. Journal of Cetacean Research and Management 7:153.

Wentz FJ, Scott J, Hofflman R, Leidner M, Atlas R, Ardizzone J (2015) Remote Sensing Systems Cross-Calibrated Multi-Platform (CCMP) 6-hourly ocean vector wind analysis product on 0.25 deg grid, Version 2.0. Remote Sensing Systems, Santa Rosa, CA

Whitt AD, Powell JA, Richardson AG, Bosyk JR (2015) Abundance and distribution of marine mammals in nearshore waters off New Jersey, USA. Journal of Cetacean Research and Management 15:45–59.

Wood SN (2011) Fast stable restricted maximum likelihood and marginal likelihood estimation of semiparametric generalized linear models. Journal of the Royal Statistical Society: Series B (Statistical Methodology) 73:3–36. doi: 10.1111/j.1467-9868.2010.00749.x